Università degli Studi di Ferrara

DOTTORATO DI RICERCA IN
SCIENZE DELL'INGEGNERIA

CICLO XXVII

COORDINATORE Prof. Stefano TRILLO

ONE-DIMENSIONAL HYDRODYNAMIC MODELS IN RIVER RESOURCE MANAGEMENT AND POLICY DESIGN

Settore Scientifico Disciplinare ICAR/01

Dottorando
Dott. Bernardi Dario

Tutore
Prof. Schippa Leonardo

Anni 2012/2015

Doctoral thesis in Engineering Science, XXVII cycle – Bernardi Dario

Department of Engineering, University of Ferrara – Italy

Supervisor: Dr. Leonardo Schippa, PhD, LPE

Università degli Studi di Ferrara

Ferrara, April 10th ,2015

blank

Abstract

This thesis concludes a three-year doctoral program in hydraulic engineering.

The research work focused on the development, testing and application of one-dimensional numerical models to river resources management and policy design issues, pointing out the key role numerical modeling can play to support river managers in the decision process where large-scale, eco-morphological river changes are supposed to occur. These latter may result in overwhelming environmental and socio-economic costs for the population and communities living along rivers, especially in developing countries: river morphological evolution cannot be neglected anymore when planning river resources use in large watersheds, and the need for tools capable of informing river managers is nowadays manifest.

One-dimensional models, even though introducing simplifications in the description of hydrodynamics and sediment movement processes, do have some advantages. Provided modeling assumptions are correct, they are able to provide indicators that - despite not capturing all details - allow analyzing trends of morphological processes at reach-scale or basin scale. Moreover, they are time-saving and open the way to long-term analyses and implementation in optimization procedures. Models based on the shallow water equations for the liquid phase, together with the Exner equation for river bed evolution, have been used: two different numerical schemes for solving the governing equations have been implemented trying to improve model robustness and versatility.

Even the simplest numerical models, built on simple numerical schemes, require a long case-specific model building work. Understanding of the river morphology evolution drivers and basic

physical processes, hydrological and topographical data collection and pre-processing, adaptation of the model to the specific case study and specific features (e.g. control rule for the Isola Serafini diversion barrage, time-varying bifurcation for the Red River), choice of suitable closure equations (e.g. sediment transport formula), are all essential steps that influence reliability of results and claim the same carefulness as the development of the numerical model itself. Details are given about the model building process for each case study.

We analyzed three different case studies of river system management in which numerical model simulations give a relevant contribution to the decision-making process.

- River Po (Italy), in its lower course, has undergone a severe bed lowering process during second half of the 20th century. The Isola Serafini hydropower plant, located on Po river, operating since 1962, is served by a 330 m wide barrage that still affects the hydrological regime and sediment supply downstream. Alternative operating rules for the barrage, over a time horizon of ten years, have been analyzed by the means of a one-dimensional hydro-morphological numerical model. A multi-objective optimization framework was implemented, to assess the effects of the operating rules on hydropower revenue and river bed incision. We adopted a surrogate modeling technique (Global Response Surfaces in the Learning and Planning procedure) to embed the hydro-morphological model in the optimization procedure in a multidisciplinary approach. The obtained results are encouraging and show that with a moderate loss in hydropower revenue, the decrease in river bed degradation can be remarkable.
- The Red River (*Song Hong*) in northern VietNam has experienced severe river bed degradation along its lower course as well, but over a shorter period (last 15 years). The continued decrease of the water levels in the dry season aggravated water scarcity for agriculture. These outcomes can be attributed to strong instream sediment mining, major upstream impoundments, climatic and land use changes. The IMRR (*Integrated and sustainable water Management of Red-Thai Binh Rivers System in changing climate*) project, run by the Politecnico di Milano university with several Vietnamese agencies and

authorities under the supervision of the Italian Ministry of Foreign Affairs, has faced several challenges inherent to water resources use in the Red River basin; the main river morphological evolution aspects of the last decades have been thoroughly analyzed and a finite-volume numerical model of the lower course of Red River has been set up and tested. The model has been used to evaluate the sensitivity of the river stretch to discharge modulation operated by upstream reservoirs, and to estimate instream sand mining rates to draw up some prediction scenarios. We showed that sediment mining rates, as expected, could be much larger than licensed amounts; this accelerates incision in the first reach and reverses the natural restoration trend in the following reaches, aggravating water level lowering. The flow control operated by reservoirs, conversely, appears to affect much less the morphological processes in the studied reach.

- In January 2014, a serious flooding event (due to a levee breach) occurred in the Modena Province (Italy) along Secchia River. Concerns have increased about the role of vegetation in Secchia river channel during big floods. A detailed characterization of riparian vegetation features has then been produced by the Po River Interregional Agency (AIPo) to point out critical issues about current vegetation pattern along Secchia river banks and possibly plan a maintenance - remediation strategy. This characterization report constitutes a good basis for a hydrodynamic modelling work; a 1D finite-volume model, accounting for the influence of different vegetation patterns and densities on flow resistance has been applied to a 60 km long stretch of Secchia river. The agreement between simulation results and gauged data on a real flood event is encouraging and opens the way to the use of the model for evaluating the effectiveness of future vegetation management plans.

Contents

Chapter 1

Introduction

Throughout the history of mankind, river systems and their perpetual physical changes have been the basis of development and progress of the communities living on floodplains - unquestionably the large majority of the world's population - as well as drivers of their evolution, their wealth and often cause of their fatal disasters. It is evident that the attempt to control and manage the evolution of rivers has always been a focus of the human activity: water supply, food, power, transport, are key aspects to deal with, all strongly related to river resources. Evaluation of both short term and long term river responses is essential in every phase of a project (Chang, 1988).

The aggressive exploitation and abuse of river resources can dramatically impact the environmental quality and morphological equilibrium of rivers, leading to complex processes that can quickly reverse existing trends.

In recent years, river geomorphology has become a key aspect of river management (Simon and Rinaldi, 2006) and geomorphic processes significantly affect various environmental services that fluvial systems provide to our society, ranging from flood mitigation to ecological aspects. The economical quantifications of these direct and indirect ecosystem services are difficult to estimate and a matter of recent research (Gilvear et al., 2013), but their evaluation cannot be neglected anymore when planning modern catchment management strategies.

In the last decades, in parallel with the increase in computing power, the adoption of numerical models to solve the differential equations governing the principles of hydrodynamics and sediment transport in rivers has established itself among the river scientists community.

In the case of one-dimensional unsteady open-channel flow, it is common practice to use as mathematical basis the De Saint Venant balance equations of mass and momentum. Many engineering problems involve the study of flows characterized by small vertical scales compared to other dimensions, as it generally occurs in rivers: these can be described by the shallow-water equations (SWE), which form a set of non-linear hyperbolic equations (Cunge et al., 1980, see the following chapter 2 for details).

A variety of numerical schemes have been proposed for the solution of systems of hyperbolic balance equations, both in the finite difference and finite volume frameworks: among others, we recall the contributions by Lax and Wendroff (1960), Preissmann and Cunge (1961), McCormack (1969), Harten et al. (1983), Roe (1986), Sweby (1984), Lai (1986), Hirsch (1990), Bhallamudi and Chaudhry (1991), Garcia-Navarro et al. (1992), Toro (1989 and 1994), Garcia-Navarro and Vazquez-Cendon (2000). Higher order approaches have been developed, aiming to reach any desired order of accuracy, such as the ENO (Harten et al., 1987) and ADER (Toro, 2001) schemes; the recently developed path-conservative methods (Castro et al., 2006) lead to the the PRICE (Toro and Siviglia, 2003; Canestrelli et al., 2009) methods for the system of shallow-water equations in non-conservative form. Many of these advanced solutions are applicable also to 2D and 3D flow problems.

In any case, the choice of a numerical hydrodynamics and sediment transport model in a river management problem is not only driven by accuracy in the representation of the physical processes, but also by the morphological, hydrological, anthropogenic features of the river system which have to be considered, as well as the *space and time scale* of the processes involved. Long-term modeling of morphological river evolution is a challenge involving complex phenomena in a non-static system subject to continuous and sometimes random changes. For these reasons, despite

the availability of many commercial codes for 2D and 3D modeling, one-dimensional models are still widely used by river engineers and managers worldwide: recent interesting applications of one-dimensional models to management issues, for instance, can be found in Langendoen et al (2009) on the evolution of two incised streams in northern Missisippi, Nones et al. (2013) on the investigation of the effects of large impoundments on the Zambezi River, Canestrelli et al. (2013) on a long-term modelling of an estuary in Papua New Guinea, to name a few.

In general, the models we present herein are suitable for analysis of one-dimensional flows in sinuous or meandering, mild slope rivers in their middle - lower course ("transfer zone" as defined by Schumm, 1977) , with no dramatic braiding – anastomosing phenomena.

To be useful in management decisions, a model has to provide indicators to evaluate effects of different management policies or hydrological scenarios on the river system. The evaluation of different scenarios implies several simulation runs, whose length is determined by the processes time scale ($\sim 10^1$ years), and these have to be performed in an acceptable computational time.

From here it follows that we cannot expect a detailed description of all morphological changes that the river cross sections undergo over the years. This would require at least a 2D or 3D approach: nonetheless, local random alterations unpredictable by models are always possible. Hence, computational costs would be unaffordable and still the results would be subject to uncertainty.

The choice of a one-dimensional model allows us to represent the main geomorphic processes of interest in our case studies (i.e. river bed aggradation-degradation for river reaches 10^1 – 10^2 km long) and at the same time to limit the computational time required for the several experiments planned. By means of mobile-bed, hydrodynamic models, we analyzed the effects of the Isola Serafini run-of-the-river hydropower barrage on Po river (Italy) and the impact of flow control through reservoirs and instream sand mining on Red River bed degradation (VietNam).

In chapter 5, we focus on a specific feature of the one-dimensional river modeling, namely flow resistance (hydrodynamic roughness) induced by drag force caused by vegetation. It is well known that riparian vegetation influences flow field at several scales (for thorough reviews, see

Camporeale et al., 2013; Curran and Hession, 2013) and its effects can be positive or negative on reducing flood risk downstream (Darby, 1999; Tabacchi et al., 2000; Anderson et al., 2006) depending on canopy and root characteristics, but also on local river geometry and hydrodynamics. An attempt has been made to determine lumped flow resistance coefficients along the river, starting from a riparian vegetation characterization project realized by means of satellite image analysis and a field survey. Vegetation type, plant density and age have been considered to calculate the resistance coefficients. The management problem here is to assess the flood risk with different riparian vegetation configurations.

The present thesis outlines as follows. In chapter 2, we recalled the essential features of the mathematical model and numerical schemes used throughout the work. Chapter 3, 4 and 5 respectively, present methodologies, results and discussion about the three case studies and management problems analyzed (Isola Serafini on Po River, Red River and Secchia River). Chapter 6 summarizes the conclusions and outlooks.

Chapter 2

Mathematical model and numerical schemes

2.1 Governing equations

The following system of balance equations (in conservative form) describes one-dimensional, unsteady free surface flow in channels of complex geometry (Cunge et al., 1980; Chaudhry, 1993)

$$\frac{\partial A}{\partial t} + \frac{\partial Q}{\partial x} = q \tag{2.1}$$

$$\frac{\partial Q}{\partial t} + \frac{\partial}{\partial x}\left(\frac{Q^2}{A} + gI_1\right) = g\frac{\partial I_1}{\partial x}\Big|_{zw=const} - gAS_f \tag{2.2}$$

$$(1-p)\frac{\partial A_b}{\partial t} + \frac{\partial Q_s}{\partial x} = q_s \tag{2.3}$$

where equations (2.1) and (2.2) express respectively the mass and momentum balance of the liquid phase, and equation (2.3) (Exner equation) accounts for mass conservation of the stream bed material. Hydrostatic pressure is assumed everywhere.

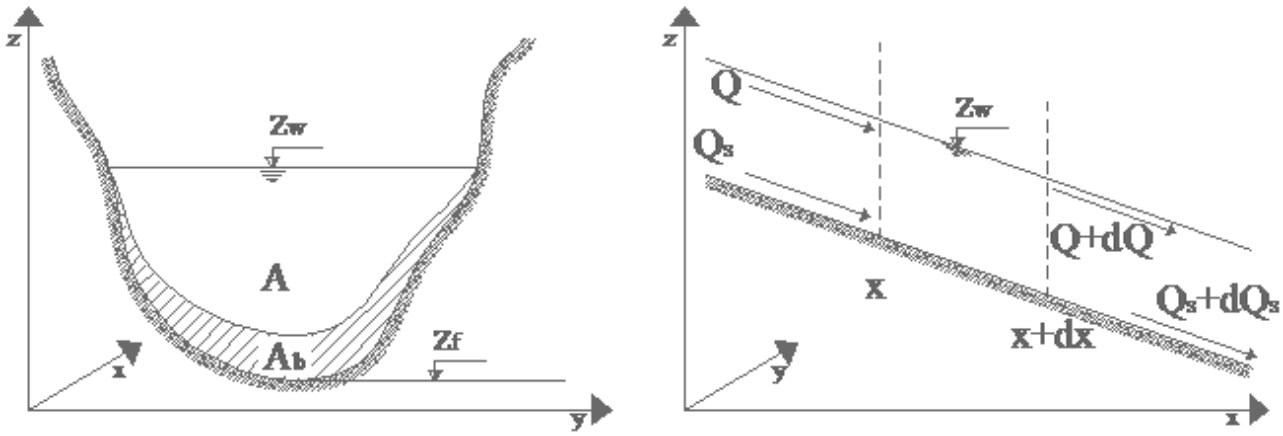

Figure 1. Cross section and longitudinal view of the stream with indication of the variables

In the equations t = time, x = longitudinal stream coordinate, A = cross-section wetted area, Q = liquid discharge, g = gravity acceleration, I_1 = static moment of the wetted area A with respect to the water surface, S_f = friction slope, A_b = sediment volume per unit length of the stream subject to erosion or deposition ("sediment area"), Q_s = sediment discharge in volume, q and q_s are the water and sediment lateral inflows (or outflows) per unit length, respectively, p is bed porosity.

In vector form, the system reads:

$$\bar{U}_t + \bar{F}(\bar{U})_x = \bar{S}(\bar{U}) \qquad (2.4)$$

In which

$$\bar{U} = \begin{bmatrix} A \\ Q \\ A_b \end{bmatrix} \qquad \bar{F} = \begin{bmatrix} Q \\ \frac{Q^2}{A} + gI_1 \\ \frac{1}{1-p} Q_s \end{bmatrix} \qquad \bar{S} = \begin{bmatrix} q \\ g \frac{\partial I_1}{\partial x}\Big|_{zw=const} - gAS_f \\ q_s \end{bmatrix} \qquad (2.5)$$

U is the vector of state variables, F is the vector of fluxes, and S contains the source terms.

The momentum balance equation is usually proposed in the following form (Cunge et al., 1980; Chaudhry, 2007):

$$\frac{\partial Q}{\partial t} + \frac{\partial}{\partial x}\left(\frac{Q^2}{A} + gI_1\right) = g\mathrm{A}\left(S_0 - S_f\right) + gI_2 \qquad (2.6)$$

(2.6) includes the local bottom slope S_0, usually defined as

$$S_0 = \frac{\partial z_\mathrm{b}}{\partial x} \qquad (2.7)$$

where z_b is the bottom elevation. However, the direct definition of local bottom slope S_0 is never easy for irregular channel geometries with abrupt changes in slope, and leads to pressure balance errors. To avoid the explicit reference to a value of local bottom slope, equation (2.6) has been changed into equation (2.2) through some rearranging steps (Valiani et al., 2001, Capart et al., 2003; Schippa & Pavan, 2008).

Equation (2.2) balances momentum correctly even if the channel geometry is not gradually varied along *x*; pressure contributions on the liquid volume boundaries due to channel slope and non-prismaticity effects are included in the gradient of the static moment I_1 (first term of the right-hand side in Equation 2.2) along the stream coordinate x, to be evaluated at a constant reference water level *zw*.

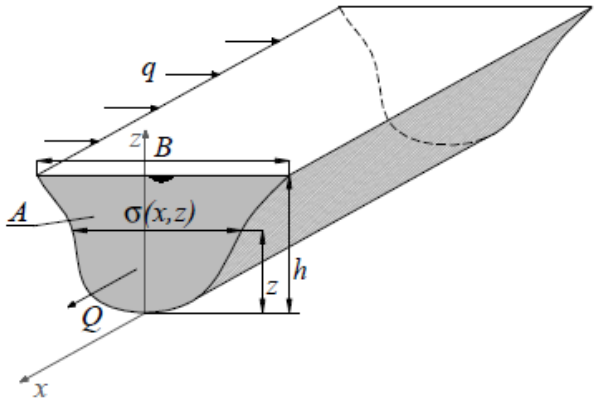

Figure 2. Variables definition for Equation (2.6) rearrangement

The static moment I_1 equals

$$I_1 = \cos\theta \int_0^h \sigma(x,z)(h-z)dz \tag{2.8}$$

θ is the angle between the river bed profile and the horizontal (if θ is small, cosθ ≈ 1: this hypothesis holds for large rivers in their middle-lower course). z is the vertical coordinate and σ is the local flow width. The presence of I_2 is due to the irregular shape of the channel cross section, and represents the variation of I_1 along the streamline direction *x* if the water depth *h* is supposed constant.

$$I_2 = \left.\frac{\partial I_1}{\partial x}\right|_{h=const} = \frac{\partial}{\partial x}\left(\cos\theta \int_0^h \sigma(x,z)(h-z)dz\right)_{h=const} \tag{2.9}$$

If Leibniz rule is applied to (2.9), (2.10) is obtained

$$I_2 = \left.\frac{\partial I_1}{\partial x}\right|_{h=const} = \frac{\partial I_1}{\partial x} - \frac{\partial I_1}{\partial h}\frac{\partial h}{\partial x} = \frac{\partial I_1}{\partial x} - A\frac{\partial h}{\partial x} \tag{2.10}$$

Given that

$$I_1 = \int_A z dx dz = \int_0^B dx \int_0^h z dz = \int_0^B h^2 dx \rightarrow \frac{\partial I_1}{\partial h} = A$$

The choice of the datum is free. Then, the following two expressions in (2.11) are equivalent:

$$\frac{\partial I_1}{\partial x} = \left.\frac{\partial I_1}{\partial x}\right|_{h=const} + A\frac{\partial h}{\partial x} \; ; \; \frac{\partial I_1}{\partial h} = A$$

$$\frac{\partial I_1}{\partial x} = \left.\frac{\partial I_1}{\partial x}\right|_{zw=const} + A\frac{\partial z_w}{\partial x} \; ; \; \frac{\partial I_1}{\partial z_w} = A \qquad (2.11)$$

Considering that $z_w = z_0 + h$ and $S_0 = -\frac{\partial z_0}{\partial x}$, solving for I_2 we have

$$I_2 = \frac{\partial I_1}{\partial x} - A\frac{\partial h}{\partial x} = \left.\frac{\partial I_1}{\partial x}\right|_{zw=const} + A\frac{\partial z_w}{\partial x} - A\left(\frac{\partial z_w}{\partial x} - \frac{\partial z_0}{\partial x}\right) \qquad (2.12)$$

And this leads finally to

$$I_2 = \left.\frac{\partial I_1}{\partial x}\right|_{zw=const} - AS_0 \qquad (2.13)$$

Substituting (2.13) in the right-hand side of (2.6), the new equation of momentum balance (2.2) is obtained.

This mathematical model is suitable for hydrodynamic modelling in natural, irregular streams as proven by Schippa and Pavan (2009).

To complete the system, two closure equations are needed to compute slope friction and sediment discharge respectively. More details will be given when analyzing single case studies applications.

Since we deal with one-dimensional models, the solution of the balance eqn. (2.3) updates the value of "sediment area" A_b at every time step. This value, in turn, has to be converted into a bed elevation variation, Δs, for every wetted point of the cross section. It is assumed herein that this variation Δs

is proportional to bed shear stress, which in turn is related to the local water depth h through a proportionality constant k:

$$\Delta s = kh \tag{2.14}$$

The variation of sediment area ΔA_b, at every time step, is given by integrating s along the wetted perimeter P:

$$\int_P \Delta s dp = \Delta A_b \tag{2.15}$$

Applying the same integral to the right-hand side of (2.14) leads to the integral of the water depth h along the wetted perimeter, which is in fact the wetted area A. it follows that

$$k = \frac{\Delta A_b}{A} \tag{2.16}$$

and the local bed elevation variation due to erosion or deposition is calculated directly by (2.14).

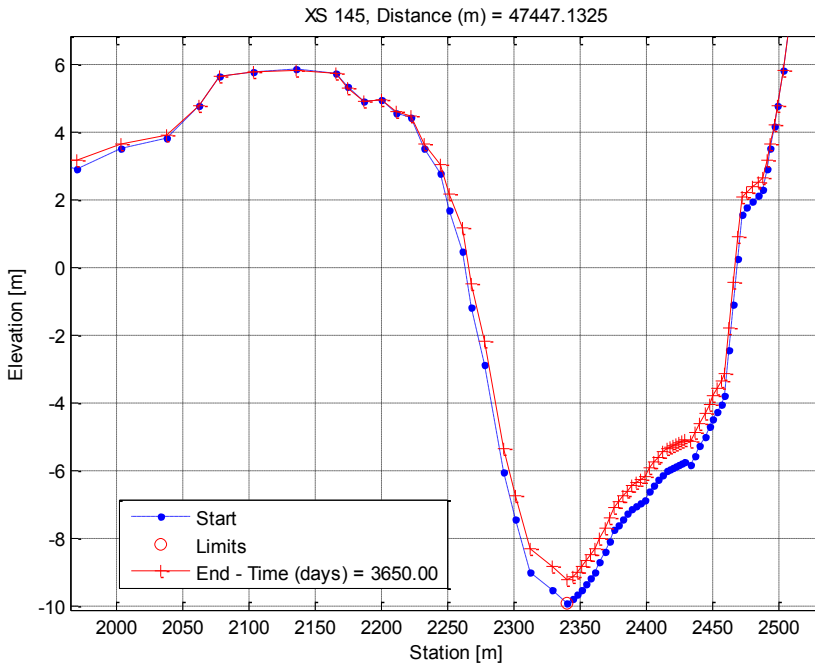

Figure 3. Example of cross section change (start-end of a simulation).

2.2 A finite difference solution: McCormack scheme

The finite difference explicit scheme developed by McCormack (1969) has been used to integrate the set of equations (2.1) - (2.3), for its simplicity to implement and ability to cope with discontinuities in the solution (the scheme is shock-capturing). It is based on a predictor-corrector procedure, where backward spatial finite differences are used in the predictor step and forward differences in the corrector step. Numerical tests and further information can be found in the work by Schippa and Pavan (2009).

If *i* is the identification number of the cross section, n is the identification number of the time step, Δx is the space interval between cross sections and Δt the time step, we may write for McCormack scheme:

Predictor: $$U_{i,P}^{n+1} = U_i^n - \frac{\Delta t}{\Delta x}(F_i - F_{i-1}) + \Delta t S(U_{av}^n) \quad (2.17)$$

Corrector: $$U_{i,C}^{n+1} = U_i^n - \frac{\Delta t}{\Delta x}(F_{i+1} - F_i) + \Delta t S(U_{av}^n) \quad (2.18)$$

The source terms $S(U_{av}^n)$ are evaluated as follows (e.g. at predictor step, but in the same way at corrector step)

- *Sf* is the average between cross sections i and i-1 at time step n;
- $\frac{\partial I_1}{\partial x}\Big|_{zw=const}$ becomes $\frac{I_{1,i+1}-I_{1,i}}{\Delta x}\Big|_{zw=const}$. Both static moments can be calculated with water level at time step n;
- q and q_s are the water and sediment lateral inflows in the space interval.

Finally, the solution U at time step n+1 is given by

$$U_i^{n+1} = \frac{U_{i,P}^{n+1} + U_{i,C}^{n+1}}{2} \quad (2.19)$$

A Courant-type stability condition is imposed to calculate the time step Δt :

$$\Delta t < CFL \frac{\Delta x(\min)}{S_{\max}} \quad (2.20)$$

Where CFL is the chosen Courant number, less than 1, and *Smax*, maximum wave propagation speed, is calculated as

$$S_{\max} = \max|V_i| + \max(c_i) \qquad (2.21)$$

Where V_i and c_i are the water velocities and celerities at each cross section.

McCormack scheme, as other second-order schemes, can lead to spurious oscillations close to discontinuities (e.g. steep wave fronts) in the solution. To overcome this, an artificial viscosity (Chaudhry, 1993) term has been added.

In subcritical flow regime, upstream boundary conditions for liquid and solid discharge and a downstream boundary condition for water level are needed.

2.3 A Godunov-type finite volume scheme

After the first application of the model to the case study of the Po River (Chapter 3), a different numerical scheme has been chosen.

A Godunov-type (Godunov, 1959) finite volume scheme, first order accurate in space and time, has been adopted to integrate the system of equations (2.4). A splitting form is implemented: the homogeneous part of the system is first solved, then with the obtained intermediate step solution $U^{n+1/2}$ the ODEs involving source terms are integrated, as follows (Toro, 2009):

$$\bar{U}_t^n + \bar{F}(\bar{U}^n)_x = 0 \rightarrow \bar{U}^{n+1/2} \qquad (2.22)$$

$$\bar{U}^{n+1} = \bar{U}^{n+1/2} + \Delta t S\left(\bar{U}^{n+1/2}\right) \qquad (2.23)$$

Once the domain has been divided in cells ("volumes"), the indexes *i +1/2* and *i -1/2* denote the boundaries of cell *i*. An exemplification is depicted in Figure 4.

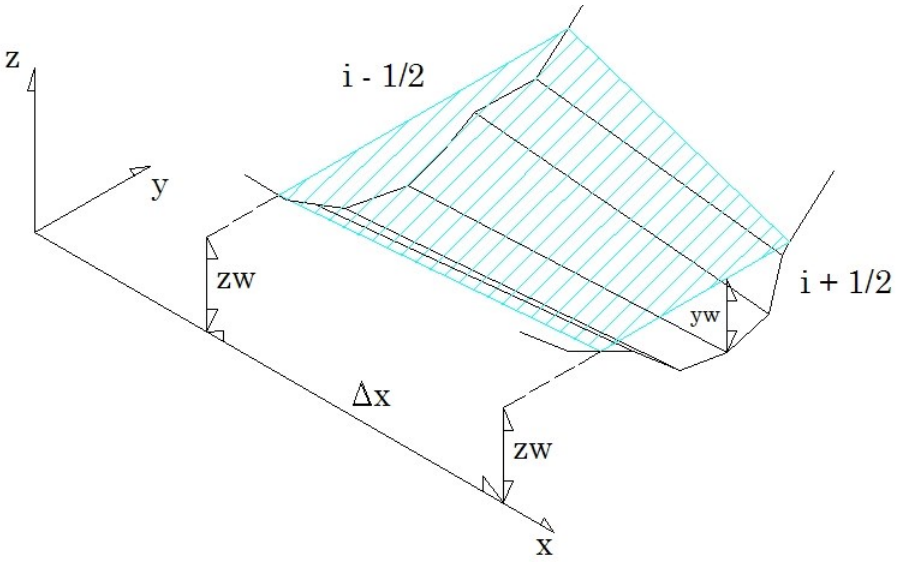

Figure 4. A cell in a finite-volume domain.

To solve the homogeneous part (2.22), numerical fluxes F have to be calculated at the interface between cells. Neglecting source terms for a moment, the scheme can be expressed in the following form

$$\mathrm{U}_i^{n+1} = \mathrm{U}_i^n + \frac{\Delta t}{\Delta x}\left[\mathrm{F}_{i-1/2} - \mathrm{F}_{i+1/2}\right] \qquad (2.24)$$

In the finite volume framework, within a computational cell the values of a state variable (vector U) are approximated by constant average values: the discontinuity in U between two cells originates waves that arise at the cell interface, forming a local Riemann problem. If we assign a local coordinate *x = 0* at the interface between cells *i* and *i+1*, he Riemann problem is an initial value problem of the form

$$\begin{cases} \mathrm{PDE}: \mathrm{U}_t + \mathrm{F}(\mathrm{U})_x = 0 \\ \mathrm{IC}: U(x,t^{(n)}) = \begin{cases} U_i^n \ \mathrm{per}\, x < 0 \\ U_{i+1}^n \ \mathrm{per}\, x > 0 \end{cases} \end{cases} \qquad (2.25)$$

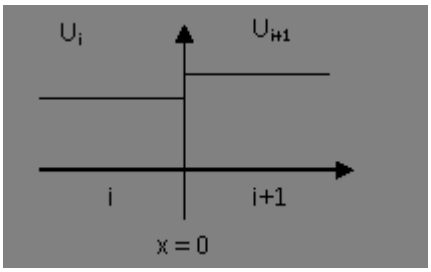

Figure 5. Local Riemann problem.

The Riemann problem can either be solved exactly or through approximate solvers: amongst the various available in the literature, we followed an approach similar to Goutière et al. (2008), where the principles of both HLL (Harten et al, 1983) and HLLC (Toro et al., 1994) solvers are used. To calculate fluxes, an estimate of the speed of the waves arising from the discontinuity is sought and a system of jump relations across each wave leads to the values of the fluxes F. In the HLL solver, only two waves are considered, and consequently only one intermediate unknown state for U; HLLC accounts for an additional wave, increasing to two the number of intermediate states.

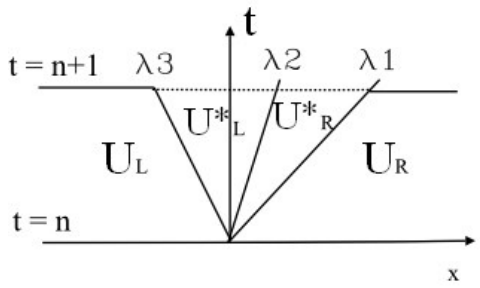

Figure 6. Sketch of a 3-waves Riemann problem in the space-time domain in a local reference system (cell boundary at x = 0).

Armanini (1999) found wave celerities expressions directly related to the Froude number for unsteady, mobile bed flow in rectangular unit-width channels. Following the same approach, Goutière et al. (2008) performed an eigenvalue analysis of the pseudo-Jacobian matrix of the system to obtain approximate eigenvalues $\lambda_{1,2,3}$ easy to implement in a Godunov-type scheme (Equation 2.26).

$$\frac{\lambda_1}{U} \cong \left(1 + \frac{1}{Fr}\right)$$
$$\frac{\lambda_{2,3}}{U} \cong \frac{1}{2}\left[\left(1 - \frac{1}{Fr}\right) \pm \sqrt{\left(1 - \frac{1}{Fr}\right)^2 - \frac{4}{(Fr^2+Fr)}\chi}\right] \qquad (2.26)$$

U is mean water velocity, Fr is the Froude number and χ is a non-dimensional factor related to sediment discharge

$$\chi = \frac{1}{(1-p)U}\frac{\partial q_s}{\partial h} \qquad (2.27)$$

where q_s is the sediment discharge, p is the bed porosity and h is the water depth.

In this work, Equation 10 is adapted to the governing equations (1)-(3) replacing the water depth with the wetted area A

$$\chi = \frac{1}{(1-p)U}\frac{\partial Q_s}{\partial A} \qquad (2.28)$$

The analytical expression of the derivative of Q_s respect to A is needed in Equation 2.28: it is convenient to choose a sediment transport formula in which this differentiation is not cumbersome. For Engelund-Hansen sediment transport formula (see following section) the derivative is easy to obtain, so facilitating the application of this particular scheme.

With the wave speeds estimation provided by (2.26), fluxes at cell boundaries can be computed. For liquid mass and momentum balance (Equations 2.1 and 2.2), following the HLL principle, only the extreme values are considered (λ_1 and λ_3): the first two components of the fluxes for the intermediate region (usually called F*) are

$$F^*(1) = \frac{\lambda_1 F_L(1) - \lambda_3 F_R(1) + \lambda_1\lambda_3(A_R - A_L)}{\lambda_1 - \lambda_3} \qquad (2.29)$$

$$F^*(2) = \frac{\lambda_1 F_L(2) - \lambda_3 F_R(2) + \lambda_1\lambda_3(Q_R - Q_L)}{\lambda_1 - \lambda_3} \qquad (2.30)$$

Subscripts L and R indicate cells on the left and on the right of the boundary, respectively. On the other hand, the computation of the third component of the fluxes vector, related to sediment continuity, accounts for the intermediate wave (λ_2). In the hypothesis that no change in A_b occurs across the fastest wave λ_1, which is not influenced by sediment movement, F*(3) reads

$$F^*(3) = \frac{\lambda_2 F_L(3) - \lambda_3 F_R(3) + \lambda_2\lambda_3(A_{b_R} - A_{b_L})}{\lambda_2 - \lambda_3} \qquad (2.31)$$

2.4 A preliminary test for the finite volume scheme

The evolution of an abrupt transition from a mild slope reach to an oversteepened reach downstream, for a steady discharge over mobile bed, has been modeled. The flow regime changes from subcritical to supercritical at the knickpoint, which is associated with a high sediment transport rate and erosion potential. This is a typical situation related to natural stream evolution phenomena.

The knickpoint progressively migrates upstream until the difference in slope between the two reaches tends to vanish. The cross section of the channel is rectangular, 0.5 m wide. The channel is 7.4 m long. The bed elevation at the upstream and downstream sections is fixed; the sediment diameter is set to 0.0016 m with density ρ_s = 2650 kg/m^3 and bed porosity is 0.4.

The knickpoint is initially located at 6.3 m from upstream cross section. Discharge is 0.0098 m^3/s and no sediment feeding is provided. Downstream water level is kept at 0.14 m. Engelund-Hansen formula has been used:

$$Q_s = 0.05\rho_s g B U^2 \sqrt{\frac{d_s}{g(s-1)}}\left(\frac{\tau_0}{\rho g(s-1)}\right)^{3/2} \qquad (2.32)$$

In Equation (2.32), Q_s is the sediment discharge in volume, B is the channel width, ρ and ρ_s are the densities of water and sediments, respectively; s is the relative density ρ_s/ρ; d_s is the sediment representative diameter; U is the water average velocity; τ_0 is the bed shear stress.

The smoothing of the knickpoint is modeled correctly, as can be seen from free surface and bed profiles in Figure 7.

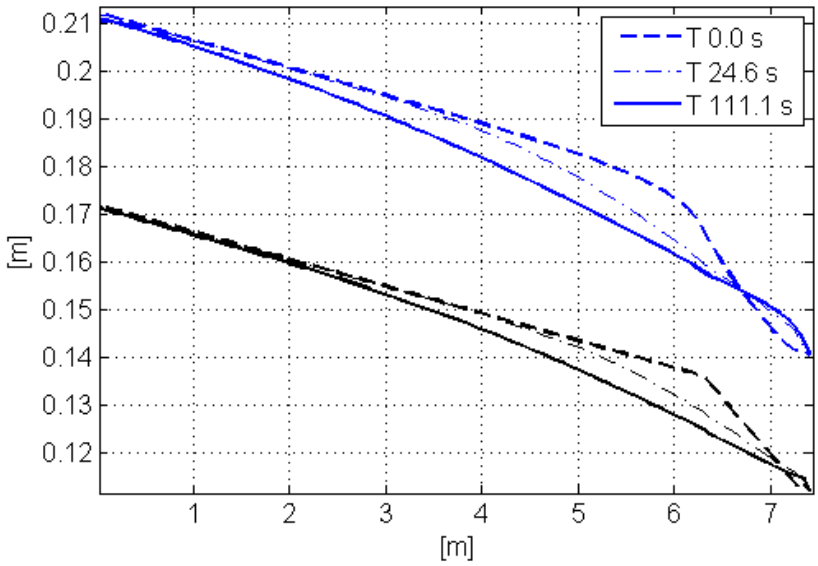

Figure 7. Free surface profiles and bed profiles variation for a knickpoint migration test.

Chapter 3

Control of river bed degradation downstream a run-of-the-river hydropower plant

This chapter reports about an attempt to integrate the understanding of the river geomorphological dynamic into planning of optimal operation rules for a barrage serving a run-of-river hydropower plant (Bernardi et al., 2013; Dinh, 2014; Bizzi et al., 2015). Physically based one-dimensional hydrodynamic and sediment transport modeling, surrogate modeling techniques and Multi-Objective (MO) optimization are combined together in this framework, in a multidisciplinary approach.

The case study is a run-of-the-river power plant on the River Po (Italy) located in the Municipality of Monticelli d'Ongina (Piacenza), Isola Serafini. The objective is to assess if a better management policy of the barrage serving Isola Serafini exists, able to mitigate the river bed lowering processes occurring downstream the barrage without affecting significantly the hydropower production.

A vast amount of literature has studied the effects of dams and barrages on river systems in terms of both geomorphological and ecological responses (Poff and Hart, 2002, Gurnell, 2005, Gupta et al., 2012.) Dams affect the hydrological regime downstream primarily through changes in timing, magnitude and frequency of high and low flows. Sediment connectivity is altered too, since a large amount of sediment load delivered by the headwaters upstream is trapped.

In response to the altered water and sediment fluxes, the river aims to a new equilibrium by a complex range of geomorphological adjustments which can undertake several steps and last many decades before reaching a more stable condition. Alterations include changes in cross-section (aspect ratio), bed material (e. g. coarsening), slope, pattern and bedforms. By trapping sediment

upstream, reservoirs can often cause the river transport capacity to exceed the available sediment supply, creating a sediment deficit downstream (Grant, 2003), which in turn triggers river erosion both on the river bed and the banks. Such adaptation processes can extend over hundreds of kilometers and last for decades.

Few frameworks have been developed to provide flexible decision making tools to assess the effects of building a dam in a specific catchment location (Grant 2003, Burke 2009). Nevertheless, when planning operating rules, only the fulfillment of the main purpose for which the structure is built is considered, very often hydropower production or water supply.

Multi-objective (MO) approaches can take into account a variety of water related interests affected by the dam construction, from flood mitigation to water supply and environmental quality and have been adopted to provide decision makers and stakeholders with valuable tools to measure the consequences of alternative operating rules from a variety of perspectives (Castelletti 2007, Yin 2009). These experiences have marked a significant progress in our ability to plan sustainable management of water resources and have provided more comprehensive insights of how dams affect the fluvial system and the related ecosystem services; however, the integration of fluvial geomorphological processes understanding when planning optimal operating rules remains very rare.

Studies that have optimized dam regulations in order to minimize their impact on channel morphological adjustments downstream are almost absent: we could find only one example in literature (Nicklow and Mays 2000, Nicklow and Ozkurt 2003). In this attempt, the authors built a single objective framework, i.e. the model is able to consider only the effect of operating rules on downstream river bed incision neglecting conflicts with other water related interests, like hydropower revenue or water supply as commonly addressed in a MO approach.

We then analyze the effects, in terms of hydropower revenue and river bed incision rate, of alternative operating rules over a time horizon of 10 years. To evaluate the effects of the different policies, a physically based one-dimensional numerical model has been used. A MO problem

providing optimal solution, in a Pareto sense, for the two conflicting management objectives is then solved, by adopting a Response Surface approach. The following sections provide information on the modeling structure and present the results obtained.

The proposed case study aims to provide river managers with tools to critically compare the effects of alternative operational policies at the barrage in terms of river geomorphic processes. The findings allow analyzing the trade-off between hydropower production and river bed incision, and open the way to plan sustainable and cost-effective measures in the long term.

The work reported in this chapter has been carried out together with the group of Professor Rodolfo Soncini-Sessa at Politecnico di Milano University; Simone Bizzi, Quang Dinh and Simona Denaro.

3.1 Introduction to the case study: the Po river and Isola Serafini

The Po is the longest river in Italy and runs for 652 km across the northern regions from the Alps to the Adriatic Sea, with a catchment area of approximately 70,000 km^2. We have focused on a 112 km long stretch in the river middle course (Figure 8) from Piacenza to Boretto, which includes the run-of-river plant of Isola Serafini.

Isola Serafini power station (Figure 9), managed by the Italian energy agency ENEL, is served by a 350 m wide barrage, located 16 km downstream Piacenza; it has a total capacity of 80 MW nowadays and has been operating since 1962. The incoming discharge is partially diverted to the hydropower plant channel on the right, which originated as a meander cut-off during the huge 1951 flood and joins again the Po river about 12 km downstream the gate, after a large meander.

Figure 8. Location of the reach of interest.

The barrage has eleven sluice gates of equal width: In two of them, for sediment-scouring purposes, the bottom is lowered by 1.5 m. Six gates can be overtopped and work as sharp-crested weirs.

There is no room for water storage behind the barrage, except for the short transitories during manoeuvres; thereafter, pondage is not a management option.

River Po environmental services are widely exploited. For instance River Po is the longest waterway in Italy and is the main irrigation supply to Po Valley, the richest and most productive agricultural area in Italy. Its high quality sands are suitable for constructions and were significantly exploited in the past decades.

Due to intense sediment mining as the main cause, the middle course of Po underwent a strong river bed degradation process in the years from 1950 to 2000 (Figure 10).

Sand mining was very intense from 1950 until 1980; after that, stricter regulations have first reduced and then stopped the activity. Surian (2003) state that instream mining increased from about 3 million m^3/year to about 12 million m^3/year in the period 1960-1980, and then it decreased back to about 4 million m^3/year. The peak volume (12 million m^3/year) is estimated to be not far from the assessed average annual sediment yield of the basin. Licensed amount in 1980 for instream mining was around 6 million m^3/year (Italian Ministry of Agriculture, 1990):

estimating a double amount is then realistic, controls from public authorities were insufficient at the time.

Figure 9. Aerial view of Isola Serafini run-of-river hydropower plant (flow upwards). The barrage diverts part of the flow to the power station on the right.

Along with sediment mining, also low water training for navigation purposes and the presence of dams in the upper part of the Po basin affect the overall sediment balance along the middle course. Besides, the presence of the IS hydropower plant plays an important role since its building in 1960. IS barrage is trapping sediment upstream, causing an abrupt decrease in sediment supply downstream and affects the hydrological regime reducing the transport capacity of the river in the meander downstream.

As a consequence of river bed lowering, several navigation and irrigation structures became unusable during low flow periods - e.g. harbor locks in Cremona, - forcing expensive interventions to rebuild them or restore their functionality. The estimated costs of the new dock in Cremona are over 40 million € (Bonomo, 2011).

For all these reasons, Isola Serafini run-of-river power station is a suitable case study where to assess the existence of an optimal operating rule balancing the conflicting needs of maximizing hydropower revenue and minimizing river bed incision rate downstream of the plant.

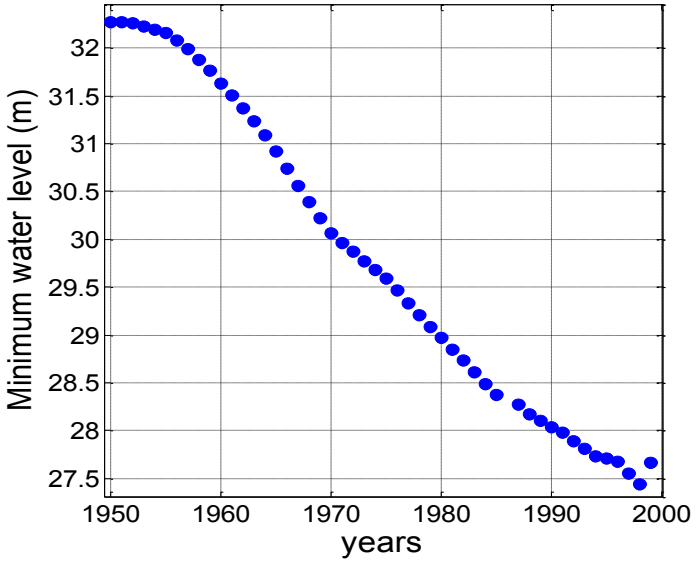

Figure 10. Minimum water levels recorded at Cremona gauging station.

3.2 Modeling the system: the power station operating rule

The current operating rule of Isola Serafini barrage is reported in Figure 12 (bold red line) and aims at maximizing hydropower production. For this purpose, the water level upstream the dam is constantly kept at 41.00 m a.s.l., with a maximum tolerance of 0.50 m. The power production is always maximized except during floods, when the power station is stopped for safety reasons. As previously recalled, no water pondage is allowed so continuity at the bifurcation is satisfied at any time.

Variable a is the inflow from upstream and u is the amount of water diverted to the hydropower plant, the decision variable; consequently $w = a-u$ is the discharge downstream of IS (Figure 11). A MEF (minimum environmental flow) of 100 m^3/s is required through the meander at any time and the minimum flow to activate a turbine of the power station is 200 m^3/s; so, for incoming

discharges a not greater than 300 m³/s, the power station is not working and the diverted flow u is null.

When a is greater than 300 m³/s, all flow exceeding MEF is diverted to the turbines, until the maximum permitted of 1000 m³/s, so as to maximize electricity production. For a = 1100 m³/s or greater, then, the power station keeps working at his maximum capacity; all incoming flow exceeding this value passes throughout the gate and flows into the meander.

The station can work until the total incoming discharge reaches approximately 4000 m³/s; above this threshold, the head jump across the gate becomes too low for electricity generation so all the turbines are switched off (u = 0). In addition, to avoid flooding risk, all gates must be completely open to let the flood pass through.

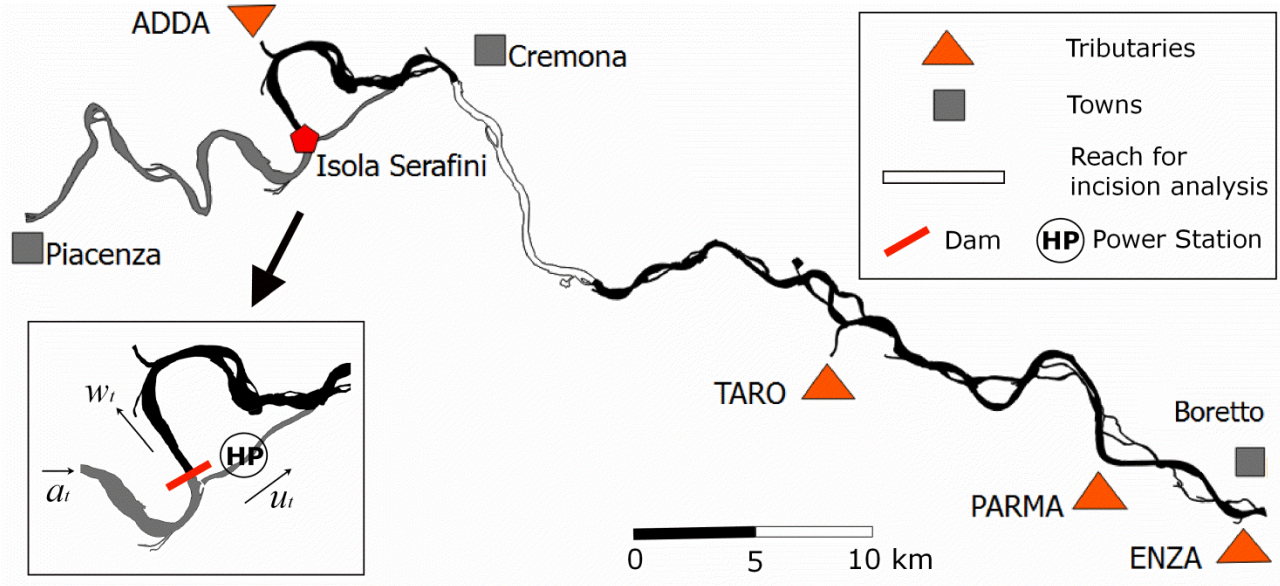

Figure 11. Scheme of the case study.

In order to build alternative regulation policies, we parameterized the current operation rule. The physical constraints for the variables are given by the MEF in the meander, the minimum and maximum flow through the turbines and the safety limit against flood risk. In addition, to enclose

the alternatives in an effective domain, a critical value of the discharge Q_{crit} must be defined, i.e. a value of discharge below which sediment transport can be considered negligible. Recent modeling studies in Po river (Rosatti, 2008) stated Q_{crit} equals 800 m³/s. This threshold has been decreased to 700 m³/s.

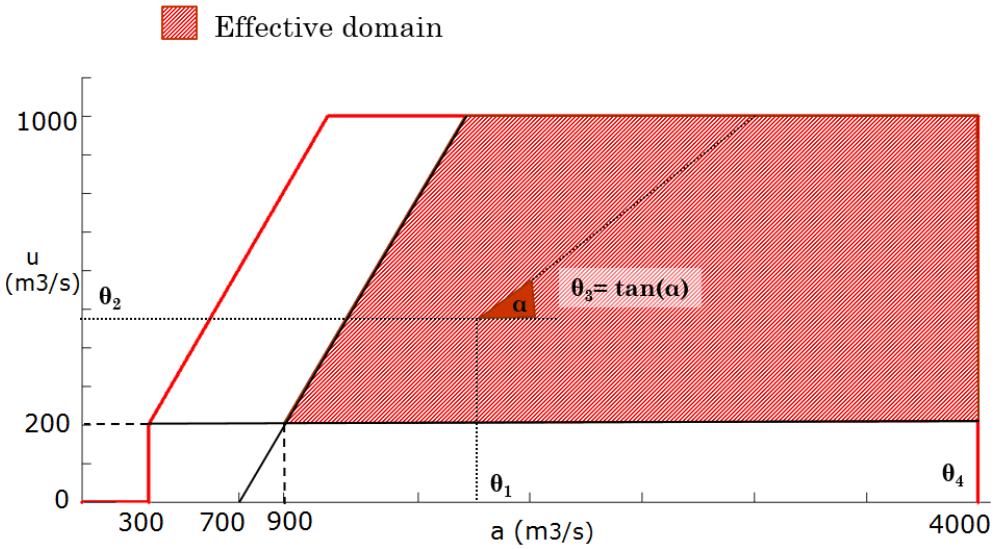

Figure 12. Current Isola Serafini operating rule and domain of alternatives.

Alternative policies should be planned to reach two main purposes: the increase of the sediment supply to the downstream reach and the increase of the transport capacity in the meander to mobilize settled sediment. Moreover, they should conflict as less as possible with the hydroelectricity production.

The operation rule can be defined by a class of piecewise-linear functions (such as the BAU operating rule or a new one e.g. bold black line in Figure 13), specified by a vector containing a set of 4 elements, θ_1, θ_2, θ_3 and θ_4. The fourth parameter, θ_4, is the discharge threshold at which the gates are completely open. This parameter affects primarily sediment supply to the downstream reach and secondly also the transport capacity in the meander; θ_1, θ_2, and θ_3 affect mainly transport capacity in the meander by reducing the discharge u through the turbines (so increasing the discharge through the barrage) when the power station is on. In detail, θ_1 and θ_2 are the

coordinates of a point in the effective domain and θ_3 is the slope of the line connecting (θ_1,θ_2) with the boundary of the domain (see Figure 13)

The class of functions is defined as follows:

$$\begin{cases} u = 0 & \text{if } 0 \le a \le 200 + MEF \\ u = \min(a - MEF, 1000) & \text{if } 200 + MEF < a \le \theta_1 \\ u = \min(\theta_2 + \theta_3 \cdot (a - \theta_1), 1000) & \text{if } \theta_1 < a < \theta_4 \\ u = 0 & \text{if } a > \theta_4 \end{cases} \quad (3.1)$$

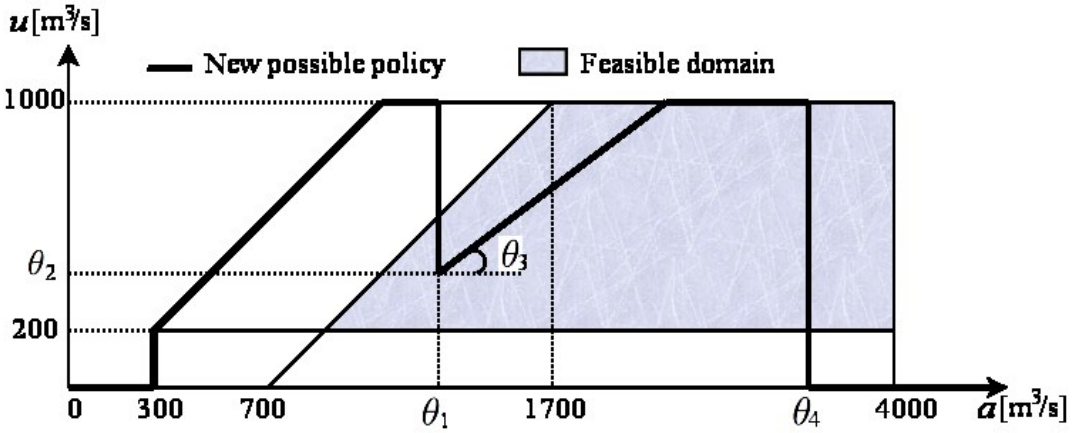

Figure 13. Domain of alternatives with a new possible policy diagram

Taking care of all constraints, the feasible effective domain is specified by the following conditions:

$$\begin{cases} 2000 \le \theta_4 \le 4000 \\ 900 \le \theta_1 \le \theta_4 \\ 200 \le \theta_2 \le \min(\theta_1 - 700, 1000) \\ 0 \le \theta_3 \le 1 \end{cases} \quad (3.2)$$

The business as usual operating rule (Figure 12), for instance, can be obtained by setting $\theta_1 \ge 300$; $\theta_2 = 1000$; $\theta_3 = 0$; $\theta_4 = 4000$.

3.3 Modeling the physical system: hydrodynamics and sediment transport

Before describing the model building steps, it is worth recalling that the results of hydro-morphological modeling are more significant in terms of comparison between different operating rules rather than looking at absolute values. The inherent uncertainty in modelling morphological processes also suggests this precaution.

To represent correctly the river bed evolution processes at the reach scale over a 10-years horizon, and to avoid overburdening computational times, given the high number of simulations to run, the choice fell on a one-dimensional hydro-morphological model able to represent 1D flows with mobile bed in natural channels of complex geometry. We elaborated the model presented by Schippa and Pavan (2009) and adapted it to the specific requirements of the case study.

The main features of the mathematical model can be found in Chapter 2. The model is based on a set of three differential equations (equations (2.1)-(2.3) in Section 2.1) stating mass and momentum conservation for the liquid phase (shallow water equations) and mass conservation of the solid phase (Exner equation) along the main stream direction. We recall them here:

$$\frac{\partial A}{\partial t} + \frac{\partial Q}{\partial x} = q \tag{3.3}$$

$$\frac{\partial Q}{\partial t} + \frac{\partial}{\partial x}\left(\frac{Q^2}{A} + gI_1\right) = g\frac{\partial I_1}{\partial x}\Big|_{zw=const} - gAS_f \tag{3.4}$$

$$(1-p)\frac{\partial A_b}{\partial t} + \frac{\partial Q_s}{\partial x} = q_s \tag{3.5}$$

The finite difference explicit scheme developed by McCormack (1969, see section 2.2) has been chosen to integrate the system of governing equations.

As stated in Chapter 2, two closure equations are needed to solve the system, for friction slope S_f and sediment discharge Q_s.

For slope friction, the common Manning formula has been used:

$$Sf = \frac{n^2 Q^2}{A^2 R^{4/3}} \qquad (3.6)$$

Where n is the Manning resistance coefficient, A is the cross-section wetted area, Q is liquid discharge, R is hydraulic radius.

For sediment discharge, the Engelund-Hansen (Equation 3.7, Engelund and Hansen, 1964) formula has been chosen. Previous studies on the Po river (Italian Ministry of Agriculture, 1990) have shown that this formula, compared to others, is the most suitable to correctly represent sediment movement in the Po river. Since then, no more complete field campaigns about sediment transport all along the Po have been performed.

Moreover, Engelund – Hansen formula has several advantages: it is simple to implement, and it is a total transport formula. Being the grain size in the studied stretch (around 0.5 mm) well inside the applicability limits, we assessed that Engelund-Hansen formula could be a fairly accurate starting point. Of course, implementing a different formula for sediment transport in the model is straightforward.

$$q_s = 0.05 \cdot \rho_s g U^2 \sqrt{\frac{d_s}{g(s-1)}} \cdot \left(\frac{\tau_0}{\rho g (s-1)} \right)^{3/2} \qquad (3.7)$$

In (3.7), q_s is the solid discharge per unit width; ρ and ρ_s are the densities of water and sediments, respectively; s is the relative density ρ_s/ρ; d_s is the sediments representative diameter; U is the water average velocity; τ_0 is the bed shear stress.

Engelund-Hansen formula is used also to calculate sediment contribution from the tributaries. Cross section features of the tributaries at the mouth and data about the slope and sediment diameters are reported in *Po Acquagricolturambiente* (Italian Ministry of Agriculture, 1990).

In subcritical flow regime, upstream boundary conditions for liquid and solid discharge and a downstream boundary condition for water level are needed.

The cross sections along Po river are available from the topographical surveys by AIPO (*Interregional Po Agency*), carried on in 2009. There are 67 surveyed cross sections in the reach of interest, one every 1.69 km in average. On every cross section plot, the boundaries of the overbanks and the thalweg are identified: then, to improve spatial accuracy, cross sections are linearly interpolated up to a distance of 450 m, i.e. the number of cross sections along the reach is increased to 250. Flow resistance coefficients were calibrated during previous studies (Schippa et al., 2006)

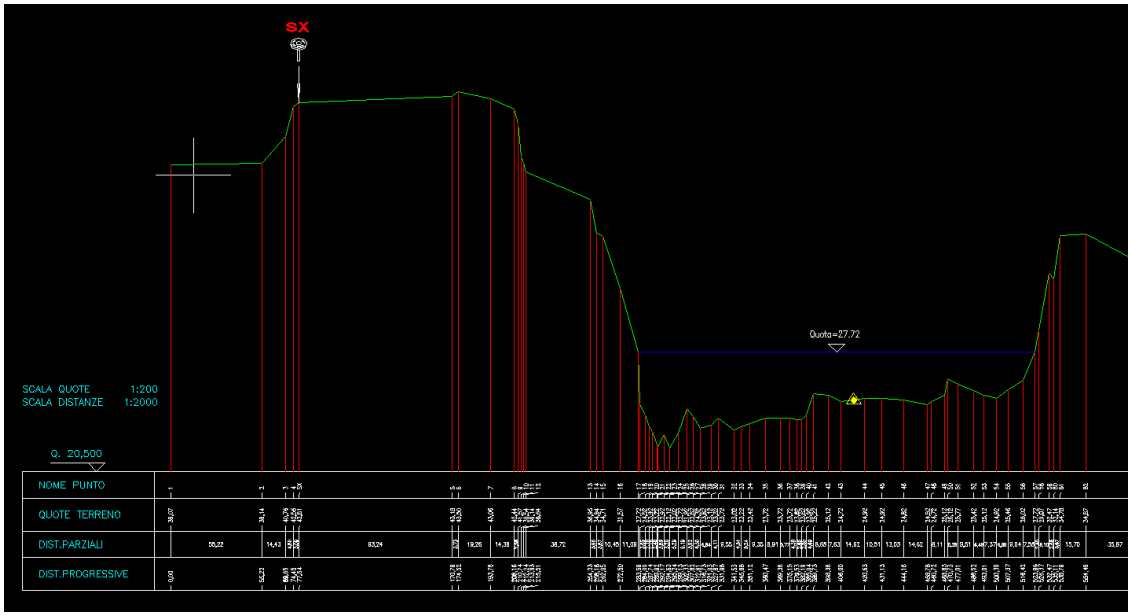

Figure 14. Cross section plot.

The river stretch is split in two sub-stretches, A from Piacenza to IS gate and B from IS to Boretto (Figure 11). The first is 30 km long whereas the length of the second is almost 82 km. All 4 tributaries (Adda, Taro, Parma and Enza) join the river in reach B. The power station channel joins the river between the Adda confluence and Cremona.

In subcritical flow regime, upstream boundary conditions for liquid and solid discharge and a downstream boundary condition for water level are needed.

At upstream boundary (Piacenza station) and along the lower course of the tributaries, a long time series of data is available from ARPA (*Regional Agencies for Environment*) records. We refer to a 10-year long historical time series of water inflows recorded at Piacenza and at the tributaries' mouths from 1964 to 1973. For this period, data are readily available and can be representative also for the future, since no relevant changes in the hydrological regime have occurred at basin scale.

At downstream station (Boretto), the stage-discharge relationship is provided by ARPA hydrological bulletins as well.

A specific subroutine implements the control rule of the barrage, and makes the model switch between two different operating conditions.

Case 1. When the power station is on, (a <= θ_4, see section 3.2), the water level upstream the barrage is kept at 41 m a.s.l. and the two reaches A and B are disconnected. This means that the upstream boundary condition for reach A is the inflow at Piacenza, whereas the downstream boundary condition is the imposed water level.

The operating rule of the barrage provides the upstream boundary conditions for reach B , namely water and sediment discharge entering the meander. Downstream condition for reach B is provided by the stage-discharge relationship.

It is evident that we do not include in the model the numerical solution for the equations in proximity of the barrage: this purpose is clearly beyond the scope of our work, for the complexity of the physical phenomena occurring when the flow approaches the gates. The equations we use for the 1D model are no longer valid in the area close to the gates, clearly dominated by 3D flow patterns.

For these reasons, modeling the sediment transport across the barrage, taking into account all the local physical processes, requires assumptions to introduce a simplification keeping as close as possible to reality. In Case 1, when the power station is operating and the gates are at least partially closed, $Q_{up,B}$ -the sediment discharge entering stretch B, is calculated as

$$Q_{up,B} = Q_{dw,A} \cdot 0.7 \cdot \left(\frac{w}{a} \right)^{1.7} \qquad (3.8)$$

Where $Q_{dw,A}$ is the sediment discharge approaching the barrage, w is the liquid discharge flowing across the gates, a is the total incoming flow (see Figure 11).

The empirical reduction coefficient - 0.7 - is applied to take into account the fact that not all of the eleven gates are open when power station is operating, so part of the sediment is retained. Anyway, it has to be noticed that when power station is on, water velocity and transport capacity close to the barrage are really small: the backwater effect slows down the flow well before getting to the barrage, so the sediment supply to the downstream reach is limited.

Case 2. When the flow rate is above the safety limit against flood risk ($a > \theta_4$, see section 3.2) all the gates are fully open. No flow is diverted to the power plant channel ($u = 0$, see Figure 11) and the two reaches A and B are linked, without an internal boundary condition.

In *Po Acquagricolturambiente* (Italian Ministry of Agriculture, 1990), it is stated that most of the sediments taking part in the bed evolution processes are transported, during high flows, in suspension and only a small part by traction near the bed; so we decided, as a first step, to assume that for the highest flows, with all gates of the barrage open, nearly all sediments pass through the gate. Moreover, the opening of the gate and the subsequent increase in flow velocity in the adjacent zone upstream, if compared to the condition of barrage closed, could bring back in suspension previously settled fine material and convey it downstream. A study by the Po River basin management authority (AdbPo, 2007) shows that material with diameter up to 1 ψ (0.5 mm) can be transported in suspension. For this reason we decided to assume that full continuity is satisfied also for sediment transport.

The cross section of the barrage is unerodible by definition.

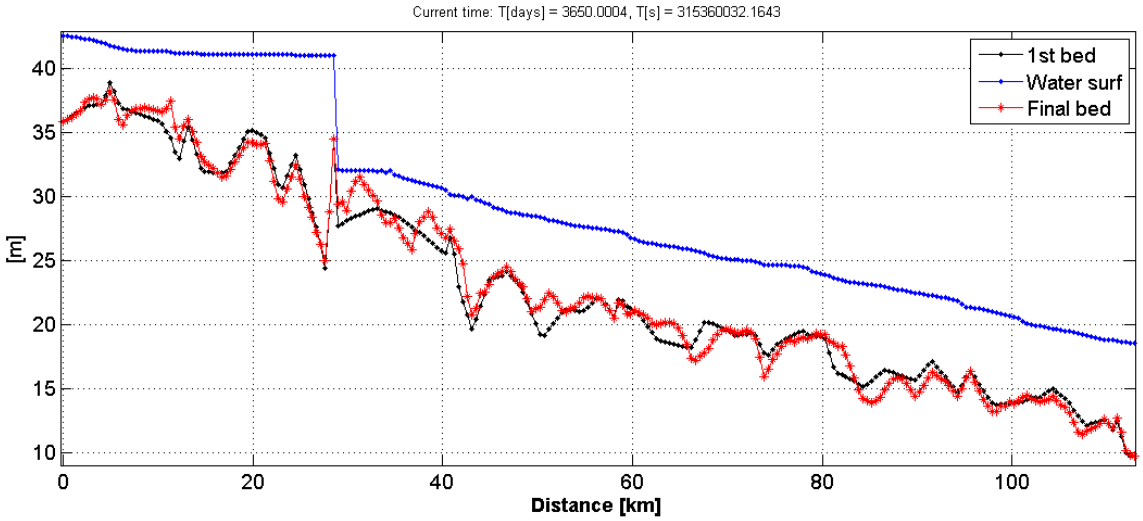

Figure 15. Water and river bed profiles (Case 1)

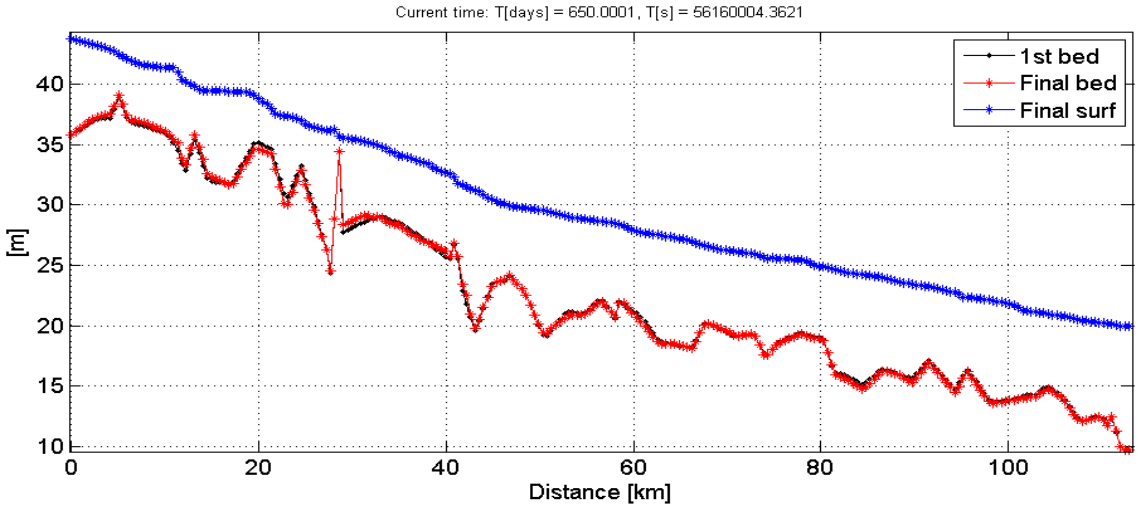

Figure 16. Water and river bed profiles (Case 2)

3.4 Indicators

The two conflicting objectives of hydropower production revenue and reduction of river bed incision are quantified through suitable indicators, in order to implement them in the optimization process.

The physically based model simulation provides a final configuration of the bed (e.g. Figure 15). A low-discharge, steady flow simulation (300 m^3/s) is run over both the initial and final bed configurations. The two water surface profiles are then compared and an indicator of river bed incision is calculated measuring the difference in water levels, zw_{final} - $zw_{initial}$.

To obtain the first indicator J_{inc} for a specific sub-reach, water level variations are averaged over the M cross sections belonging to it.

$$J_{inc} = avg(zw_{final} - zw_{initial})\Big|_{j=1...M} \qquad (3.9)$$

The indicator J_{inc} can be calculated for specific sub-reaches all along the river stretch, to investigate the system behavior.

This indicator is quite reliable: water level for a low-discharge event is able to smooth and compensate local effects, if compared to indicators referring to river bed level alone. It has a drawback though: it cannot be computed during the observation period, but only as a difference between final and initial state because an additional steady flow simulation is needed. This makes it suitable for a feed-forward approach, where outcomes of a selected alternative are checked at the end of the simulation period.

In preparation for a feedback/feedforward framework (see Section 3.7) in which real-time monitoring of river bed incision is planned, another indicator has been chosen. We monitor the evolution of the bed level in 5 pre-specified points within the main channel bed (one is the thalweg, the other four are two on its left and two on its right side) in each one of M cross sections equally distributed along the reach of interest.

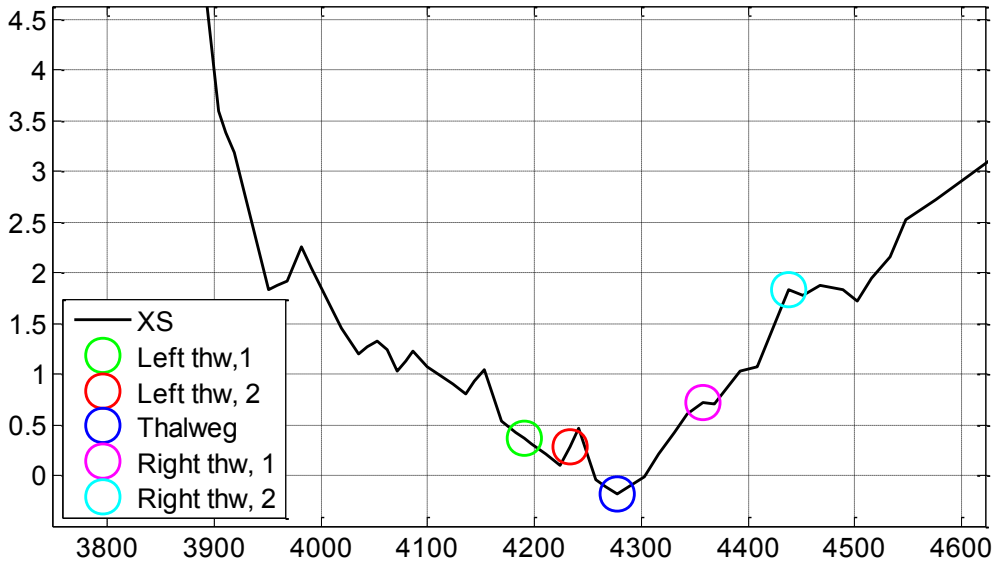

Figure 17. Indicator for river bed incision: 5 points monitoring. Example

Let's denote with $z_{b,ij}(0)$ the bed level in the i-th point (i=1, …, 5) of the j-th cross section (j=1,…,M) the first day of the y-th year of the evaluation horizon. The bed level variation J_y in the reach downstream from Cremona at the beginning of the y-th year is then defined as the average difference of level between time zero (the starting of the evaluation horizon) and that instant all over the sampled points, i.e.

$$J_y = \frac{1}{5M} \sum_{i=1\ldots5} \sum_{j=1\ldots M} (z_{b,ij}(y) - z_{b,ij}(0)) \qquad (3.10)$$

The indicator of total river bed incision can be considered as J_y for y = N, where N is the number of years in the evaluation horizon. It is convenient, however, to refer to an average incision rate per year

$$J_{inc} = \frac{J_N}{N} \qquad (3.11)$$

If *J* is negative – in both versions (3.9) and (3.10) - we may assume that the river bed is undergoing degradation. It is evident that it is not possible to condensate all information related to river morphological evolution in a single indicator without strong simplifications: however, J_{inc} is certainly representative of an overall erosion (or deposition) trend occurring in the analyzed river reach.

As for hydropower , the revenue of hydropower (€) over n days is the sum of the product of the daily energy production P_t (kWh) by a time-varying energy unit price π_t. This revenue can be divided for the number of years N to obtain a yearly revenue (€/year):

$$J_{hp} = \frac{1}{N} \sum_{t=1}^{n} \pi_t \cdot P_t \qquad (3.12)$$

In turn, the daily production P_t is given by the product of water density ρ and gravity acceleration *g* by the flow release *u* through the turbines, the head jump H and the turbine efficiency η (with . H is the difference between the water level upstream the gate and the level just downstream the turbines (h_{up} - h_{down}).

$$P_t = \rho g \eta_t u_t H_t t \qquad (3.13)$$

In turn, the daily production Pt is given by the product of water density ρ and gravity acceleration *g* by the flow release *u* through the turbines, the head jump H and the turbine efficiency η and the time. H is the difference between the water level upstream the gate and the level just downstream the turbines (h_{up} - h_{down}). Since flow profile in the power station channel is not calculated, h_{down} is given by an empirical relationship: $h_{down} = f(u, h_{junc})$. The dependent variables are the discharge *u* flowing into the channel and the water level at the junction between the channel and the Po river (h_{junc}, computed by the model).

3.5 Problem formulation and design of experiments

We already defined (section 3.2, Figure 11): *a* (incoming flow), *u* (flow diverted to the HP station) and *w* (residual flow passing through the gates). The flow *u* is led back into the main channel a few km downstream. The multi-objective design problem, following the formulation of Soncini-Sessa et al., (2007) for water resources problem, can be so formulated:

$$\begin{aligned} & min|_{\theta}\, \mathbf{J}\left(\boldsymbol{x}_{t=0\rightarrow h-1,}\, u_{t=0\rightarrow h-1,}\, a_{1\rightarrow h}\right) \\ & x_t = f\left(\boldsymbol{x}_{t-1}, u_{t-1,}\, a_{\mathrm{t}}\right) \\ & u_t = \mathrm{m}(a_{\mathrm{t}}, \boldsymbol{\theta}) \\ & \mathrm{t} = 0,1, \ldots, \mathrm{h} \end{aligned} \qquad (3.14)$$

a is the incoming flow from time 1 to time h (given). The management objectives pursued (see sect. 3.4, hydropower production revenue and reduction of river bed incision) are expressed by the indicators J_{hp} and J_{inc} that condense the information provided by the hydromorphological model *f*. We seek optimal operating rules *m* (function of the inflow a and the design parameter vector **θ** with the four parameters $\theta_1, \ldots, \theta_4$ listed in sect. 3.2) to maximize both J_{hp} and J_{inc} . The physically based model *f* gives us information on the states *x* (water and river bed levels) at time *t* provided we have information on states at time *t-1* and we chose an operating rule *m* among the feasible rules.

The solution of this problem would require thousands of runs of the physically based model. Surrogate modeling techniques can handle this issue and partially replace the hydromorphological model. Section 3.7 will recall the essential features of the Response Surface Methodology (Castelletti et al., 2010) which was chosen to set up the multi-objective optimization.

However, to start the surrogate modeling, we need to test a certain number of appropriate instances of the operating rules; different values of the design parameter vector $\boldsymbol{\theta}$ are chosen and the corresponding objective values J_{hp} and J_{inc} are determined via simulation of the hydro-morphological model. This introductory step is called Design of Experiments (DOE): the first set of simulation runs allows to better understand the behavior of the system and may lead to interesting results that will facilitate the following optimization procedure.

The number of initial runs is a compromise between the need of properly covering the feasible set of the design parameter vector and the concern of keeping the simulation time within acceptable limits.

In addition to the business as usual (BAU) simulation, we run 49 different alternative operating rules, varying the 4 parameters within their domain. Experiments for different θ_4, from 2000 to 4000 m^3/s were simulated in order to assess the importance to restore sediment connectivity more frequently between stretches A and B. At the same time, alternative options for diversion of the incoming water to the hydropower plant were implemented varying the values of θ_1, θ_2, and θ_3, to assess their effects on transport capacity immediately downstream the gate.

3.6 Design of Experiments: results

Incision was analyzed in two reaches in the meander (named Me1 and Me2) and a longer one close to Cremona: from an economic perspective the latter suffers the most from river bed degradation, due to the presence of the industrial harbors. J_{inc} in this paragraph refers to the form in Equation 3.9. In the following sections we only will use form 3.11.

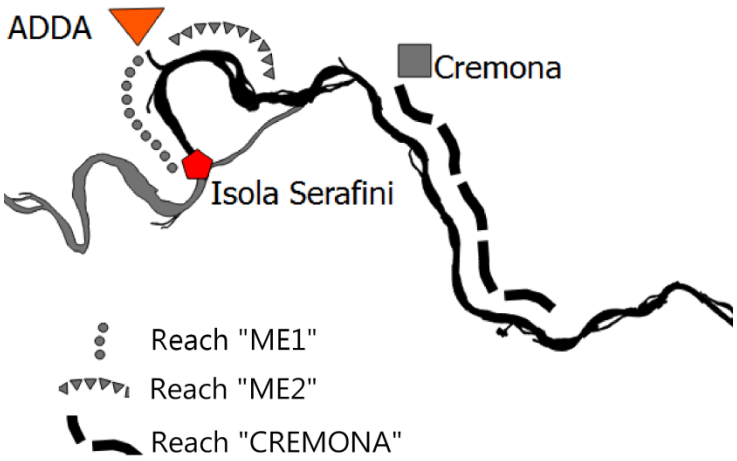

Figure 18. Details of river reaches analyzed for river bed incision.

Results of this first set are summarized in Figure 19 and Table 1.

Figure 19 reports the results of all experiments. The BAU policy leads to an hydropower generation worth 34.28 mil€/year and to a J_{inc} in Cremona of -0.63 m in ten years. The square markers represent the Pareto efficient solutions amongst the simulated ones. The results are quite encouraging and show that it would be possible to reduce remarkably the incision process in Cremona with a moderate loss in hydroelectricity production.

Table 1 reports the Pareto efficient solutions ordered by decreasing incision. River bed incision is decreasing coherently not only in Cremona but also in upstream reaches: results of J_{inc} in the two reaches of the meander (Me1 and Me2, see fig. 1), indeed, show that the effects of alternative regulation policies are stronger closer to the gate.

The first columns of Table 1 report the values of θ parameters for the Pareto efficient solutions. Please notice that setting θ_2 to 1000 means not to change the BAU, except for θ_4.

These results reveal a characteristic system response: θ_4 is the most sensitive driver of river bed evolution. The best performing alternatives (i.e. those with the best J_{hp} / J_{inc} trade off) are the ones implementing the current operating rule, changing only θ_4 : re-establishing hydraulic and sediment connectivity during high flow events, through a decrease in θ_4, appears to be very effective in

tackling river bed incision, whereas significant changes in θ_1, θ_2, θ_3 entail to reduce hydropower production without reducing river incision.

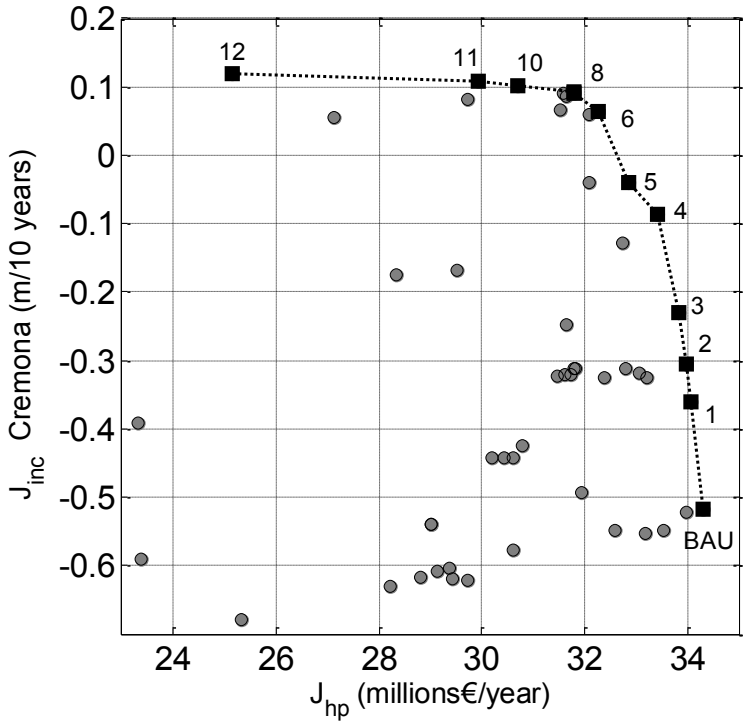

Figure 19. Design of Experiments results: incision in Cremona vs hydropower revenue.

Table 1. Design of Experiments: Pareto-optimal solutions

ID	θ_1	θ_2	θ_3	θ_4	J hp	J_{inc}, 10 years (m)		
					(M€/y)	Me1	Me2	Cremona
BAU	1700	1000	0	4000	34.28	-1.49	-0.83	-0.63
1	1700	1000	0	3200	34.07	-0.97	-0.47	-0.36
2	1700	1000	0	3000	33.97	-0.82	-0.35	-0.30
3	1700	1000	0	2800	33.83	-0.59	-0.16	-0.23
4	1700	1000	0	2450	33.40	-0.04	0.23	-0.09
5	1700	1000	0	2200	32.83	0.19	0.35	-0.04
6	1700	1000	0	2000	32.27	0.49	0.52	0.06
7	1700	900	1	2000	32.25	0.50	0.53	0.06
8	1400	400	0.5	2000	31.79	0.65	0.58	0.09
9	1700	400	0.3	2000	31.78	0.66	0.59	0.09
10	1300	400	1	2000	30.71	0.62	0.53	0.10
11	1200	320	1	2000	29.92	0.62	0.50	0.11
12	900	200	0.5	2000	25.16	0.43	0.32	0.12

3.7 A surrogate modeling algorithm: the Response Surface methodology in the Learning and Planning procedure

In this case study we adopt the Learning and Planning – Response Surface (LP-RS) procedure proposed by Castelletti et al. (2010), to solve the multi-objective design problem (Equations 3.14) using a Global Interactive Response Surface Methodology.

A wide variety of surrogate models have been developed over the past decades and their use is becoming more and more popular within the water resources community.

The Response Surface Methodology (RSM) was first proposed by Box and Wilson (1951) and was widely implemented both for Single-Objective and MO optimization problems in order to overcome computational limitations of environmental systems optimal control problems.

A classical optimization algorithm for solving a design problem as in (3.14) evolves in the space of the design parameter vector $\boldsymbol{\theta}$ (see Section 3.2) and evaluates the corresponding value of the objectives **J,** simulating the physical system behavior. The iterations end when the optimal values (in Pareto sense) of the design parameters are found.

The idea is simple: owing to the physical constraints, we are interested to understand the relationships between the objectives **J** and the design parameter vector $\boldsymbol{\theta}$: the function $\mathbf{J}(\boldsymbol{\theta})$, linking objectives and possible operating rules, is named Response Surface (RS).

If the RS function were fully known, it would be easy to solve problem (3.14) by solving its equivalent form:

$$\min \mathbf{J}(\boldsymbol{\theta}) \qquad (3.15)$$

In our case study, as previously mentioned, a direct determination of the Response Surfaces for the two objectives would require thousands of simulations of the hydro-morphological model for many different $\boldsymbol{\theta}$ (i.e. alternative barrage operating rules), thus making the problem not solvable. Thus it is mandatory to derive an approximation $\tilde{\boldsymbol{J}}(\boldsymbol{\theta})$ of the RS: that can be identified with the LP-RS procedure.

The iterative steps of the LP-RS procedure are displayed in Figure 20. At the first iteration, after the design of experiments (Step 1, see Section 3.6) a first training set, composed of 49 couples **(θ,J)** , is available and is used to identify, via interpolation, a first approximation $\tilde{\boldsymbol{J}}_{\mathbf{1}}(\boldsymbol{\theta})$ of the Response Surface (RS, Step 2). Assuming that the $\tilde{\boldsymbol{J}}_{\mathbf{1}}(\boldsymbol{\theta})$ properly represents the RS, the Design Problem would be fully solved: the Pareto front in the space **J** of the objectives (river bed incision J_{inc}, hydropower revenue J_{hp}, e.g. Figure 19) is the sought solution.

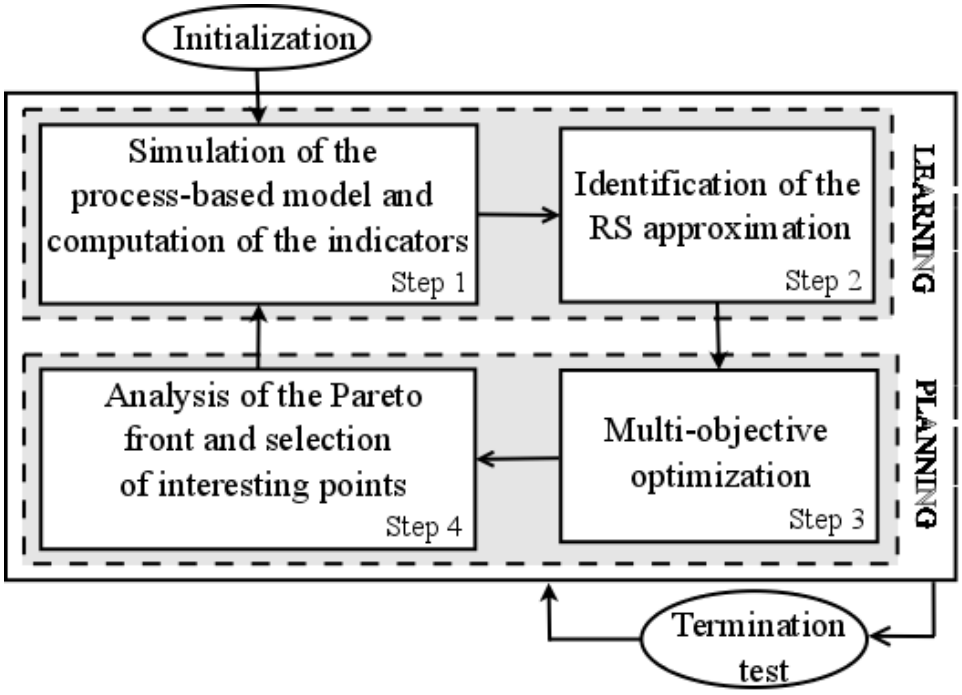

Figure 20: Learning and Planning – Response Surface process (Castelletti et al., 2010).

However, the accuracy of the RS approximation must be checked: a few values of the design parameter vector **θ** (e.g. a few operating rules) are selected on the Pareto front and simulated by the hydromorphological model. These new simulations increase the number of couples **(θ,J)** in the training set (and we are back to Step 1, starting the second iteration of the process). So, a new approximation $\tilde{\boldsymbol{J}}_{\mathbf{2}}(\boldsymbol{\theta})$ of the RS is identified (Step 2) and an updated Pareto front is available.

Starting from the second iteration, a termination test can be performed to end the procedure. Different termination criteria may be used, based either on the RS approximation convergence or on its accuracy. The latter considers the distances ε_j between the values of the j-th objective

obtained via model simulation and those given by the RS approximation at the previous iteration for the same operating rule $\boldsymbol{\theta}$. Let us consider river bed incision: If the global average distance $\boldsymbol{\varepsilon_{inc}}$ obtained averaging the single distances $\varepsilon_{i,inc}$ is below a given tolerance λ_{inc}, the Pareto front based on the RS calculated at the current iteration is considered to be a good approximation of the one that would be generated by the physically based model itself, so the procedure can be terminated. Otherwise, another iteration is performed.

The thresholds λ_j have to be set by the designer: their values are chosen according to the type of problem and the chosen objectives. Once more, the goal is to find the right compromise between the desired accuracy and the available computational power. In our case, the termination test verifies that the average distance $\boldsymbol{\varepsilon_{inc}}$ is only a small part of the range within which each objective falls. Namely, our two thresholds λj are the 6% of the difference between the maximum and minimum value assumed by the j-th objective in the current LP-RS iteration.

This means that we consider correct the values calculated by the RS approximation with a confidence rate of 94%. This is considered satisfactory for our case study, given the inherent uncertainty in modeling river morphological processes at the spatial and temporal scales proposed.

The design of experiments already revealed some characteristic system responses: starting from the results reported in section 3.6, the LP-RS procedure was implemented for two different types of control laws.

3.8 A feedforward control: implementation and results

We first implemented the LP-RS procedure for a pure feedforward control, i. e. an anticipative control law. This means that at each time *t* the inflow *a* entering the reach is measured, and a release decision *u* is determined according to the operating rule *m. m* in turn is defined by the design parameter vector $\boldsymbol{\theta}$ (see sections 3.2 and 3.5). We analyze a time horizon of 10 years and $\boldsymbol{\theta}$ is time invariant.

This feedforward control aims to affect both sediment connectivity between the two reaches A and B and the increase in discharge in the meander to mobilize settled sediments, according to the system behavior described in section 3.2. J_{inc} is evaluated only in Cremona reach for the reasons previously explained (section 3.6).

Following the steps of the LP-RS procedure (Figure 20), we started with the design of experiments (Initialization and Step 1 of the first iteration) whose results have been reported in section 3.6.

The RS in this problem is a function $\mathbf{J}\ (\boldsymbol{\theta})$ linking the four elements of the vector $\boldsymbol{\theta}$ and the two objectives J_{hp} and J_{inc} (an $\mathbf{R_4} \rightarrow \mathbf{R_2}$ function). Finding its approximation (Step 2 of the LP-RS procedure) is a traditional model identification problem, composed of model selection, calibration and model validation, reiterated at every iteration with an updated set of **(θ,J)** couples. Details on the identification of the best RS model can be found in Bizzi et al. (2015) and Dinh (2014). Five different functional classes have been considered and tested: the best interpolators for each objective J are used to build the RS approximation. Once identified the Pareto dominant solutions on the RS approximation, the selection of interesting points on the Pareto front is performed by the choice of an expert and these alternatives are simulated by means of the physically based model; the termination test decides whether a new iteration is started or the process is stopped, meaning that the RS approximation $\widetilde{\boldsymbol{J}}_{\boldsymbol{i}}(\boldsymbol{\theta})$ found at the i-th iteration is adequate compared to the RS that the physically based model itself would produce.

At the first iteration step for this feedforward control, starting from the 49 simulations of the training set (see section 3.6), 26 Pareto-dominant alternatives were found on the RS approximation. 8 of them were chosen for simulation with the hydromorphological model: both their physical meaning (the corresponding operating rules) and their proximity to the Pareto front knee have been considered as factors. The training set increased in size, yielding to a new approximation of the RS (iteration 2, Step 2) with 42 Pareto-dominant alternatives. The first termination test was performed and passed, so right at the 2nd iteration the procedure was stopped.

The quick convergence of the front is mainly due to the large number of simulations in the first training set.

The results are reported in Table 2; the Pareto front plot in the objective space is in Figure 21.

It is important to remind that the incision is reported in meters/year for modelling requirements, but in geomorphological terms it means a generalized river bed lowering – of course averaged over the reach - of more than half a meter in the next ten years, which can vary in function of the frequency and intensity of the occurring floods. However, it is worth recalling that the results of hydro-morphological modeling are more significant in terms of comparison between different operating rules rather than looking at absolute values.

Table 2 Feed-forward control, selected alternatives and objective values after 2nd iteration of LP-RS. (*BAU)

θ_1	θ_2	θ_3	θ_4	$\tilde{J}_{hp}$ (M€/y)	$\tilde{J}_{inc}$ (m/y)	J_{hp}, (M€/y)	J_{inc}, (m/y)	ε_{hp}	ε_{inc}
*1700	1000	0	4000	-	-	34.28	-0.0628	-	-
1700	700	0	2000	32.2519	-0.0034	32.0227	0.0012	0.2292	0.0046
1700	850	0	2350	33.3975	-0.0142	32.9547	-0.0071	0.4428	0.0071
1700	350	0.5	2000	31.7857	-0.003	31.7666	0.0009	0.0191	0.0039
1700	1000	0	2650	33.832	-0.0218	33.6983	-0.0212	0.1337	0.0006
1700	900	0	3600	34.1736	-0.0466	33.9808	-0.0563	0.1928	0.0097
1700	1000	0	2150	32.8346	-0.0084	32.7085	-0.0107	0.1261	0.0023
1700	1000	0	2100	32.4555	-0.0075	32.5951	-0.0109	0.1396	0.0033
1300	400	0.1	2000	30.7095	-0.0024	29.7821	0.0045	0.9274	0.0069

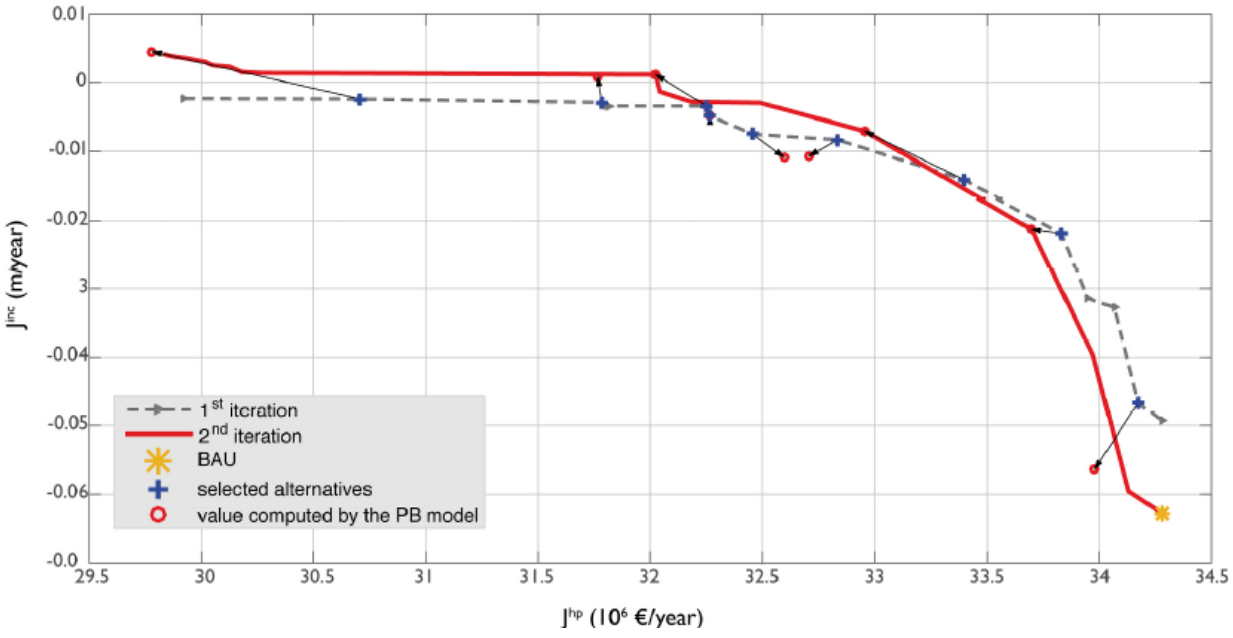

Figure 21. Pareto front with results of feed-forward control. BAU = business as usual.

Both simulated and approximated results confirm what the design of experiments showed: θ_4 is the most sensitive driver of river bed evolution.

A regression analysis has been performed over the simulated data to prove this hypothesis. A stepwise linear regression is built up over the 57 simulation results in order to infer the correlation between the components θ_i of the design parameter vector $\boldsymbol{\theta}$ and the incision rate J_{inc}. Only the correlation between θ_4 and J_{inc} shows statistical significance, which means that altering only the transport capacity in the meander is ineffective in reducing the incision rate downstream the barrage and, at the same time, it conflicts with power plant revenue. On the other hand, re-establishing hydraulic and sediment connectivity during high flow events, through a decrease in θ_4, appears to be very effective in contrasting riverbed incision. Based on these evidences we propose a second framework, where the value of θ_4 is determined by a feedback law.

3.9 A feedback – feedforward control: implementation and results

In this development of the initial control problem, based on the above listed results, the system is controlled by a feed-forward operating rule as in 3.8, but, at the end of each year, on the base of the the river bed level variation i_y observed, a *feedback* operating rule m_b modifies the value of the parameter θ_4 of the feedforward operating rule m. The new θ_4 value is maintained all over the following year. The values of θ_1, θ_2, θ_3 are fixed to the values they have in the current (Business as Usual, BAU) rule.

Thus, the parameters of the previous feedforward rule turn out to be all fixed except θ_4 ; the design parameter vector $\boldsymbol{\theta}$, this time, is composed of the parameters that specify the feedback rule only.

The aim of the control is to keep the yearly rate of river bed level change i_y close to a target value δ (e.g. δ=0), i.e. to maintain a constant yearly rate of incision (or deposition). This means that, at the beginning of each year y of simulation, the controller will determine a new value for the parameter θ_4 based on the difference between the observed i_y and the target δ. In mathematical terms, in the y-th year the value of θ_4 is given by the following expression:

$$\text{m: } \theta_4 = \alpha + \beta\left(i_y - \delta y\right) \qquad (3.16)$$

(3.16) is the feedback rule, and α, β and δ are the elements of the design parameter vector. Once chosen α, β and δ, with the information i_y coming from the model simulation, θ_4 is determined at the beginning of each year, hence for a given inflow scenario *a* the decision variable *u* is determined at every time *t*.

The response surface RS is then a function of α, β and δ.

Chosen δ, the alternatives we are interested in are those for which the feedback control law is effective; that means it produces an average yearly incision rate J_{inc} = δ. These alternatives are associated to the intersecting plane between the incision δ and the surface $\tilde{J}_{inc}(\alpha, \beta, \delta)$ in a 4D space: an exemplification in a 3D space is reported in Figure 22 (of course the dependence from α cannot be shown, for graphical impossibility). Among the alternatives on the intersected plane, only those maximizing the hydropower revenue J_{hp} are Pareto dominant.

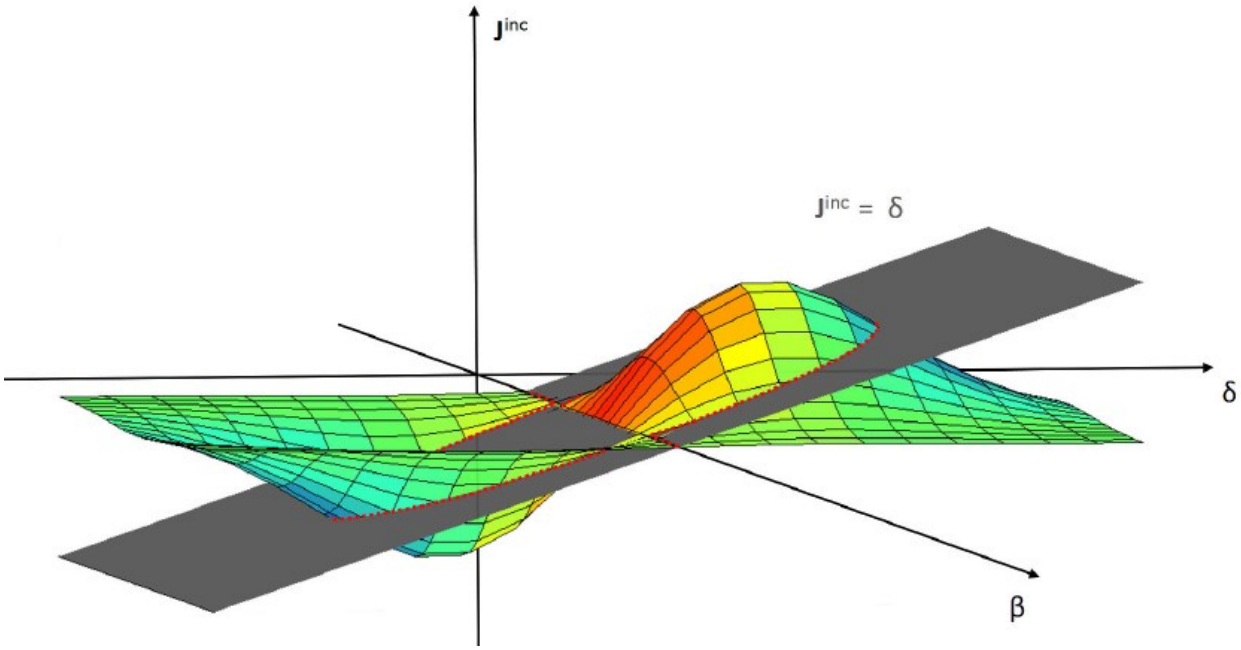

Figure 22. Effective alternatives in the feed-back control procedure are the intersection points between the plane Jinc = δ and the response surface.

The feedback control had to be tested in order to determine the most suitable range for each of the new components α, β and δ. An example of results for a simulation run of the hydromorphological

model, where θ_4 is determined by equation (3.16), is reported in Figure 23: the trajectory of J_{inc} coming out from the model is compared to the target trajectory determined by δ.

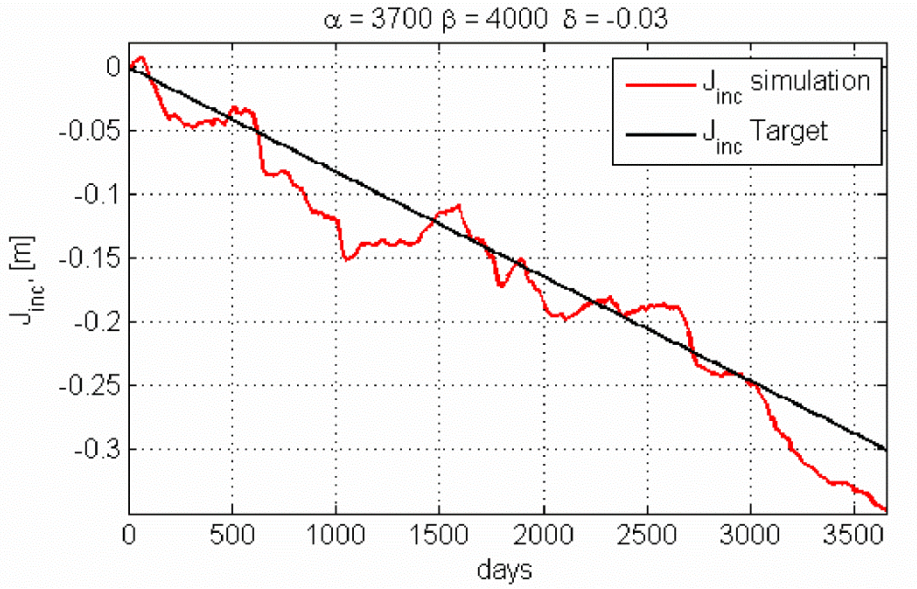

Figure 23. Jinc vs time: simulated and target trajectories

Several tests were performed, with α, ranging from 1200 to 4000, β from 1000 to 7000, and δ from -0.06 to 0.06 m/year. 25 simulation runs were effectively included in the training set to start the LP-RS procedure. Four iterations of the process were necessary to pass the termination test. A total of 58 simulations of the hydro-morphological model were run: 25 for the first iteration, 11 for the second, 10 for the third and 12 for the fourth. As the training set increases in size at each iteration, the RS approximation improves. The results are reported in Table 3; the Pareto front plot in the objective space is in Figure 24 .

Table 3. Feedback control, selected alternatives and objective values after 4th iteration of LP-RS. (*BAU)

α	β	δ	θ_4	$\tilde{J}_{hp}$ (M€/y)	$\tilde{J}_{inc}$ (m/y)	J_{hp}, (M€/y)	J_{inc}, (m/y)	ε_{hp}	ε_{inc}
*-	-	-	4000	-	-	34.28	-0.0628	-	-
1200	2000	0.06	f(t)	31.8052	0.06	31.7043	0.05	0.1008	0.01
2700	4900	-0.01	f(t)	33.5017	-0.01	33.607	-0.02	0.1052	0.0058
1600	4900	0.02	f(t)	32.7972	0.02	32.4471	0.01	0.3501	0.0136
1500	3600	0.03	f(t)	32.6136	0.03	34.138	-0.05	0.063	0.0011
4000	3000	-0.05	f(t)	34.2067	-0.05	34.1116	-0.05	0.0686	0.0034
3600	1900	-0.04	f(t)	34.1139	-0.04	33.7493	-0.03	0.0023	0.0087
2900	2100	-0.02	f(t)	33.7055	-0.02	32.6376	-0.01	0.0437	0.0096
2000	4700	0.01	f(t)	33.0908	0.01	32.3724	0.04	0.4531	0.0163
1200	3700	0.04	f(t)	32.4047	0.04	31.9913	0.04	0.0323	0.0044
1400	2100	0.05	f(t)	32.1352	0.05	31.719	0.06	0.1438	0.0119
1200	1900	0.06	f(t)	31.7471	0.06	33.9543	-0.04	0.028	0.0013
3700	4000	-0.04	f(t)	34.045	-0.03	32.5505	0.03	0.0907	0.0073

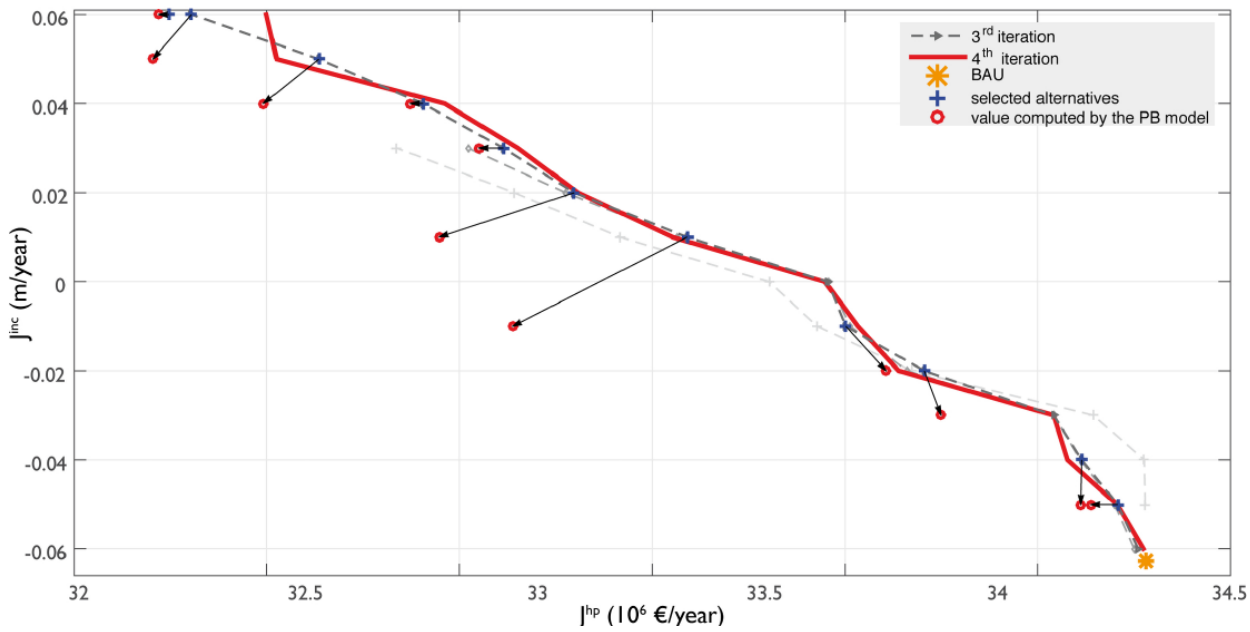

Figure 24. Pareto front with results of feedforward-feedback control at 3rd-4th iteration. BAU = business as usual.

3.10 Comments to results

As observed when commenting results in section 3.8, the Pareto front of Figure 24 shows that a significant reduction of incision process can be achieved with a moderate loss in the hydropower revenue. A comparison between the Pareto fronts obtained with both controls is shown in Figure 25. Such a case study shows how a fairly simple hydro-morphological numerical river model can play a key role, together with a surrogate model in an optimization framework, to provide river managers relevant information for decisions.

Feedback control (Scheme "B") is conceptually more advanced than a simple feedforward control ("Scheme A"), since it provides an *online control* on the river bed level variation rate: it allows designing operating rules that aim to achieve a user-defined incision rate in the reach of interest. Conversely, the performances of feedforward control might depend on the hydrology series considered, whereas the feed-back control of Scheme B leads to performances which, thanks to the online control, are independent from the hydrology inputs considered in the analyses. Pareto front of Scheme B dominates the one obtained with Scheme A.

Keeping in mind that the identification of the Pareto dominant solutions can be affected by significant uncertainty, since the physically based numerical modeling of river channel behavior is inherently affected by limited understanding, some conclusions can be drawn, in particular:

- stopping the incision would cost 2.5 M€ per year due to the consequent reduction in the hydropower revenue (about 7.3 % of the current yearly production) when adopting a simple feedforward control, but only 0.8 M€ per year (about 2.6 % of current yearly production) when adopting a feedback additional control.
- halving the current rate of incision in the reach downstream from Cremona would cost 0.5 M€ per year (about 1.5 % of current yearly production) with Scheme A, and 0.2 M€ with Scheme B (0.6 % of current yearly production).

In reality, adopting a feedback control would mean to implement a yearly cross-section extensive survey programme. This implementation is not straightforward from the technical point of view, nor the investment for such a monitoring is negligible. However, it is important to show how the online control gives a relevant reward in terms of revenue.

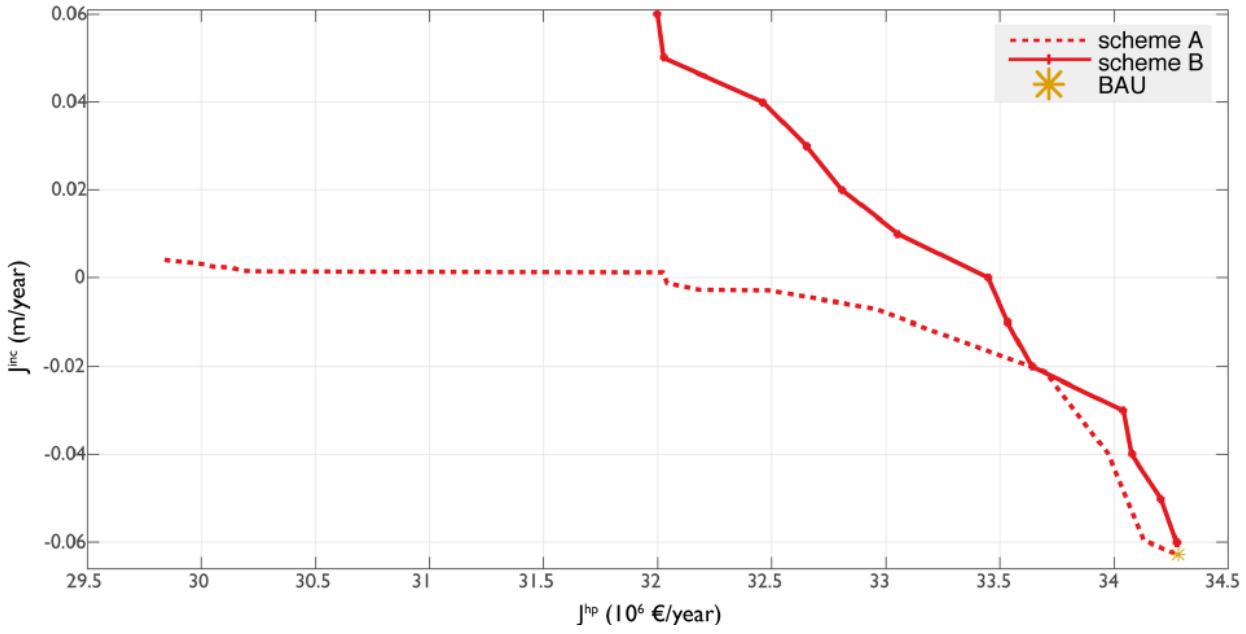

Figure 25. Pareto fronts obtained with feedforward control (scheme A) and feedforward-feedback control (scheme B).

Chapter 4

Hydromorphological modeling of Red River (Vietnam)

In the context of the IMRR (Integrated Management of Thai Binh - Red River basin – *www.imrr.info*) cooperation project, funded by the Italian Ministry of Foreign Affairs, led by Politecnico di Milano University and carried on together with several Vietnamese Ministries and Agencies, the analysis of past morphodynamic river changes and the study of the evolution scenarios of Red River morphology are of prominent importance.

From a multi-objective management perspective, the development of a numerical physically based model for the midterm-long term analysis of reach-scale morphological evolution of a large sandy river in a developing country is certainly challenging but turns out to be a great research opportunity.

This chapter reports about the part of the project related to the morphodynamic analysis and modelling of the lower course of Red River (Bernardi et al., 2014, Bernardi and Schippa, 2014, Schippa and Bernardi, 2014), with a special focus on human activities that deeply impact the river morphological conditions and influence the river system management.

The work reported in this chapter has been carried out together with the leader of IMRR Project, Professor Rodolfo Soncini-Sessa at Politecnico di Milano University and his group: Quang Dinh, Rafael Schmitt and Marco Micotti.

4.1 Introduction

Red River (*Song Hong*) rises in Yunnan province (China) and flows south-east towards VietNam and the Tonkin Gulf (Figure 26). Its total length is 1140 km and the total basin area is 157,000 km^2. Red

River is actually named *Thao* up to the confluence with Da and Lo tributaries, located close to Viet Tri. Right upstream the VietNam capital, HaNoi - a dynamically expanding urban area situated at the banks of the River - a large bifurcation with Duong River partially diverts the flow towards the city of Pha Lai. The lower course ends in a wide delta and is surrounded by many large and populated agricultural districts. After the Mekong Delta, the Red River Delta is Vietnam's second most important rice production area.

Figure 26: Red River (*Song Hong*) basin (source Wikimedia Commons, user: Kmusser).

The management of Red River basin has to take into account a large number of conflicting socio-economic issues. Instream sand mining is deeply affecting river morphology enhancing the bed incision process. The big reservoirs in the upstream catchments (*Thac Ba* on Lo river and *Hoa Binh, Son La* on Da river) constructed to match the increasing hydroelectricity demand, also act as flood control structures, and significantly alter sediment supply downstream and consequently river equilibrium (Kondolf, 1997; Dang *et al.*, 2010). At the gauging stations of Son Tay, HaNoi and Thuong Cat a strong decrease of the minimum water levels has been recorded from 2000 on (Figure 27). The noticeable acceleration in river bed degradation is a danger for agriculture water supply as well as for infrastructure stability. River bed incision dramatically changed the flow distribution pattern at the bifurcation with Duong River.

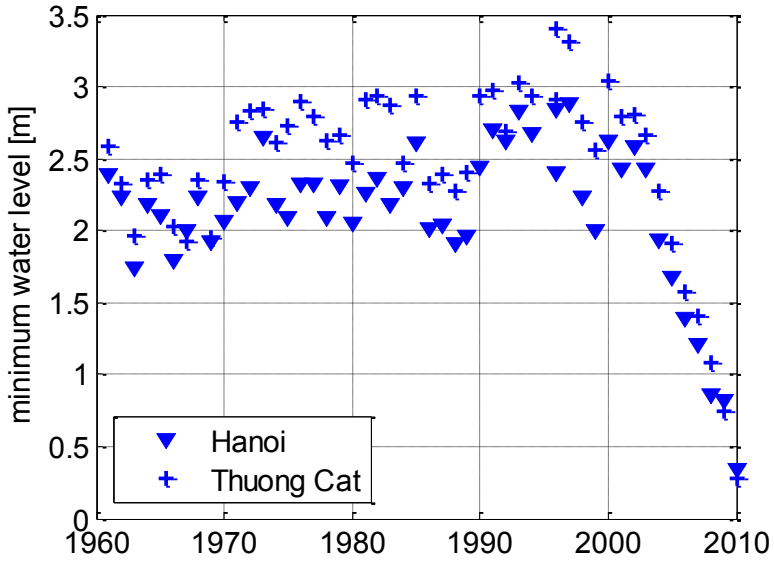

Figure 27 Minimum water levels recorded at Hanoi (Hong) and Thuong Cat (Duong River)

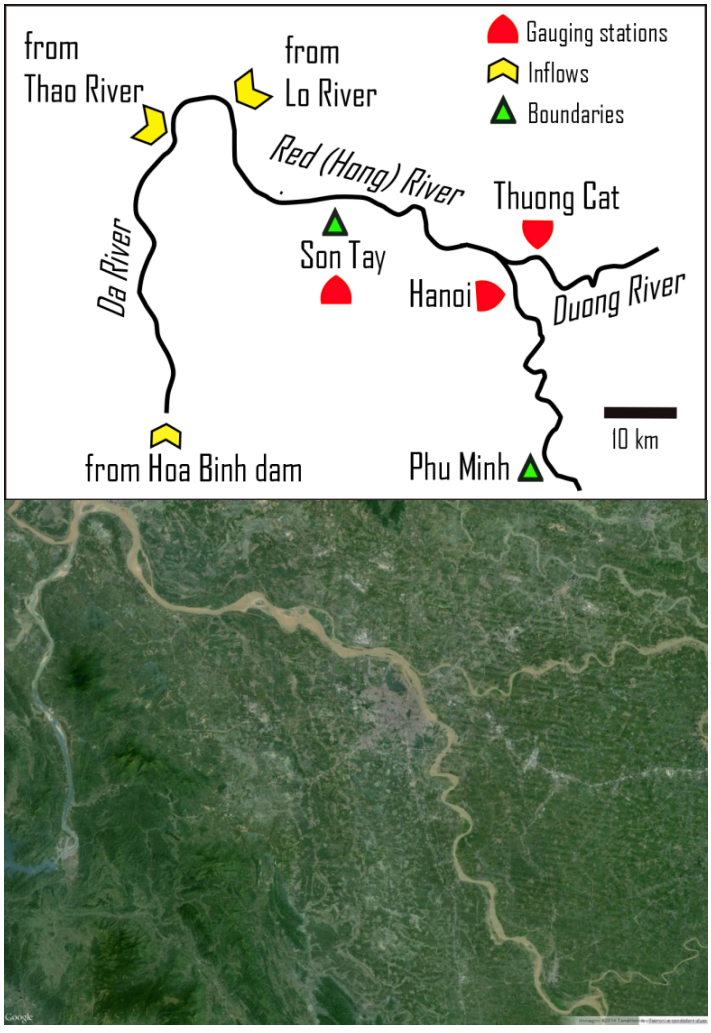

Figure 28. Scheme and satellite image of the studied river reach.

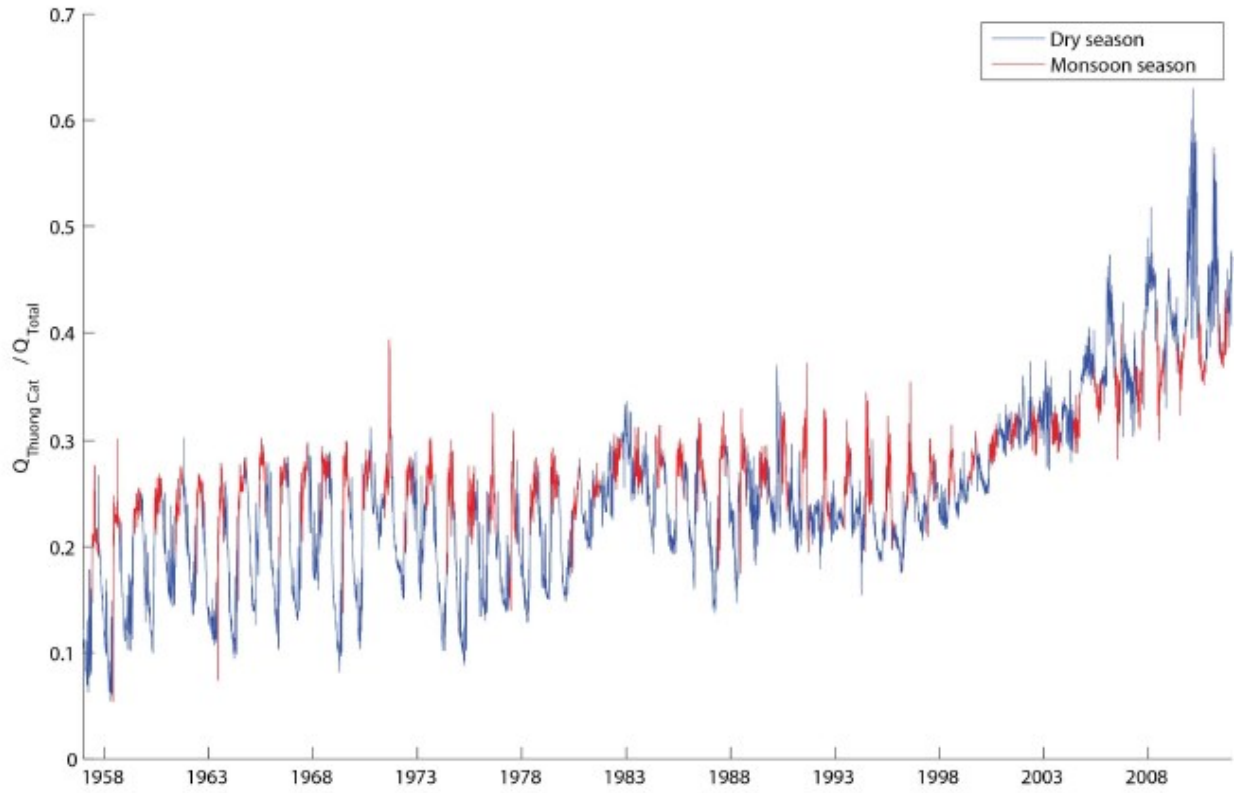

Figure 29. Flow distribution pattern vs time at the bifurcation between Hong and Duong rivers (ratio of flow towards Duong over total incoming flow ,Schmitt, 2014).

4.2 Model building: data collection and pre-processing

Collecting up-to-date information is essential to the model reliability. The main aspects to investigate are

- River geometry (cross section surveys)
- Flow and hydrology (discharge, water level time series)
- Sediment characteristics and sediment transport
- Location and relevance of water supply infrastructures (lateral outflows)

After data collection, a selection has been made to retain only useful information, always taking as a reference the desired accuracy in representing the modeled processes.

River cross sections geometry

Detailed cross section surveys have been performed along the reach of interest in 2000. The reach of interest is 82 km long and 75 cross sections were surveyed along this reach. In the following years, some of the cross sections surveyed were updated: the most important update was carried on in 2009, but still some information is lacking. However, 2000 and 2009 surveys constitute a solid basis of topographical information: the average distance between cross sections is less than 1 km.

Surveys of cross sections are very detailed: we are mainly interested in the morphology evolution of the river active channel. Many detailed information about presence of structures, buildings, little rills and artificial channels in the wide overbanks are not relevant to our study. Surveys had to be analysed and simplified, reducing the number of points per cross section via algorithms and manually, in order to retain only useful points and decrease computational time. In Figure 29, an example of survey detail next to a levee is reported (light blue crosses are surveyed points) together with its model implementation (straight lines approximation). In the active channels, instead, all details are retained.

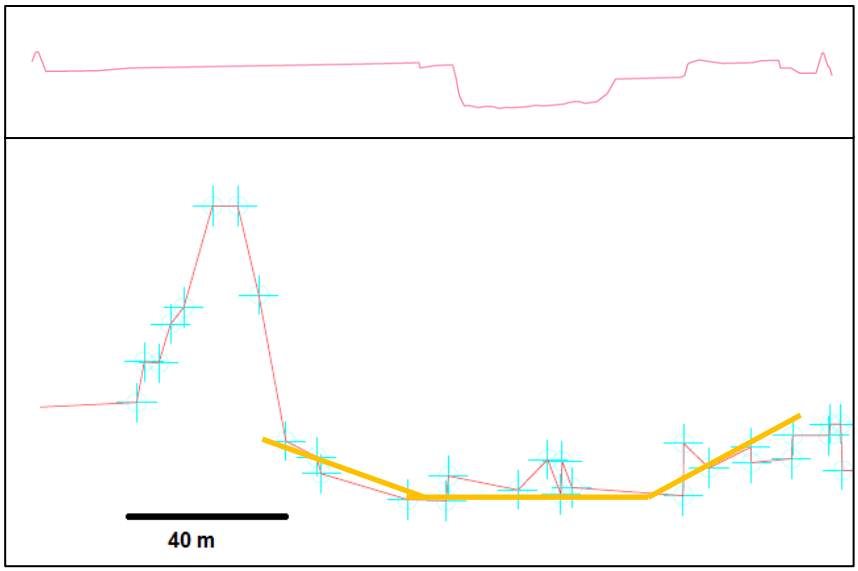

Figure 30: cross section survey detail and simplification.

On every cross section, the boundaries of the overbanks and the thalweg are identified, then to improve spatial accuracy a linear interpolation between surveyed cross section is made up to an interval of 330m (250 cross sections on the entire reach). Interpolated cross sections are the boundaries between computational finite volume cells (see the following sections and Chapter 2 for the numerical model description)

Table 4. Cross sections surveyed along the reach of interest.

ID	River Station (m)	ID	River Station (m)	ID	River Station (m)	ID	River Station (m)	ID	River Station (m)
45	26378.00	*61*	*45473.00*	*76*	*61211.00*	*90*	*72822.00*	*108*	*88804.00*
46	29117.00	62	46173.00	*77*	*61554.00*	91	73605.00	109	89916.00
47	*30546.00*	63	46982.00	78	62431.00	92	74598.00	110	91868.00
49	32149.00	64	48184.00	79	63370.00	94	75791.00	*111*	*92744.00*
50	33214.00	65	49548.00	79	63430.00	95	77567.00	*112*	*94358.00*
51	*34036.00*	*66*	*50591.00*	80	64647.00	96	78207.00	113	94755.00
52	34431.00	67	51715.00	81	65651.00	97	79884.00	114	96732.00
53	35780.00	68	52511.00	82	66648.00	100	80990.00	115	98322.00
54	37169.00	69	53145.00	83	67671.00	*101*	*81674.00*	116	100345.00
55	*38410.00*	70	55349.00	84	69639.00	102	82200.00	117	101906.00
56	39654.00	71	56384.00	85	70505.00	*103*	*82852.00*	118	104107.00
57	*42062.00*	72	57848.00	86	71287.00	104	83920.00	119	104687.00
58	43081.00	73	58694.00	*87*	*71757.00*	*105*	*84890.00*	*120*	*107348.00*
59	44468.00	74	59567.00	*88*	*72036.00*	106	85705.00	*121*	*108698.00*
60	45113.00	*75*	*60726.00*	89	72516.00	*107*	*87584.00*	*122*	*111161.00*

On every cross section, the boundaries of the overbanks and the thalweg are identified, then to improve spatial accuracy a linear interpolation between surveyed cross section is made up to an interval of 330m (250 cross sections on the entire reach). Interpolated cross sections are the boundaries between computational finite volume cells (see the following sections and Chapter 2 for the numerical model description)

Table 4, together with Figure 31 gives an overview of all data available. Italic numbers indicate that the cross section has not been updated in 2009.

Since no cross section surveys are available before 2000, this will be the starting year for the simulation runs.

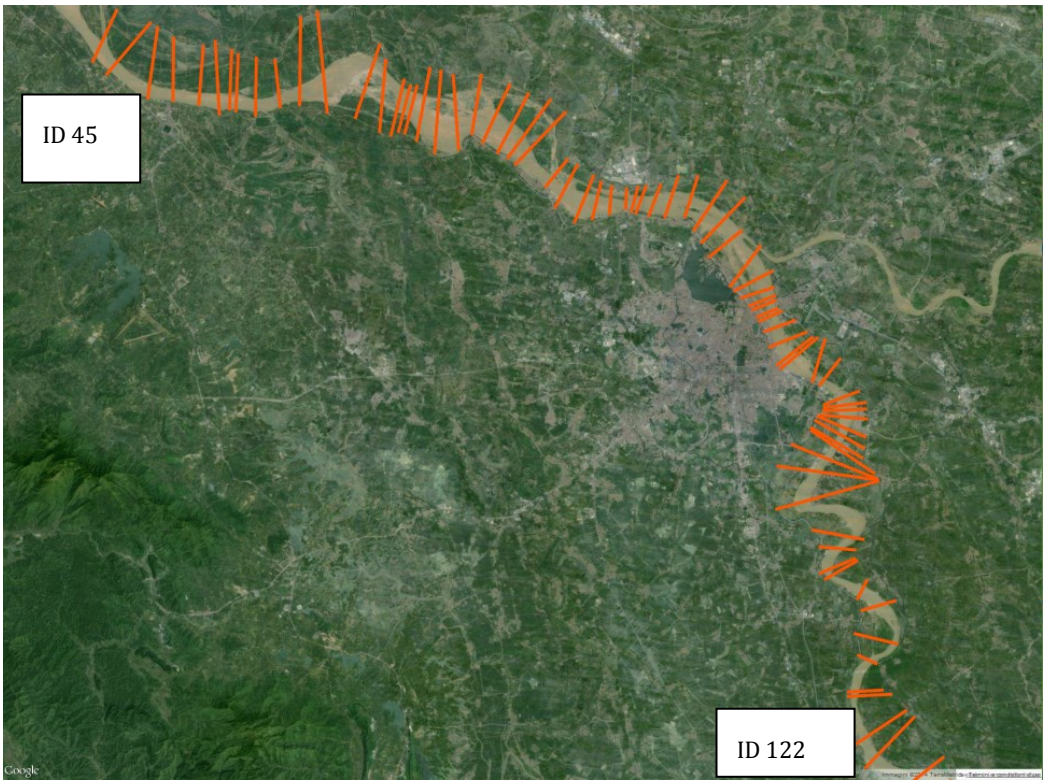

Figure 31: Plan of cross sections survey in the reach of interest.

Hydrology

At the gauging stations of Son Tay, Hanoi and Thuong Cat (Figure 28) time series of daily discharge and water level are available from 1960 on. This database allows a validation of the model and helps treating the bifurcation in the correct way. The observed hydrograph in Son Tay will be the upstream boundary condition. The discharge hydrograph in Hanoi together with water level measurements in Hung Yen (20 km downstream the closure section) helps in building a stage-discharge relationship as downstream boundary condition.

Apart from numerical modelling, these data were useful for a detailed analysis of the geomorphological evolution of the river system, including the changes in bifurcation behavior observed from early 2000s (analysis performed by Schmitt, 2014).

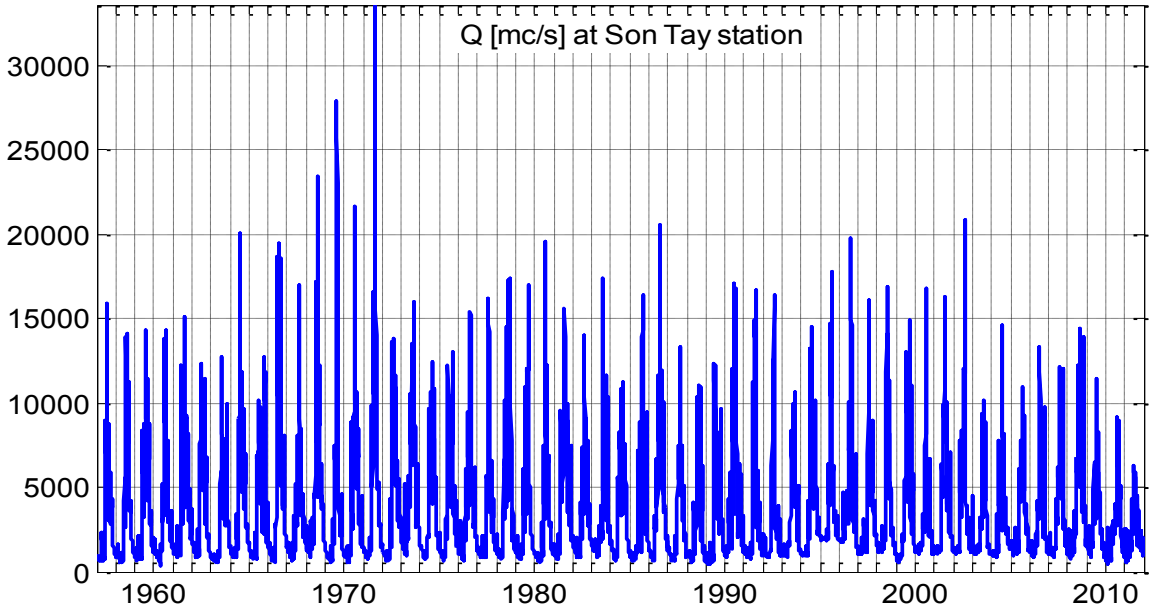

Figure 32. Discharge time series at Son Tay station

Sediment characteristics and sediment transport

An essential feature that describes river alluvium is the representative diameter: its estimation is always necessary in the use of sediment transport formulae, relating sediment flow to liquid flow given some characteristics of sediments.

No recent measurements of grain size have been performed along Red River recently and almost no data were found. In the archives of IWRP only old measurements from the 1970s were available: from these, we estimated the sediment representative diameter of 10^{-4} m – 0.1 mm all along the reach. Different hypotheses on grain size should be based upon more recent and reliable data.

Daily suspended solids (SS) concentration data (g/m^3) are available; these include washload, which is ineffective in terms of morphological evolution, whereas bedload is neglected. However, considering the strong prominence of suspended load in a large sandy river as Red River (above 85%, Uyen, 2011), and taking into account the uncertainty that affects measurements, these data could be representative of suspended sediment transport and are useful for validating and testing sediment transport formulae.

Location and relevance of water supply infrastructures

A large number of water supply structures (pumping stations, gates) are located on Red River banks, supplying water to large canals and agricultural districts.

From the data available we assessed that irrigation supply has limited effects on river morphology because:

- Water is derived in dry season, when sediment transport is already at minimum if compared to large floods
- The withdrawn flow doesn't exceed 10-15% of total discharge

For these reasons, irrigation lateral outflows are neglected.

The sediment transport formula

The sediment discharge can be computed with different formulae. The choice fell on Engelund-Hansen total load formula and a preliminary test was carried on to assess if it is representative of the sediment movement in Red River

$$Q_s = 0.05\rho_s g B U^2 \sqrt{\frac{d_s}{g(s-1)}} \left(\frac{\tau_0}{\rho g(s-1)}\right)^{3/2} \qquad (4.1)$$

A daily value of total suspended discharge *Qs* has been derived from SS concentration and discharge time series at the cross section of Son Tay, and then compared with simulated values obtained from a representative run of the model (year 2000 only). The daily values of Q_s have been divided in Nc classes (0.01 m^3/s wide). Extreme values larger than 2 m^3/s are part of a single last class. For each class, the relative frequency RF(i) has been calculated. As reported in Figure 33, results can be considered satisfactory. The statistical expected values J_{Qs} for the recorded and simulated *Qs* differ by less than 10%.

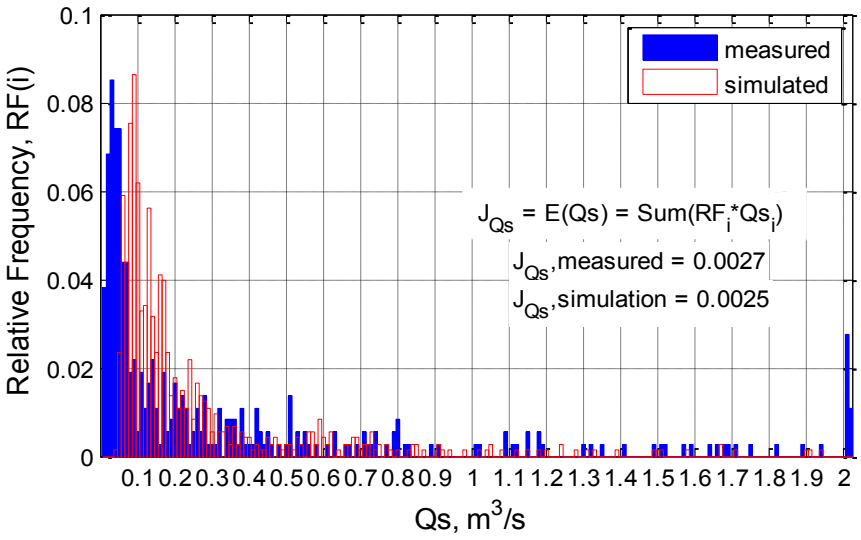

Figure 33. Test of sediment transport formula.

Van Rijn formula was also tested: results of its performance in terms of expected values were similar, with a ratio of bed load over total load very close to expected values - 10-15% or lower, as estimated also in Vietnamese reports (Uyen, 2011). Due to its simpler mathematical form, Engelund – Hansen formula has been preferred.

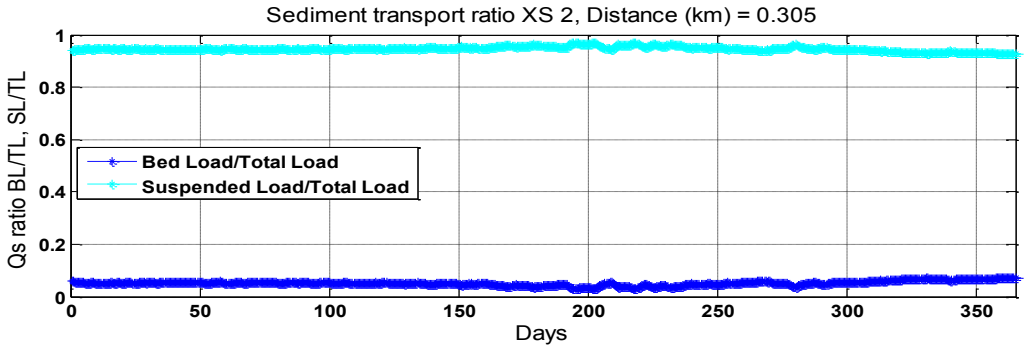

Figure 34. Ratio of suspended and bed load over total load at Son Tay cross section – test of Van Rijn formula.

Bifurcation modeling

The discharge flowing towards Duong river (Q_{DU} in Equation 4.2) is ruled by conveyance and friction slope ratios with Hong river, as follows:

$$Q_{DU} = \frac{K_{DU}\sqrt{Sf_{DU}}}{K_{DU}\sqrt{Sf_{DU}}+K_{HO}\sqrt{Sf_{HO}}} Q_{in} \qquad (4.2)$$

where subscripts DU and HO indicate Duong River and Hong River respectively; K_{DU}, K_{HO} are the conveyances (known if cross section geometry at bifurcation and water level are known) and Sf_{DU}, Sf_{HO} are the friction slopes; Q_{in} is the discharge approaching the bifurcation. Hence, flow distribution is driven by the geometry evolution of both distributaries (Figure 35): however, only Hong river is modelled herein. A *priori* hypotheses have to be assumed on the behavior of the Duong cross section at the bifurcation and on friction slope ratio between the two branches during the simulation time.

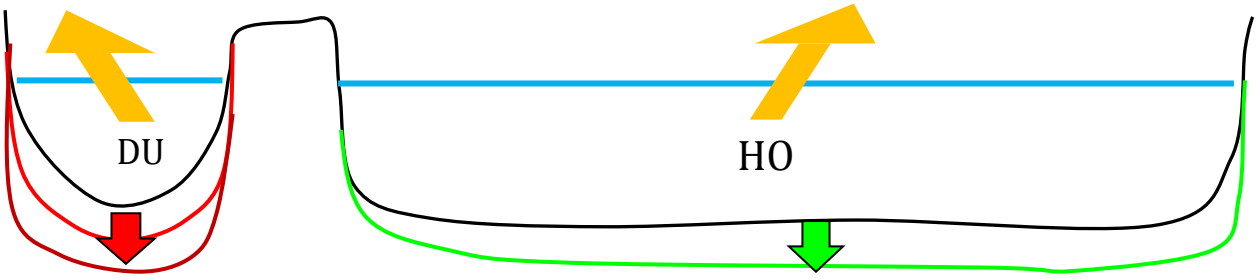

Figure 35. Sketch of flow distribution at the bifurcation.

For instance, bifurcation behavior is adjusted during the model validation process for the period 2000-2009 (see following sections), testing different bed lowering trends of Duong river initial cross section, to calibrate conveyance ratio (see Eq. 4.2) and match the complex flow distribution pattern observed during those years (Figure 29). Lowering trends are inferred from recorded minimum water levels in the cross section of Thuong Cat on Duong River, just downstream the bifurcation.

In the same way, historical data about water surface slope in dry and wet season can be analyzed to estimate ratio of friction slope between the two branches (water surface slopes can be a good approximation of friction slopes).

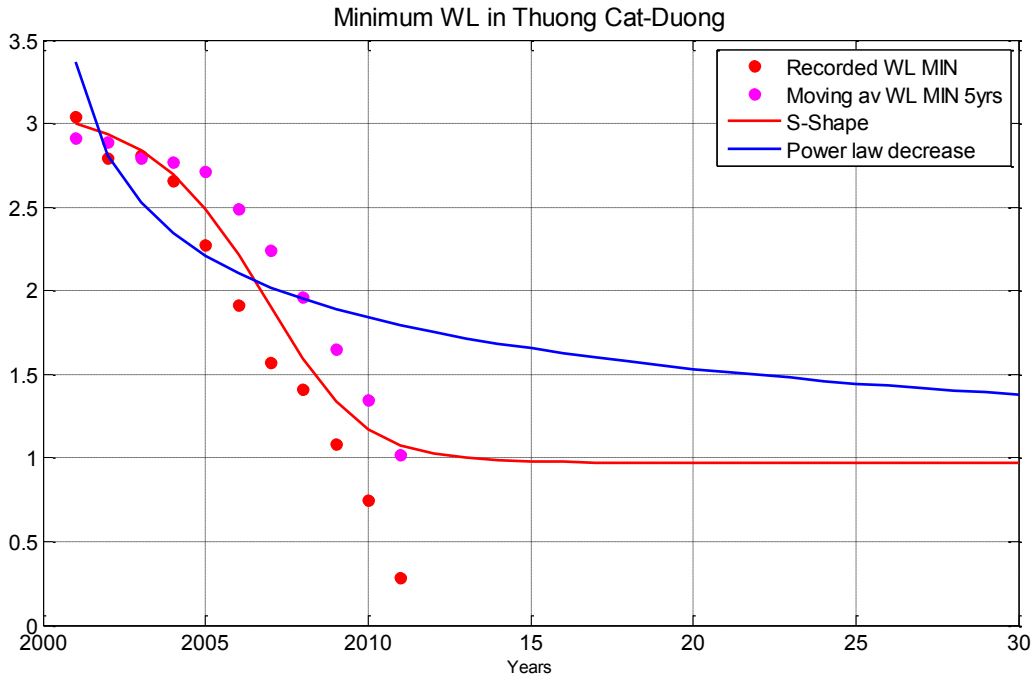

Figure 36. Lowering trends of minimum water levels at Thuong Cat cross section.

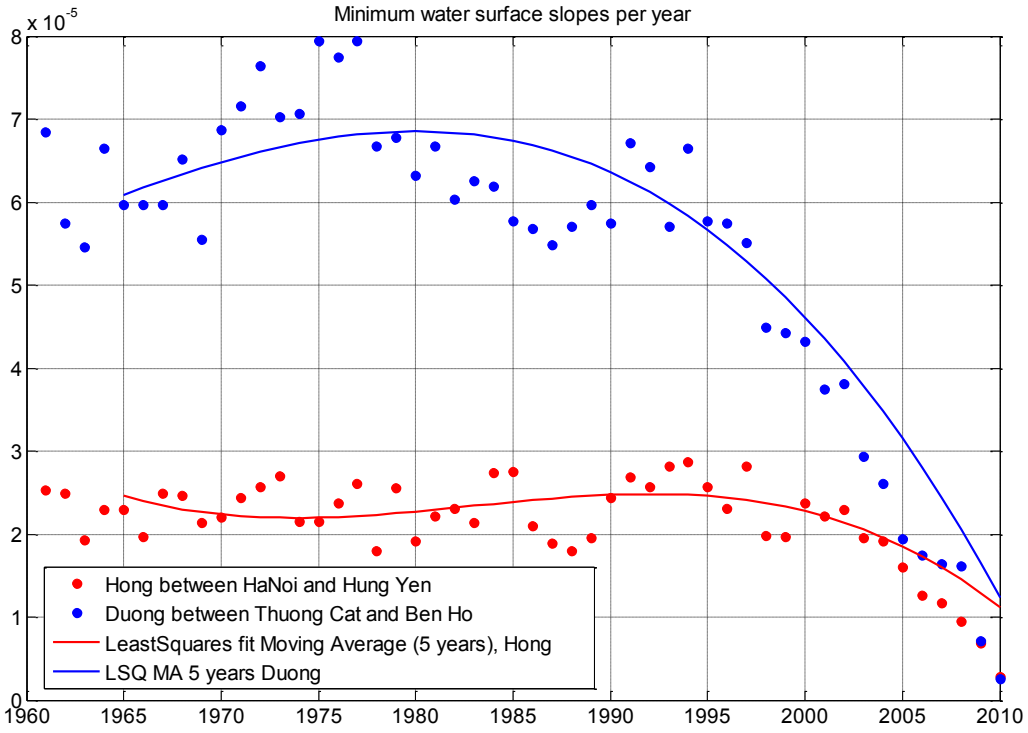

Figure 37. Trends of minimum water surface slope in Hong and Duong.

4.3 Numerical scheme

A Godunov-type finite volume scheme, first order accurate in space and time, has been adopted to integrate the system of equations (2.1)-(2.3) (see section 2.3). A splitting form is implemented: the homogeneous part of the system is first solved, then with the obtained intermediate step solution $U^{n+1/2}$ the ODEs involving source terms are integrated. A finite volume scheme implicates the solution of Riemann problem at computational cell boundaries: among the large number of approximate Riemann solvers available in the literature, we followed the HLLC-type approach (Harten et al., 1983; Toro et al. 1994) presented in the work by Goutière : (2008) where the speeds of the waves originating at cell boundaries and delimitating the intermediate constant states are estimated by an eigenvalue analysis of the system matrix. Details are reported in section 2.3.

4.4 Validation and sensitivity analysis

Two main purposes drive the choice of simulation runs model: the validation, taking advantage of the available flow and topographical data (2000-2009), and a preliminary sensitivity analysis of the effect of sand mining and flow control through reservoirs on river reach morphology.

Validation of the model was performed taking as initial condition the cross sections surveyed in 2000, and running 10-year long simulation runs with the recorded discharge series in Son Tay (2000-2009) as upstream boundary condition. Bifurcation behavior was adjusted during this process, testing different bed lowering trends of Duong river initial cross section, to calibrate conveyance ratio and flow distribution (see Eq. 4.2). Lowering trends are inferred from recorded minimum water levels at the cross section of Thuong Cat on Duong River, just downstream the bifurcation. Bed roughness in the reach is assumed as invariant. The results of these runs (codes VD1 and VD2, see Table 5) are compared with recorded time series of discharge at Duong bifurcation, and water level in HaNoi.

As for the influence of anthropogenic activities, a reference simulation was run for the period 2000-2009 with the recorded upstream incoming discharge as input, in the hypotesis of no sand mining

along the river (code REF). Then, two different scenarios of sand mining (code SM1, SM2) are analyzed: a starting value (sm_0) of sediment mining rate is provided in the report by MARD (Uyen, 2011): sm_0 = 6.6 Mm^3/year in the reach Son Tay - Hanoi and sm_0 = 2.3 Mm^3/year downstream Hanoi. This value was increased by 50% to run SM2. In addition, a steady low-discharge simulation (1100 m^3/s) was run accounting for the bed configuration resulting from the 10-year simulations and for the cross sections surveyed in 2000 and 2009; resulting water surfaces profiles have been compared to assess the reliability of the model.

The morphological effects of flow control through reservoirs are estimated substituting the recorded input hydrograph with a reconstructed "natural" flow hydrograph (code NAT, Figure 41) provided by previous studies at Hanoi IWRP (Institute of Water Resources Planning), supposing the absence of large impoundments upstream and consequently increasing peak flows. In this run series, both roughness and bifurcation behavior are always kept constant.

Table 5. Simulation runs summary.

CODE	INPUT HYDROGRAPH	SAND MINING RATE	DUONG RIVER BED LOWERING
VD1	Recorded	sm_0	Power-law decrease
VD2	Recorded	sm_0	S-shape decrease
REF	Recorded	0.0	No
SM1	Recorded	sm_0	No
SM2	Recorded	sm_0+50%	No
NAT	Reconstructed	0.0	No

Results: validation

The agreement between simulated and recorded data series in 2000-2009 is analyzed. Concerning bifurcation, flow in Duong distributary is slightly overestimated during dry season (Figure 38). In VD1, the Duong bed lowering (see previous section) follows a power-law decrease, with faster lowering at the beginning of the run, while in VD2 the lowering follows a S-shape curve, with faster lowering in the middle years. The total decrease is 2 m for both simulation runs. Moreover, we tried to calibrate a distinct friction slope ratio (see Eqn. 4.2) for dry and wet seasons, following once again the observed data. On the other hand, peak flow in the Duong is slightly underestimated by

the model. The overestimation of flow in the distributary leads to an underestimation of water level in Hanoi (Figure 39) during the first three-four years. Maximum levels provided by the model are in excellent agreement with recorded data.

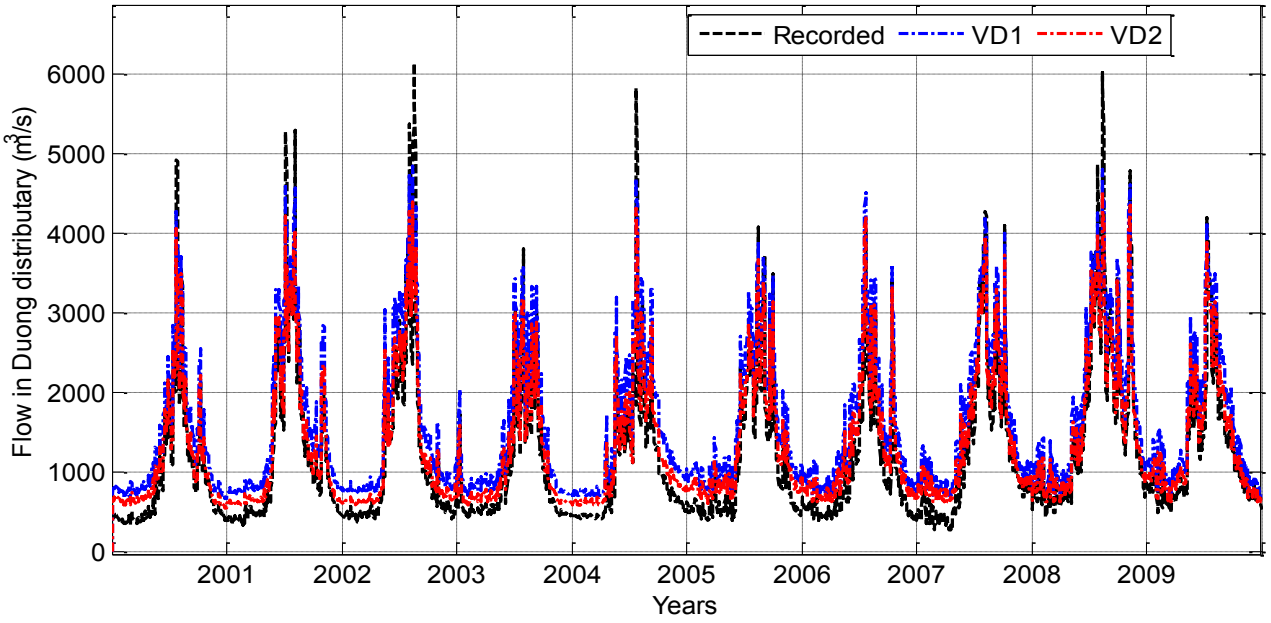

Figure 38. Discharge in Duong distributary, simulation runs VD1 and VD2.

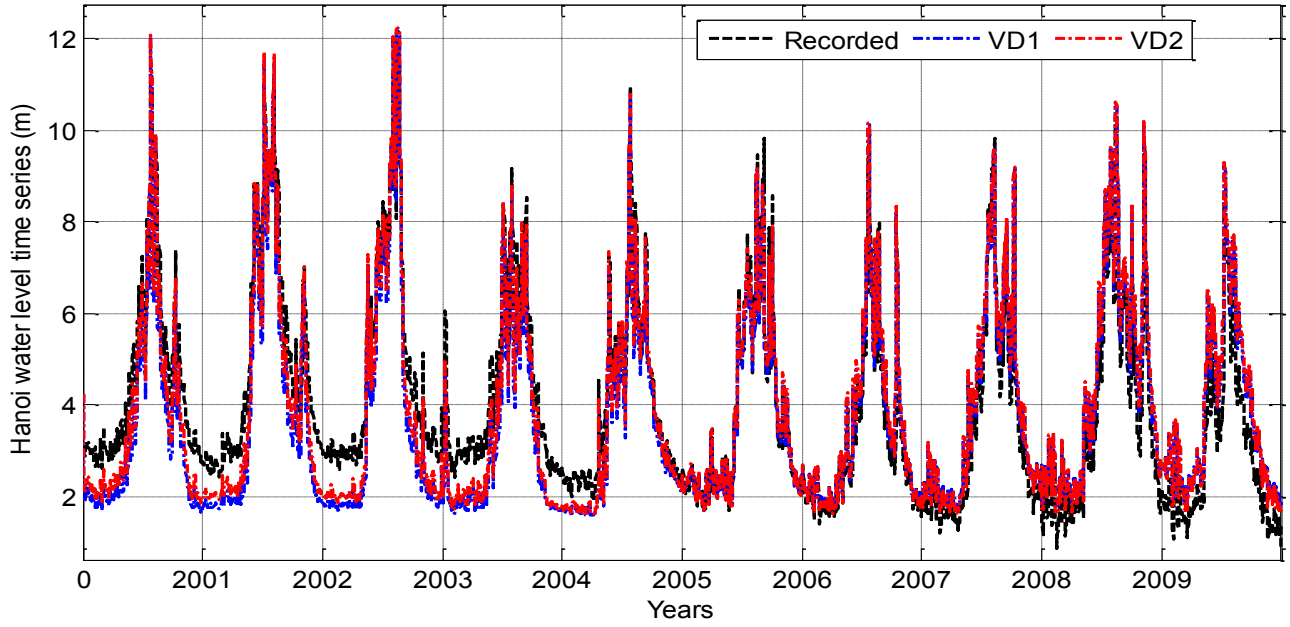

Figure 39. Water level in Hanoi, simulation runs VD1 and VD2.

Results: sensitivity analysis

To check the morphological sensitivity of the system to flow control and sand mining, we adopted the indicator J_{inc} previously introduced (Equation 3.10, section 3.4): we monitored the evolution of 5 representative points of the main channel bed (the thalweg, two left and two right) for every cross section. Starting value of this indicator is zero: negative values mean that the river is undergoing incision in that reach. We analyzed 4 reaches of equal length (20 km each, numbered from upstream, Figure 40, see also Figure 28).

Figure 42 compares the evolution of J_{inc} in time for simulation REF and NAT; in Figure 43 the same evolution for simulation runs REF, SM1, SM2 is compared.

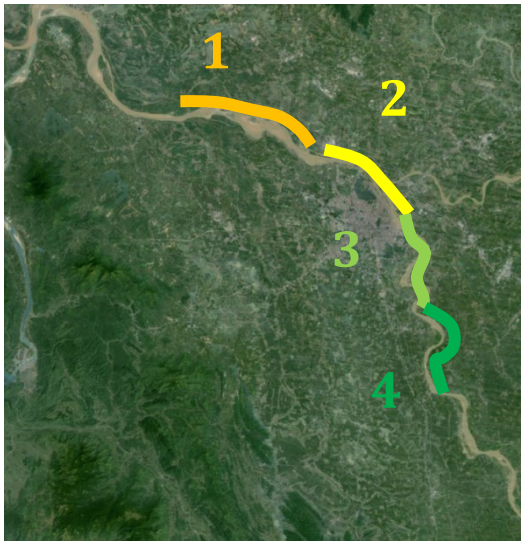

Figure 40: sub-reaches analyzed

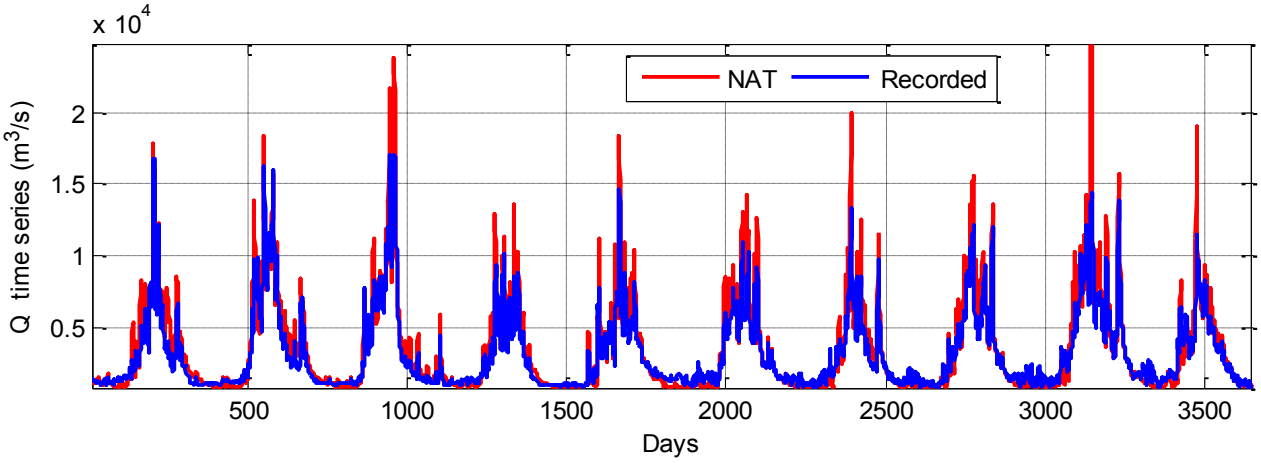

Figure 41: Recorded hydrograph at Son Tay and reconstructed "natural" hydrograph for NAT simulation.

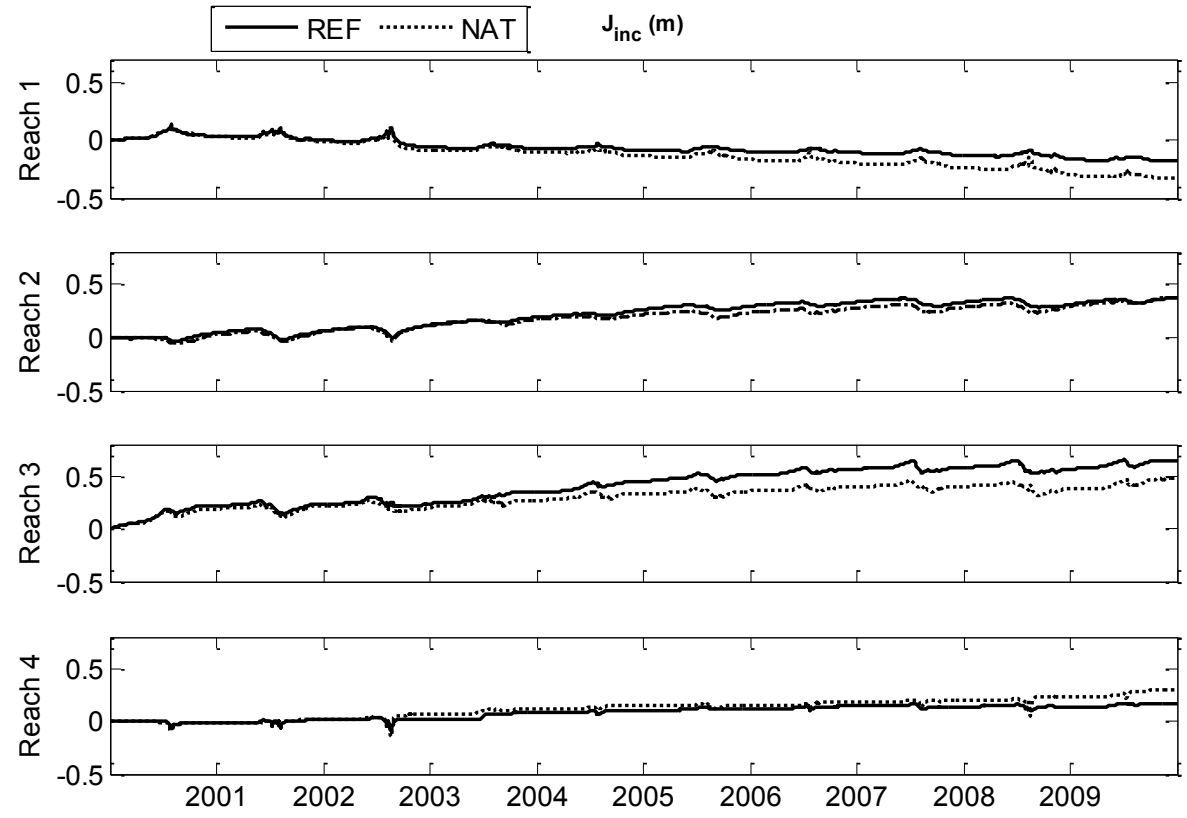

Figure 42 Indicator Jinc evolution in time, for simulations REF-NAT.

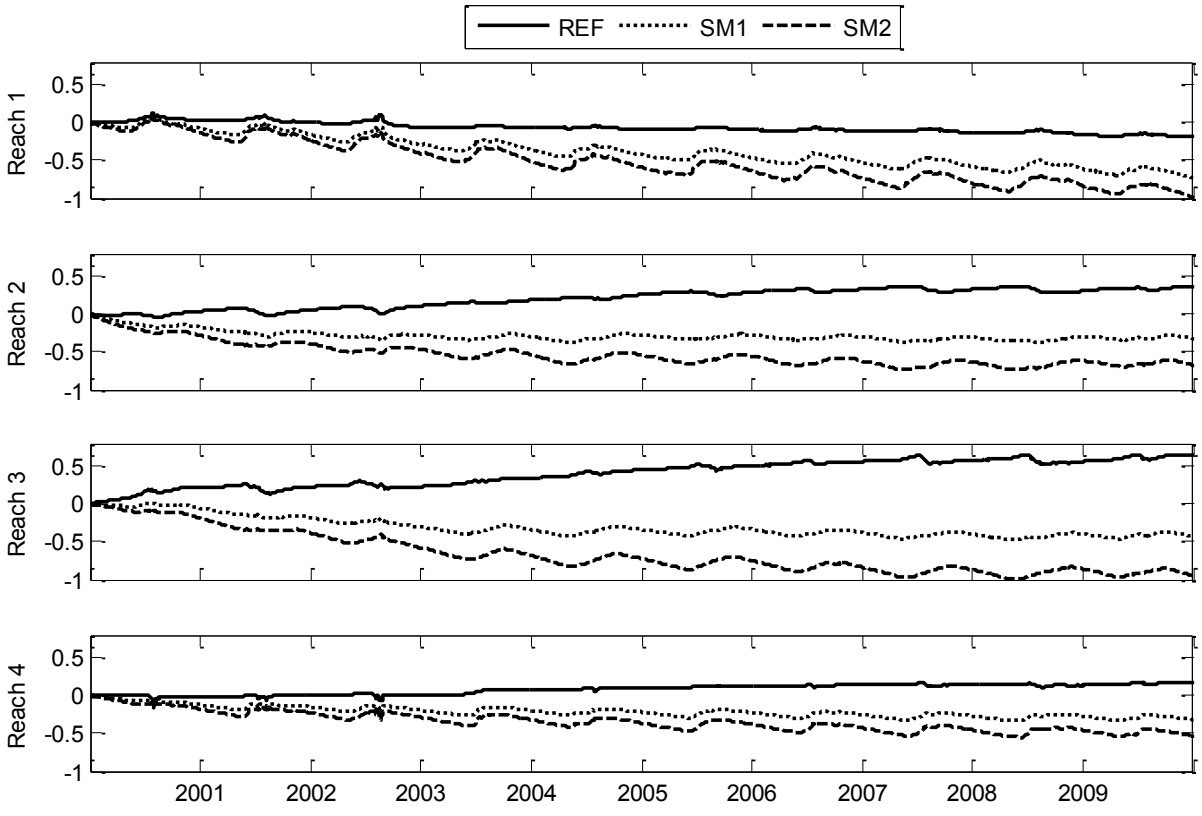

Figure 43. Indicator Jinc evolution in time, for simulations REF, SM1, SM2.

It is interesting to notice that in the REF simulation, the tendency to river bed degradation is visible only in the first reach. A natural process of slope decrease would probably occur, with deposition starting from the second reach analyzed. Sand mining instead, as expected (simulations SM1 and SM2), accelerates incision in first reach and reverses the trend in the following three reaches. Stopping or decreasing sand mining would probably start a restoring process. The flow control, conversely, appears to affect much less the morphological evolution (Figure 42). The reconstructed hydrograph (Figure 41) is supposed to remove any effect of the impoundments upstream, in presence of the same precipitation pattern. For this reason, every release policy would result in inflows discharges between the recorded and "natural" one. The results indicate that the effect of flow control alone on morphology is very limited in the studied stretch, in comparison to sand mining.

Water surface profiles related to a steady, low-discharge simulation (1100 m^3/s) have been compared (Figure 44), in a sort of visualization of indicator J_{inc} previously introduced in equation 3.9 (check section 3.4). for the bed configurations of 2000, 2009 (surveyed) and after simulations SM1 and SM2 (simulated); incision process has progressed faster than these two simulation runs show. Sediment mining rates could be larger than what initially estimated.

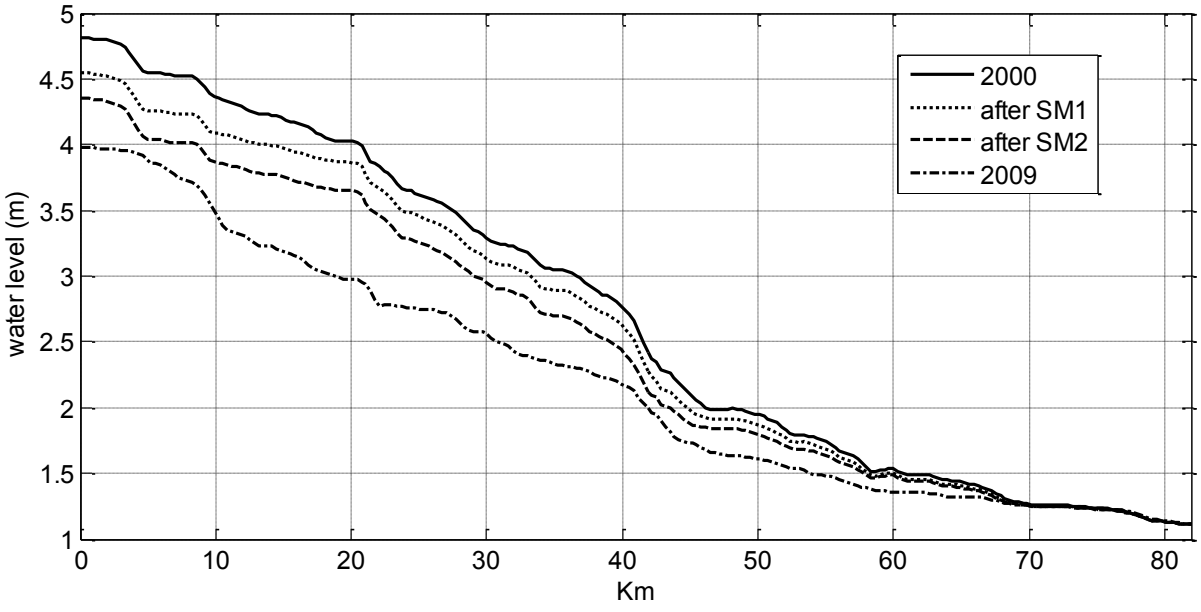

Figure 44. Water surface profiles for a steady, low discharge simulation (1100 m^3/s) on different river bed configurations.

4.5 A focus on sand mining

After the simulation runs performed in the model set-up phase, further data about sand mining activity along the river –one of the most important morphology evolution drivers as demonstrated - have been collected trying to build a reasonable scenario in order to carry on simulations with the hydromorphological model of Red River in predictive mode.

Bases of this section are a couple of reports provided by Vietnamese Authorities together with satellite image analysis.

The estimation of sand mining along Red river is subject to uncertainties, both in total volumes withdrawn and spatial distribution; taking into account preliminary simulations results and the data kindly provided by VN offices, we aim to provide an overview as reliable as possible. Sand requirements for building up to 2020 and sand reserves available along the rivers, estimated by Hanoi People Committee (PC) for Hanoi province, are a good starting point as well as the report by MARD (Uyen, 2011) that performs an analysis *a posteriori* on sand mining effects, by the mean of inspection of some river cross sections; we used the results of this analysis to obtain the starting value of our sand mining sensitivity analyses.

The MARD report provided a value that we called sm_0 = 6.6 Mm^3/year in the reach Son Tay - Hanoi and sm_0 = 2.3 Mm^3/year downstream Hanoi, in the years from 2000 to 2008.

The report from Hanoi PC (February 2013) confirms that forecasted sand requirements and planned licenses for sand mining in Hong River are consistent between them. It is reported that for the HaNoi province only, the required sand up to 2020 is around 28 Mm^3 (gravel is not included). Licensed sand mining for the Hanoi province jurisdiction is planned in 3.4 Mm^3/year.

But also part of Vinh Puc and Hung Yen provinces boundaries run along the Red River reach we are studying, the first on the northern region up to Hanoi (left bank) and the second downstream Hanoi, still on left bank. The estimated licenses for these provinces are 0.882 and 1.882 Mm^3/year, respectively. The total is then around 6.1 Mm^3/year.

As explained in the introduction, the river reach chosen for the analysis includes the most part of the instream sand deposits, besides several are located upstream; almost none of them, instead, is located downstream the closure section of the model at Phu Minh. Storage data (sand deposits estimated amount) can help in identify how much required sand comes, at the end, from sources different than the Red River.

Reserves stored along Red River are estimated in 146.7 Mm3. Other reserves in the Hanoi province are identified:

-on Da river, 16 Mm3;

-on Cong river, 15 Mm3;

-on Duong river, 2.5 Mm3;

-on Ca Lo river, 6 Mm3;

Reserves on Red River are nearly 80% of the total. It is reasonable then to assume that, to meet required amounts, 80% of the sand will be mined from Red River. If this proportion holds for the other provinces (where detailed information on requirements are lacking), the estimation of sand mined along Red River - based upon the licenses - would be around 5 Mm^3/year, well below the value provided by MARD (Prof. Uyen) studies. Anyway, the dimension of sand reserves themselves suggests that sand mining rates could be much higher, and also we didn't mention illegal sand mining which unfortunately is taking place, increasing the amount of withdrawn sand far beyond the "sustainability" limits set by the licenses. In some areas of the world, illegal sand mining is a real business and is often reported to double the legal amount, due to the difficulties and large expenses in monitoring all the sites along large rivers where illegal miners potentially can operate.

As for the spatial distribution of the sand mining along the river reach, we could rely upon the Hanoi People Committee report that establishes the location and magnitude of sand reserves. It is reasonable to hypothesize a direct correlation between the location of potential reserves and the location where sand is mined, given the high number of possible mining sites identified by the authorities all along the river (we count 18 of them only along the studied reach).

To introduce other facts revealing more about sand mining activity location, some satellite images were analyzed detecting and counting barges carrying sand, operating along the river.

We divided the studied stretch into four reaches, changing a little their extension with respect to the previous simulations: from upstream, 20.1 km, 22.3 km, 18.8 km, 20.8 km respectively. The second reach includes Hanoi city.

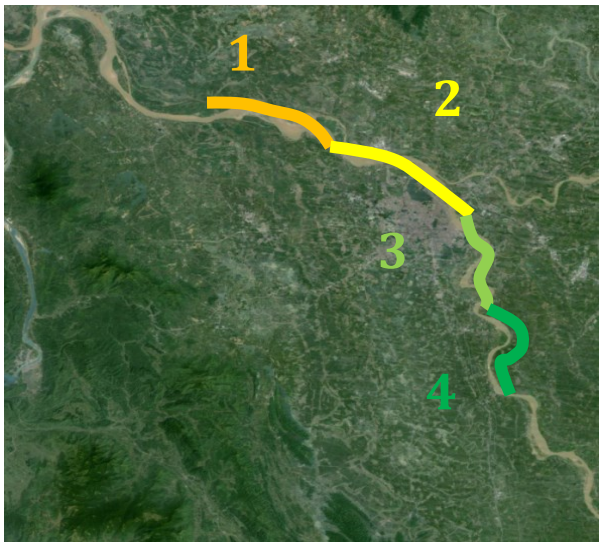

Figure 45. Sub-reaches for sand mining detailed analysis.

Spatial distribution of the deposits reveals that 88 % of the sand is stored along the first two reaches; consistently, operations of the barges (they can carry up to 70 m^3 sand) also look more intense in the upstream stretch, with almost 60% of the barges operating upstream Hanoi and only 40 % downstream.

Based on the data listed above, and starting from the simulations SM1 and SM2, we planned new 10-years long simulations (see Table 6). Always referring to the same indicator (Eqn (3.9), see previous sections and Figure 44) water surface profiles related to a steady, low-discharge simulation run on different river bed configurations have been compared. Water surface profiles for the surveyed river beds of 2000 and 2009 are available; in between there are the flow profiles obtained with the river bed at the end of our 10-years long simulations running from 2000 on.

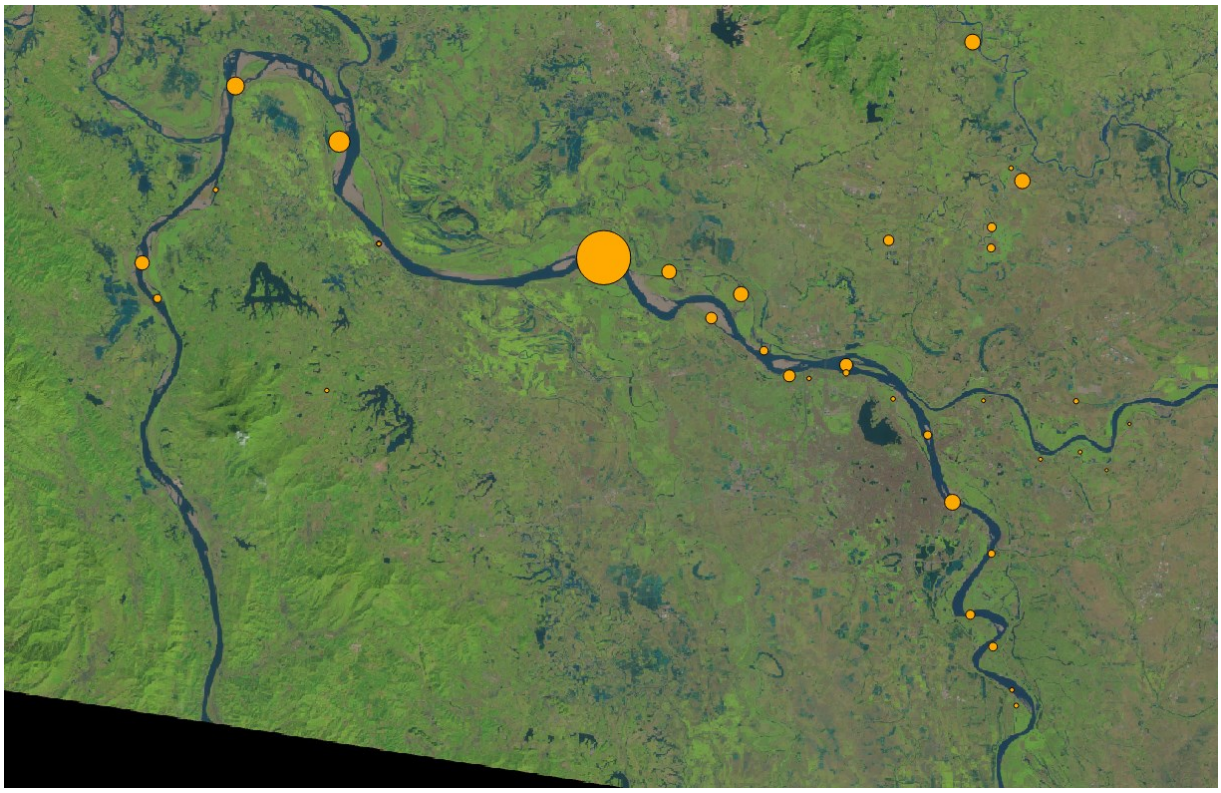

Figure 46. Location and relative magnitude of sand reserves along Da and Hong (Red) River.

Different sand mining rates and distributions along the river allow to improve progressively the matching with the water surface profile of 2009. The aim is to assess, with this sort of back analysis, a realistic sand mining rate (average) that occurred in the 2000-2009 decade and then use this scenario to run the model in prediction mode.

We start from a simulation (exp2) in which the total withdrawn sand amount along the stretch is the double of SM2– with a distribution of mined sand of 20%-50%-20%-10% respectively in the four sub-reaches. The 2nd reach includes the bifurcation and Hanoi. In the last two reaches, for exp2 the matching with flow profile of 2009 is already satisfactory.

We keep this 4- reach splitting also in the following sims (exp3a –exp3e), where we progressively increase the amount of mined sand per year in the first two reaches. In exp 3e we adopted a slightly different sub-reach splitting (boundary between 1st and 2nd reach) and distribution starting from the total amount of exp 3b.

In all runs 3a-3e, sand mining rate is uniform in time. We also decided to test a change in the temporal distribution of sand mining rates, keeping the total amount constant. Namely we kept the total of 3e, increasing rates in the first two reaches by 20%-40% in the first 5 years and reducing them by 20%-40% from the 5th year on (exp 4a and 4b respectively).

Table 6. Sand mining simulation runs: main features.

ID	Sub-reach 1		Sub-reach 2		Sub-reach 3		Sub-reach 4		Total
	Final XS (km)	Mm³ /year	Final XS (km)	Mm³/ year	Final XS (km)	Mm³/ year	Final XS (km)	Mm³/ year	Mm³/ year
exp2	20.1	3.56	42.5	8.80	61.3	3.39	82.4	1.78	**18**
exp3a	20.1	4.45 (exp2+25%)	42.5	11.0 (exp2+25%)	61.3	3.39	82.4	1.78	**21**
exp3b	20.1	5.34 (exp2+50%)	42.5	13.2 (exp2+50%)	61.3	3.39	82.4	1.78	**24**
exp3c	20.1	6.23 (exp2+75%)	42.5	15.4 (exp2+75%)	61.3	3.39	82.4	1.78	**27**
exp3d	20.1	7.12 (exp2+100%)	42.5	17.6 (exp2+100%)	61.3	3.39	82.4	1.78	**30**
exp3e	10.0	2.22	42.5	15.8	61.3	3.39	82.4	1.78	**23**
exp 4a	10.0	1.2*exp 3e for years 1 to 5; 0.8*exp3e for years 5 to 10	42.5	1.2*exp 3e for years 1 to 5; 0.8*exp3e for years 5 to 10	61.3	3.39	82.4	1.78	**23**
exp 4b	10.0	1.4*exp 3e for years 1 to 5; 0.6*exp3e for years 5 to 10	42.5	1.4*exp 3e for years 1 to 5; 0.6*exp3e for years 5 to 10	61.3	3.39	82.4	1.78	**23**

4.6 A focus on sand mining: results

We read the results of simulation runs as we did in Figure 44: after 10 years of simulation, we save the river bed configuration and we simulate over this a steady, low-discharge flow (1100 m³/s) with fixed bed. Water surface profiles can be compared, to evaluate river bed lowering due to sand mining.

Whereas exp2 profile is still well above the water surface profile calculated for 2009, exp3a looks the best approximation to it. From exp 3b on, mining rates are too intense and degradation is disproportionate. The small change in distribution operated by running exp3e has negligible effects; profiles from 3b and 3e are almost coincident.

Time variation of sand mining rates (exp4a-4b) leads to some interesting outcomes. As noticed in previous runs ("REF", section 4.4), in absence of sand mining, the system recovers fast from bed

degradation, restoring an equilibrium by the mean of deposition. A confirmation can be found looking at water surfaces for exp 4a and 4b, compared to 3e (Figure 48) , it is clear that decreasing extraction rates at some point has a positive effect – even if in the first part of the simulation mining rates are higher.

Our estimations point out that the mining rates per year in the studied reach could range between 18 and 23 Mm^3, a value which is around 3-4 times the licensed value (see section 4.5). Of course, as previously mentioned, results of such a physically based modeling are subject to several uncertainties, but no doubt the sand mining rates are clearly exceeding licensed values, and if continued with these trends, sand mining poses some serious threats to the future overall conditions of the river system and agricultural services.

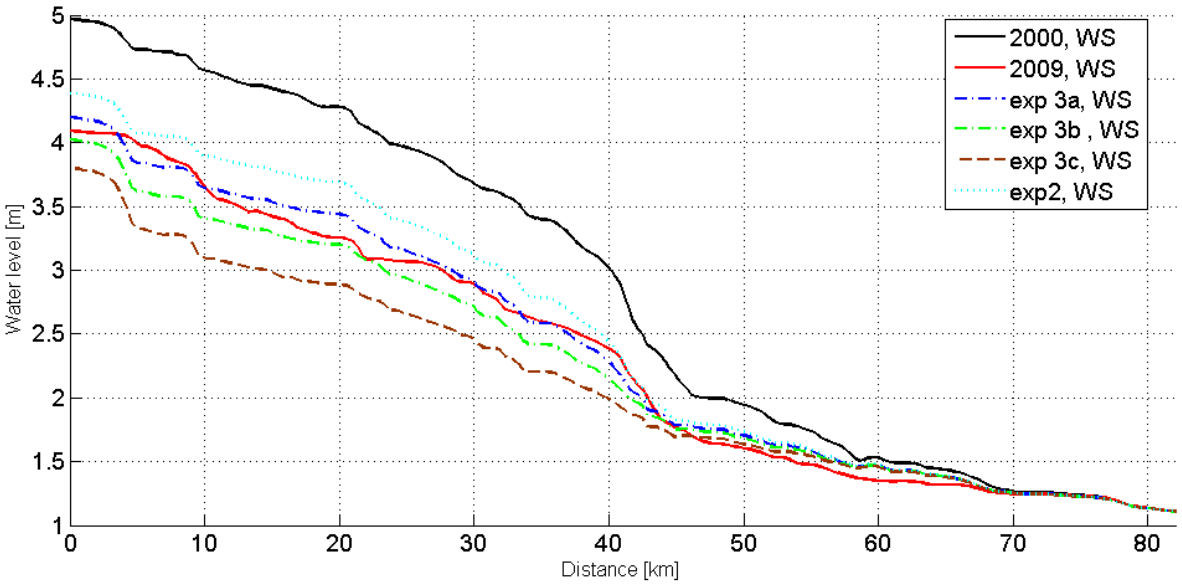

Figure 47. Water surface profiles. Comparison among sand mining simulation runs 2-3c.

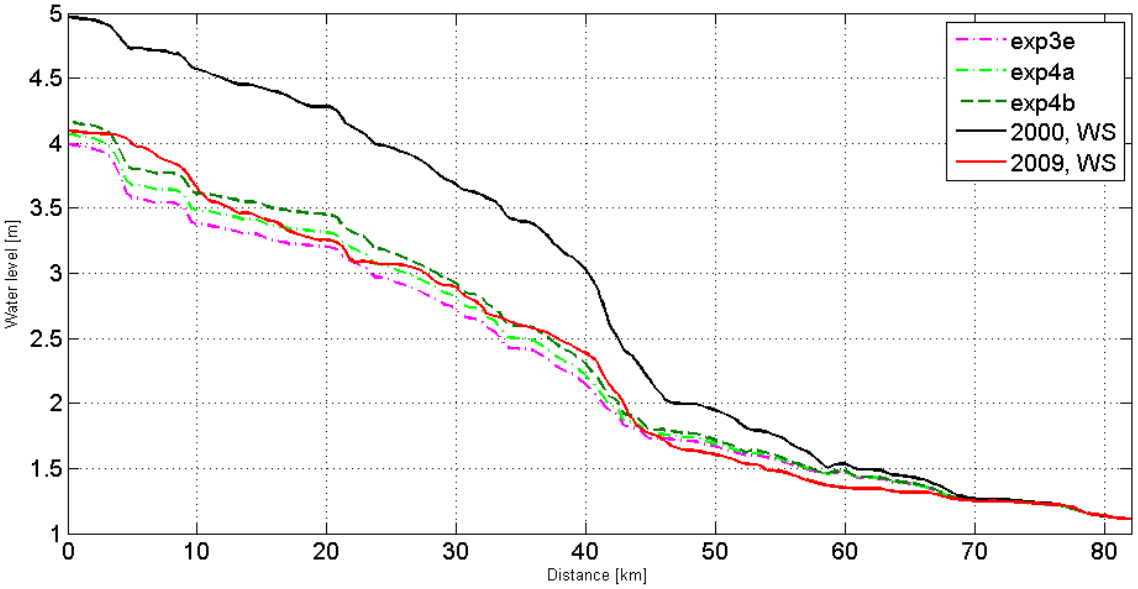

Figure 48. Water surface profiles. Comparison among sand mining simulation runs 3e, 4a, 4b

Chapter 5

A vegetation roughness model for Secchia River

In January 2014, a serious flooding event (due to a levee breach) occurred in the towns of Bastiglia and Bomporto, located in the Modena Province (Northern Italy) along Secchia River. Since then, concerns have increased about the role of vegetation in Secchia river channel during big floods.

We used a detailed characterization of riparian vegetation features performed by the Po River Interregional Agency (AIPo – Parma, Italy, that kindly provided the data) as basis for a hydrodynamic modelling work; a one-dimensional model accounting for the influence of different vegetation patterns and densities on flow resistance has been applied to a 60 km long stretch of Secchia river and validated, to support management choices and possibly check in the future the effectiveness of a proposed vegetation plan in reducing flood risk.

5.1 Introduction

After 3 days of intense precipitation on the Secchia river basin (average 120 mm total), a breach opened in the early morning January 19th , 2014 on the right levee, 5 km upstream the town of Bastiglia, close to the village of Albareto. More than 36 Mm^3 of water flew through the breach, mainly towards the towns of Bastiglia and Bomporto; the report by D'Alpaos et al. (2014) estimates a peak discharge of 400 m^3/s. The damage was worth more than 200 M€.

The reasons of the collapse of the levee have been investigated (D'Alpaos et al. ,2014). There are some eyewitnesses reports and photo-video evidences that the collapse could have started from tunnels dug across the levee by wild animals, a frequent problem in the lower course of confined rivers in the Po Valley. The high stress conditions triggered the collapse of the tunnels, and this

quickly turned into a failure of the levee. Apart from the maintenance of the levees, there were concerns about vegetation management on banks and overbanks.

It is well known that riparian vegetation influences flow field at several scales (for a thorough review, see Camporeale et al., 2013) and its effects can be positive or negative on reducing flood risk downstream (Tabacchi et al., 2000, Anderson et al., 2006) depending on canopy and roots characteristics, but also on local river geometry and hydrodynamics.

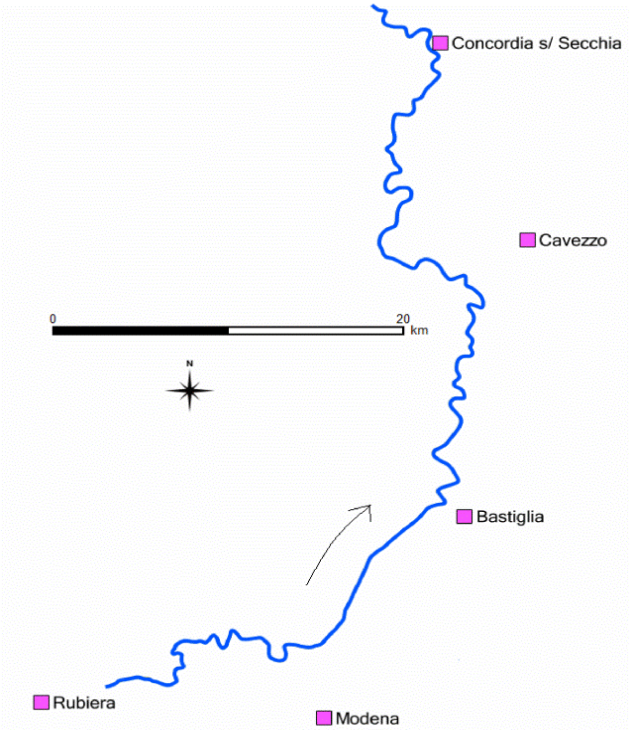

Figure 49. General map of the reach of interest.

Among several urgent measures, a detailed riparian vegetation characterization plan was commanded by Regione Emilia-Romagna after the failure. The Interregional Agency of Po River (AIPo), responsible for vegetation management in the Secchia river channel, organized and ruled the activities related to this characterization project, with the final purpose to go beyond the usual emergency-driven, ineffective countermeasure consisting in indiscriminate cutting and removal of every species; the key idea is to approach solutions at reach scale accounting for the different hydrodynamic conditions during floods, arising from a succession of sub-reaches of homogeneous morphological features, very different among them.

A framework to convert the data from the AIPo characterization report – a combination of satellite images and on-field analyses – to a set of vegetation density values and related dynamic flow resistance coefficients has been set up. We took into account factors such as the type of cover (mainly trees or shrubs) and age of plants.

5.2 Riparian vegetation and flow resistance parameters

AIPo riparian vegetation classification

AIPo (Adorni et al., 2014) has attempted a classification of the vegetated banks adjacent to the stream, following the guidelines of the technical guide SDAGE (Schéma Directeur d' Aménagement et Gestion des Eaux - Agence de l'Eau Rhone – Mediterranée et Corse, 1998) already applied in previous studies (Anselmo and Terzolo, 2001).

Riparian ecotones along Secchia river banks have been first mapped and classified into zones of homogeneous features by means of satellite images analyses, at the maximum available resolution. Once identified the main features clearly visible in the images, such as the type of cover, a GIS shapefile was created with polygons of 6 different classes; the classification was then refined by extensive on-field surveys, that improved the mapping of polygons boundaries, increased the number of final classes to 13 and added several important details that significantly help to understand the influence on the flow field (trees and shrubs density, age of plants) as well as other features of ecological interest (e.g. presence of species of high ecological value, or invasive species). See Figure 50 for a detail of the final shapefile.

In classes from 3 to 8 and 13 (step 2), trees cover dominates over shrubs but shrubs can be present; in classes 9-10, shrubs dominate over trees. All over the classified stretch, from the town of Rubiera to Concordia s/Secchia, class 4 is ranked first with 30.4% of the total cover; class 3 (24.6%) and class 9 (13.3%) follow. We notice here that *Amorpha Fruticosa* is highly invasive and quickly colonizes areas that were previously cleared.

Table 7. Classification of riparian vegetation: satellite images analysis (step 1) and field survey (step 2) (from Adorni et al, 2014)

ID	STEP 1	ID	STEP 2
1A	Bare soil	**1**	Bare soil
		2	Recent cutting/clearing
2A	Willow forest	**3**	Willow forest
3A	Willow forest w/other	**4**	Willow forest w/other trees or shrubs <20%
4A	Other trees forest	**5**	*Populus alba* forest (poplar)
		6	*Populus nigra* forest (poplar)
		7	*Robinia pseudoacacia* forest
		8	*Acer negundo* forest
5A	Shrub vegetation	**9**	Shrub vegetation (mainly *Amorpha Fruticosa*)
		10	Shrub vegetation w/trees >25%
6A	Unclassified	**11**	Herbaceous vegetation
		12	Previously cultivated, undergoing colonization
		13	Recent artificial revegetation

The attribute table of every classified polygon includes:

- predominant vegetation structure (trees or shrubs)
- trees density index (TDI), in a scale from 1 (absent) to 4 (very dense). An average distance between plants is provided for each class: > 6 m for class 2, between 2 and 6 m for class 3 and <2 m for class 4;
- trees age – this index is related to the average diameter of the stem (3 classes from young to mature – average diameter <7 cm for class 1, between 7 and 15 cm for class 2, >15 cm for class 3)
- shrub density index (SDI), in a scale from 1 to 4 again; in this case, the index is merely qualitative, indicating a sparse or continuous presence.

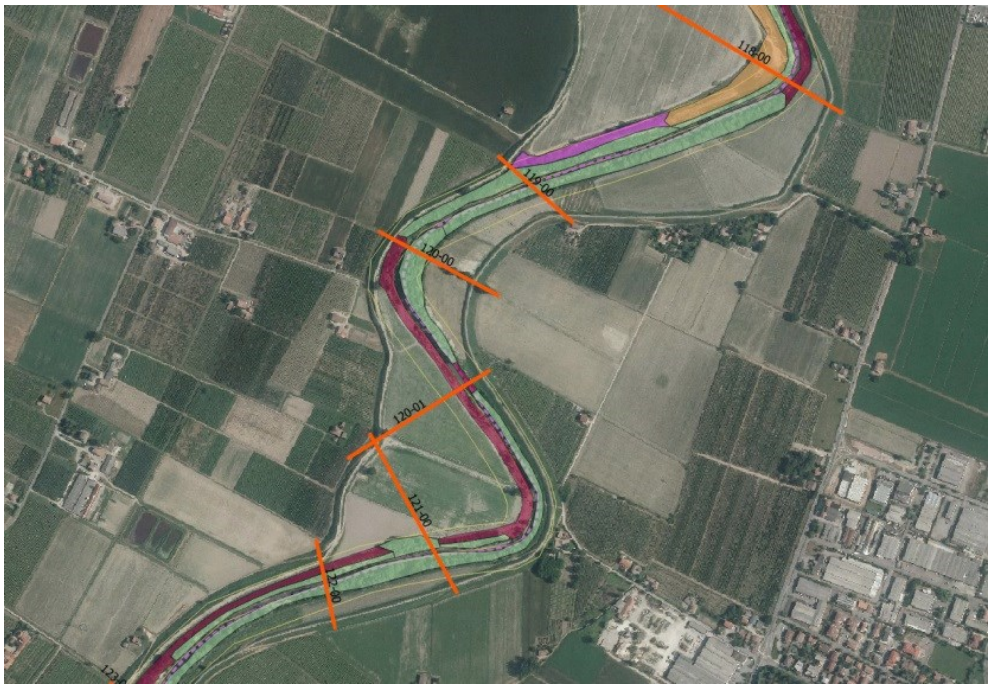

Figure 50. Adorni et al. (2014). Classification of riparian vegetation: detail of final shapefile with polygons of homogeneous features overlapped to a satellite image. Transversal lines are surveyed river cross sections.

5.3 Vegetation density

Hydrodynamic vegetation density per unit channel length *Dv* [1/m] is expressed as

$$Dv = \frac{\sum A_i}{AL} \tag{5.1}$$

Where A_i is the projected area of the vegetation element (m^2), A is the surface area of the plot in side view (m^2) and L is the channel length (m).

Several ways to measure *Dv* on the field may be found in literature (for a review see Fischenich and Dudley, 2000). Unfortunately, none of them was applied during the field survey. We built tables linking the value of *Dv* to the values of the density indexes listed in Table 7. For trees, we assumed that vegetation density *Dv'* may be related to the number of stems per square meter N and their average diameter d, as follows (Warmink 2007).

$$Dv' = \frac{\sum A_i}{AL} = Nd \tag{5.2}$$

Dv' can be calculated locally along the river on every polygon, assuming reference values for distance between plants (RD) and stem diameter (d). We finally add the shrubs density *Dv''* to *Dv'* to obtain the total *Dv*: *Dv''* has a fixed value for each SDI provided in the AIPo report. We referred for comparison to field values of *Dv* reported in the works by Asselman et al. (2002) and Warmink (2007). In the hypothesis that tree growth takes advantage from sparse or absent shrubs, we slightly increased the values of N if the SDI is lower than 3. In Tables from 8 to 10 the final values for Dv, given SDI, RD and d, are listed.

Table 8.Vegetation density Dv (1/m) for shrub density index SDI = 2. Dv'' = 0.05.

TDI	RD (m)	N (1/m²)	Dv (D = 0.07 m)	Dv (D = 0.12 m)	Dv (D = 0.2 m)
1	-	0	0.0500	0.0500	0.0500
2	6	0.016	0.0511	0.0519	0.0532
3	2.5	0.092	0.0565	0.0611	0.0685
4	1.2	0.401	0.0781	0.0981	0.1302

Table 9. Vegetation density Dv (1/m) for shrub density index SDI = 3. Dv'' = 0.1.

TDI	RD (m)	N (1/m²)	Dv (D = 0.07 m)	Dv (D = 0.12 m)	Dv (D = 0.2 m)
1	-	0	0.1000	0.1000	0.1000
2	6	0.016	0.1011	0.1019	0.1032
3	3	0.064	0.1045	0.1077	0.1128
4	1.5	0.257	0.1180	0.1308	0.1513

Table 10. Vegetation density Dv (1/m) for shrub density index SDI = 4. Dv'' = 0.12.

TDI	RD (m)	N (1/m²)	Dv (D = 0.07 m)	Dv (D = 0.12 m)	Dv (D = 0.2 m)
1	-	0	0.1200	0.1200	0.1200
2	6	0.016	0.1211	0.1219	0.1232
3	3	0.064	0.1245	0.1277	0.1328
4	1.5	0.257	0.1380	0.1508	0.1713

Hydrodynamic roughness

The concept of drag generated by the fluid moving through vegetation is employed to calculate the resistance coefficients for use in the hydrodynamic model. The tables of vegetation density Dv (Tables 8-10) allow us to link flow resistance directly to vegetation features. We assume vegetation is partially submerged and, among the many available, we select two different equations, presented

by McKenney et al. (1995, Equation (5.3)) and Baptist (2005, Equation (5.4)). The first one calculates a Manning-type resistance coefficient, the latter a Chézy-type conveyance coefficient.

$$n = R^{2/3}\left(\frac{C_d \sum A_i}{2gAL}\right)^{0.5} \tag{5.3}$$

$$Cr = \left(\frac{1}{\frac{1}{C^2{}_b} + \frac{1}{2g} C_d N d h}\right)^{0.5} \tag{5.4}$$

In Equation (5.3), n is the resistance coefficient, R is the hydraulic radius, Cd is the drag coefficient, g is gravity acceleration and other terms are defined as in Equation (5.1) In Equation (5.4,) Cr is the Chézy-type conveyance coefficient, C_b is the Chezy coefficient for the bed roughness with no vegetation, C_d is the drag coefficient, h is the water depth and N and d are defined as in Eq. (5.2) Equation (5.4) proved to be too dependent from the reference coefficient C_b and not enough sensitive to vegetation density variations; for this reason we kept Equation (5.3) as closure equation for the hydrodynamic model.

The empirical estimation of dimensionless drag coefficient C_d is complex due to the interaction and superposition of many factors influencing the drag force; C_d changes with the type of vegetation but also with the hydrodynamic conditions (e.g. Reynolds number, see Fischenich and Dudley, 2000). The range of values of C_d for several species, in different conditions (e.g. stressed-unstressed, with leaves-leafless) is very broad (for references, see Rahmeyer et al.1995, Fischenich, 2000, Wunder et al., 2011) and the assignment of different drag coefficients to each vegetation class turns out to be a disproportionate effort compared to the overall accuracy of this model. We assumed the following empirical relationship for Cd, proportional to local hydrodynamic conditions

$$C_d = K\frac{A}{B} \tag{5.5}$$

A is the local wetted area, B is the width (both referred to the sub-section), K is a constant single value that is calibrated to obtain the best matching of the simulation results (water level -

discharge) with gauged values. The final values of C_d are coherent with ranges found in literature (citations above).

5.4 The numerical scheme

For this case study, we don't need a mobile bed model. The system of equations includes only equations (2.1) and (2.2) (See chapter 2).

The same finite-volume numerical scheme used for the model of Red River, described in section 2.3, has been adopted to integrate the equations.

5.5 Model setup and results

We modeled a 50 km long reach of Secchia river, from Rubiera to Concordia s/ Secchia (see Figure 49). Topographical surveys of 92 cross sections are available (AdBPo, 2004). Overlapping cross sections surveys with vegetation classification polygons (see Figure 50), we obtain vegetation features for each cross section: SDI, TDI, age index (see section 5.2).

For bare soil and areas with recent clearings, we adopted a constant Manning coefficient n = 0.035. We set a bounded range for the coefficients determined by vegetation density, between n = 0.02 and n = 0.1.

We tested the model with an important flood event of 6 days, December 2013. Hydrological data are available at AIPo gauging stations and ARPA (Agenzia Regionale Prevenzione Ambiente, Emilia Romagna) hydrological bulletins (input hydrograph and stage-discharge relationship at final cross section).

The agreement at Ponte Pioppa (41.7 km from upstream) and Concordia s/Secchia stations is satisfactory. The best value of K (see Equation 5.5) to calculate *Cd*, found with a trial and error procedure, is K = 0.035. Plots of recorded and simulated values are reported in Figures 50 and 51;

as an example, Figure 53 shows the frequency distribution of Manning coefficients during the rising limb of the flood. The agreement between simulation results and gauged data is encouraging and opens the way to the use of the model for evaluating the effectiveness of future vegetation management plans.

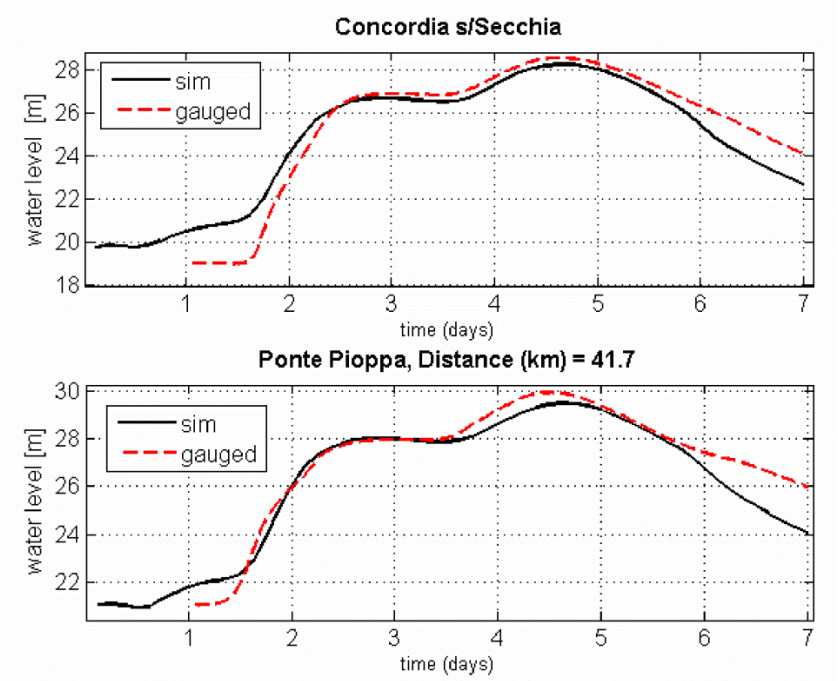

Figure 51. Recorded and simulated water levels at Ponte Pioppa and Concordia s/Secchia

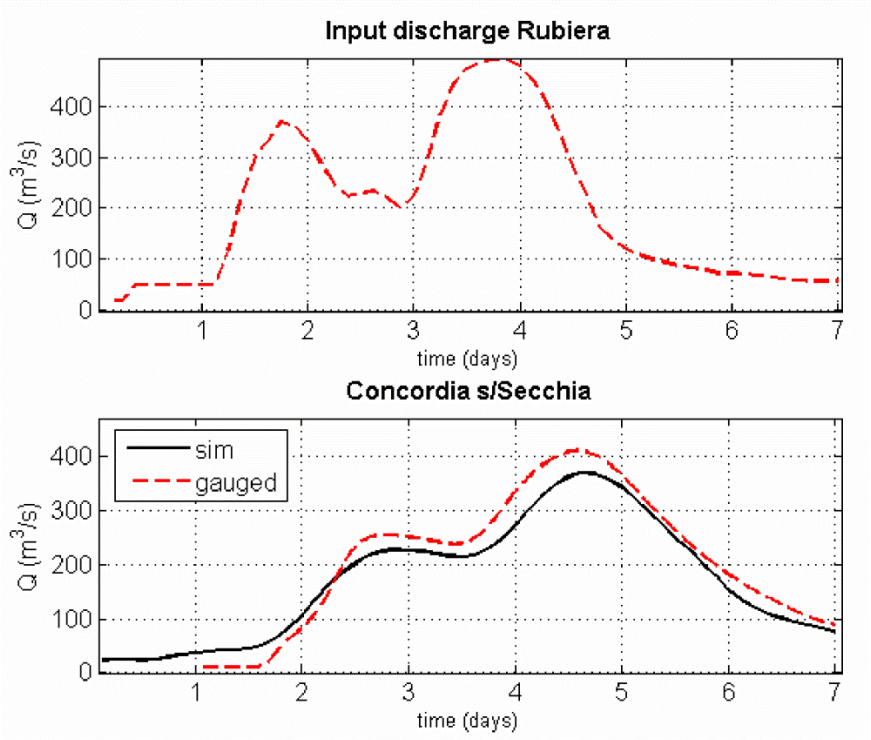

Figure 52. Recorded and simulated flow rates

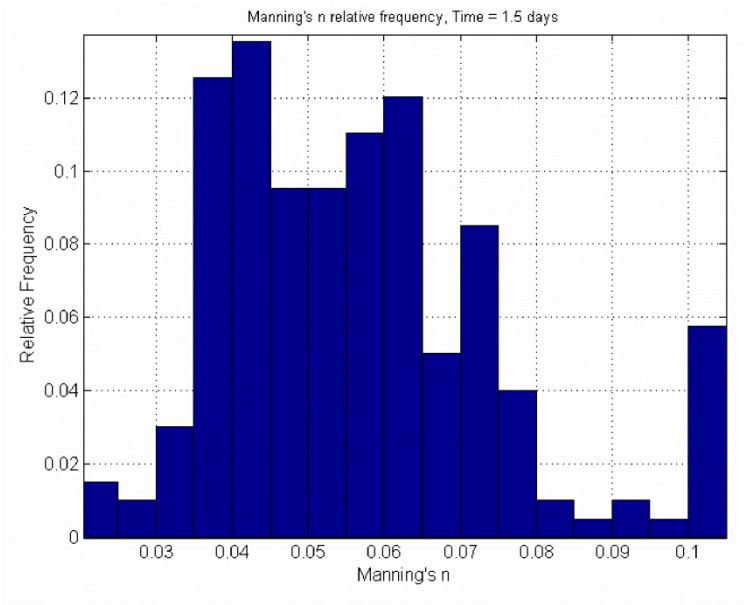

Figure 53. Relative frequency distribution of resistance coefficients during simulation at time T = 1.5 days.

Conclusions

The purpose of this work is not to contribute (or very little) to the field of numerical schemes and techniques to solve the hyperbolic system of differential equations describing free surface flows and sediment transport. Numerical models are reaching nowadays unbelievable levels of accuracy, taking advantage from an increased computing power but most of all from the frequent and multiple advances in the field of computational fluid dynamics. The community of river scientists has nowadays a broad range of tools available for detailed river geomorphological and hydrodynamic modeling (a few of these relevant contributions have been cited in the introduction).

The aim of this work is different, namely the application of cheap to run one-dimensional models, with simple but robust and reliable numerical schemes, to relevant problems of river resource management at reach or basin scale.

At these spatial scales and for long time horizons, capturing all details of such complex morphological evolution phenomena, subject to relevant randomness factors (at least locally) becomes challenging and implies a computational burden. Still, the need for tools capable of informing managers, stakeholders and agencies is apparent. We took into exam three different applications, to point out the relevant contribution of numerical models in practical problems involving management decisions which will influence the river basin evolution but also life of the communities established along the rivers, in terms of social, economical and environmental costs.

In Chapter 3, as a first attempt to include fluvial channel adjustment as a relevant factor in planning optimal operating rules of a hydropower barrage, (Bizzi et al., 2015; Dinh, 2014) we provided a procedure to design optimal operating rules for a run-of-river power plant, in a multi-objective optimization framework. Besides maximizing the energy production, the designed rules aim to

reduce the river bed incision rate downstream from the plant. The one-dimensional mobile bed numerical model provided the fundamental understanding of the hydromorphological dynamics in the river system and was coupled to the Response Surface Methodology in the Learning and Planning procedure (Castelletti et al., 2010)- a surrogate modeling approach, - to provide Pareto dominant solutions for our conflicting objectives: hydropower production and reduction of river bed incision. Without a surrogate model, thousands of simulations would be required to integrate the hydro-morphological model itself within an optimization routine, leading to unaffordable computational costs.

The obtained results are encouraging and show that with a moderate loss in hydropower revenue, the decrease in incision can be remarkable. The Pareto front is an effective tool to inform decision makers: however, future developments should focus primarily at quantifying the uncertainty related to the identification of the front. Such outlook is here particularly relevant, given the significant uncertainties that affect numerical modeling of river channel behavior. We showed the potential of coupling the advances in hydrodynamic modelling with progresses in surrogate modeling; the implementation of the proposed procedure requires tools that are available to many water resources experts.

In chapter 4, we analyzed the severe morphological degradation process of the lower course of Red River (VietNam) - driven by human-related activities: strong instream sediment mining, major upstream impoundments, climatic and land use changes - by means of a one-dimensional hydrodynamic and sediment transport model with a first-order accurate finite-volume numerical scheme.

The management of Red River basin has to take into account a large number of conflicting socio-economic issues: among those, water supply to the agricultural district of the delta is threatened by the fast rate river bed lowering. Integrated river basin management plans are still hard to accomplish in VietNam, even if strong efforts and progress have been made (Molle and Hoanh, 2011).

A validation of the model in the period 2000-2009 has been carried on. As for the simulation runs concerning sand mining and flow control, it is interesting to notice that in absence of sand mining, tendency to river bed degradation is visible only in the first reach, whereas a natural process of slope decrease would probably occur from the second reach due to deposition. We showed that sediment mining rates, as expected, could be much larger than licensed amounts and this accelerates incision in the first reach and reverses the restoring trend in the following reaches, aggravating water level lowering. The flow control operated by reservoirs, conversely, appears to affect much less the morphological processes in the studied reach.

In chapter 5, the development of a vegetation roughness model was described. The purpose of the model is to implement in a hydrodynamic numerical model a set of important information collected during a riparian vegetation characterization project on Secchia River (Italy), carried on by AIPo. Data about trees and shrubs type, density and age were collected both by means of satellite image analysis and field surveys: we converted these data to Dv (1/m) hydrodynamic vegetation density values and then used them to calculate Manning-type flow resistance coefficients accounting for vegetation-induced drag. The agreement between simulation results and gauged data is encouraging and opens the way to the use of the model for evaluating the effectiveness of vegetation management plans.

Bibliography

Autorità di Bacino del Fiume Po (AdBPo), 2004. Studio di fattibilità della sistemazione idraulica del fiume Secchia nel tratto da Castellarano alla confluenza in Po. AdBPo internal report (in italian).

Autorità di Bacino del Fiume Po (AdBPo), 2007. Programma generale di gestione dei sedimenti alluvionali dell'alveo del fiume Po – Stralcio: confluenza Arda – incile Po di Goro. Relazione Tecnica, Maggio 2007. (in italian).

Adorni M., Boz B., Gualmini M., Piovani P., 2014. Caratterizzazione della vegetazione ripariale dei fiumi Secchia e Panaro, in Provincia di Modena, dalle casse di espansione al confine provinciale. AIPo Parma, Italy, internal report (in italian).

Agence de l'Eau Rhone-Méditerranée & Corse, 1998. Guide technique SDAGE (1996-2009) n.1: La gestion des boisements des Rivières - Fascicule 2 - Définition des Objectifs et conception d'un plan d'entretien- Septembre 1998 www.rhone-mediterranee.eaufrance.fr

Anderson B. G., Rutherfurd I.D., Western A.W., 2006. An analysis of the influence of riparian vegetation on the propagation of flood waves, *Environmental modelling and software* **21**, 1290-1296.

Anselmo V., Terzolo P., 2001. Linee di gestione della vegetazione ripariale del Fiume Secchia nel tratto compreso tra le origini delle arginature e Chiesa Motta. AIPo internal report (in Italian).

Armanini, A. 1999. *Principi di Idraulica Fluviale.* Cosenza: BIOS (in italian).

Asselman N., Niddelkoop H., Ritzen M., Straatsma M., 2002. Assesment of the hydraulic roughness of river flood plains using laser altimetry, The Structure, Function and Management Implications of Fluvial Sedimentary Systems, Alice Springs, Australia 2002, IAHS Publ. no 276.

Baptist, M. J., 2005. *Modelling floodplain biogeomorphology*. Ph.D. thesis, Delft University of Technology, Delft University Press, Delft.

Bernardi D., Schippa L., 2014. A mobile bed 1D numerical model to support Red River (VietNam) basin management, *River Flow 2014*, Lausanne, Switzerland, CRC Press.

Bernardi, D., Bizzi, S., Denaro, S., Dinh, Q., Pavan, S., Schippa, L., Soncini-Sessa, R. 2013. Integrating mobile bed numerical modelling into reservoir planning operations: the case study of the hydroelectric plant in Isola Serafini (Italy). *WIT Transactions on Ecology and the Environment*, Vol. **178**.

Bhallamudi S.M., Chaudhry H., 1991. Numerical modeling of aggradation and degradation in alluvial channels, *Journal of Hydraulic Engineering*, **117 (9)**, 1145-1163.

Bizzi S., Dinh Q., Bernardi D., Denaro S., Schippa L., Soncini-Sessa R., 2015. On the control of river bed incision induced by a run-of-river hydropower plant, *Water Resources Research*, submitted for publication.

Bleninger, T., Fenton, J., & Zentgraf, R., 2006. One-dimensional flow modelling and a case study of the river Rhine. *River Flow 2006, Proc. Int. Conf. on Fluvial Hydraulics*, eds. R.M.L. Ferreira, E.C.T.L. Alves, J. G. A. B. Leal & A.H. Cardoso, pp. 1963-1972, Lisbon.

Bonomo F., Casazza L., 2011. La nuova conca di Isola Serafini. *Cemento e Calcestruzzo*, November 2011, pp. 105—115 (italian).

Box G.E., Wilson K., 1951. On the experimental attainment of optimum conditions. *Journal of the Royal Statistical Society*. Series B(Methodological), **13(1)**, 1-45.

Camporeale C., Perucca E., Ridolfi,L., Gurnell A. M. 2013. Modeling the interactions between river morphodynamics and riparian vegetation, *Review of Geophysics* **51**, doi: 10.1002/rog.20014

Canestrelli, A., Lanzoni S., Fagherazzi S., 2013. One-dimensional numerical modeling of the long-term morphodynamic evolution of a tidally- dominated estuary: The Lower Fly River (Papua New Guinea), *Sedimentary Geology*, http://dx.doi.org/10.1016/j.sedgeo.2013.06.009

Canestrelli, A., Siviglia, A., Dumbser, M., Toro, E. 2009. Well-balanced high-order schemes for non-conservative hyperbolic systems. Application to shallow water equations with fixed and mobile bed. *Advances in Water Resources,* **32**: 834-844.

Cao, Z., Day, R., Egashira, S. 2002. Coupled and decoupled numerical modelling of flow and morphological evolution in alluvial rivers. *Journal of Hydraulic Engineering*, **128(3)**: 306–321.

Capart, H., Eldho, T. I., Huang, S. Y., Young, S. Y., Zech, Y. 2003. Treatment of natural geometry in finite volume river flow computations. *Journal of Hydraulic Engineering* **129(5)**: 385–393.

Castelletti, A., Pianosi, F., & Soncini-Sessa, R., 2007. Integration, partecipation and optimal control in water resources planning and management. *Applied Mathematics and Computation*, **206(1)**, 21–33.

Castelletti, A., Pianosi F., Soncini-Sessa R., and Antenucci J. P., 2010. A multiobjective response surface approach for improved water quality planning in lakes and reservoirs, *Water Resources Research*, **46(6)**, doi:10.1029/2009WR008389.

Castro M.J., Gallardo J. M., Parés C., 2006. High order finite volume schemes based on reconstruction of states for solving hyperbolic systems with nonconservative products. Applications to shallow water systems, *Matematics of. Computation* **75**, 1103-34.

Chang, H. H., 1988. *Fluvial processes in river engineering*, Krieger Publications.

Chaudhry, M. H., 2007. *Open Channel Flow*, 2nd ed. Springer, Berlin.

Correia, L. R. P., Krishnappan, B. G., Graf, W. H. 1992. Fully coupled unsteady mobile boundary flow model. *Journal of Hydraulic Engineering* **118 (3)**: 476–494.

Cunge, J. A., Holly, F. M., Jr., and Verwey, A. 1980. *Practical aspects of computational river hydraulics,* London: Pitman.

Curran, J. and Hession, W. 2013. Vegetative impacts on hydraulics and sediment processes across the fluvial system. *Journal of Hydrology*, **505**, 364-376.

D'Alpaos, L. et al. 2014. Relazione tecnico-scientifica sulle cause del collasso dell'argine del fiume Secchia avvenuto il giorno 19 gennaio 2014 presso la frazione San Matteo, Regione Emilia-Romagna, web publication *www.regione.emilia-romagna.it*

Dang, T. H., Coynel, A., Orange, D., Blanc, G., Etcheber, H., Anh Le L., 2010. Long term monitoring of the river sediment transport in the Red River watershed (Vietnam): temporal variability and dam-reservoir impact. *Science of the Total Environment*, **408**: 4654-4664.

Darby S., 1999. Effect of Riparian Vegetation on Flow Resistance and Flood Potential. *Journal of Hydraulic Engineering*, **125(5),** 443–454.

Dinh, Quang Nhat 2014. *Multi-Objective Evolutionary Algorithm, Dynamic and non-dynamic emulators in the design of optimal policies for water resources management*. Doctoral Dissertation, Politecnico di Milano, Italy.

Engelund F. & Hansen E. 1967. *A monograph on sediment transport in alluvial streams,* Copenhagen: Teknisk Forlag.

Fischenich C., Dudley S., 2000, Determining Drag Coefficients and Area for Vegetation, ERDC Technical Note EMRRP-SR-08, Vicksburg, MS, USA.

Fischenisch C., 2000. Resistance due to vegetation, ERDC Technical Note TN-EMRRP-SR-07, Vicksburg, MS, USA.

Garcia-Navarro, P. and Vázquez Cendón, M., 2000. On numerical treatment of the source terms in the shallow water equations. *Computers & Fluids*, **29(8)**, 951-979.

Gilvear, D. J., Spray, C. J., & Casas-Mulet, R., 2013. River rehabilitation for the delivery of multiple ecosystem services at the river network scale. *Journal of Environmental Management*, **126(0)**, 30–43.

Godunov S. K., 1959. A finite difference method for the numerical computation of discontinuous solutions of the equations of fluid dynamics. *Math Sbomik* **47(3)**:271-306

Goutière, L., Soares-Frazão, S., Savary, C., Laraichi, T., Zech, Y. 2008. One-dimensional model for transient flows involving bed-load sediment transport and changes in flow regimes. *Journal of Hydraulic Engineering,* **134(6)**: 726-735.

Gupta, H., S.J. Kao, and M. Dai, 2012. The role of mega dams in reducing sediment fluxes: A case study of large Asian rivers, *Journal of Hydrology*, **464–465 (0)**, 447-458

Harten, A., Lax, P. D., van Leer, B. 1983. On upstream differencing and Godunov-type schemes for hyperbolic conservation laws. *SIAM Rev.* **25(1)**: 35-61.

Harten A., Engquist B., Osher S., and Chakravarthy S. R., 1987. Uniformly high-order accurate essentially nonoscillatory schemes, III. *Journal of. Computational Physics* , **71**, 231-303.

Hirsch, C., 1990. *Numerical Computation of Internal and External Flows*, vol. 2, Wiley, New York.

Italian Ministry of Agriculture, 1990. *Po AcquAgricolturAmbiente - 2: l'alveo e il delta*, (*Po: Water, Agriculture and Environment - volume 2: the river bed and the delta*) Il Mulino, Bologna (in Italian)

Lamberti, A. & Schippa, L., 1994. Studio dell'abbassamento dell'alveo del fiume Po: previsioni trentennali dell'abbassamento a Cremona, Supplement to *Navigazione Interna* **3/4**, July-December 1994.

Langendoen, E., Wells, R., Thomas, R., Simon, A., and Bingner, R. 2009. Modeling the Evolution of Incised Streams. III: Model Application. *Journal of Hydraulic Engineering*, **135(6)**, 476–486.

Lai C., 1986. Numerical Modeling of Unsteady Open-Channel Flow. *Advances in Hydroscience*, vol. 14, Academic Press, New York., pp. 161-333

Lax P. D., Wendroff B., 1960. "Systems of conservation laws". *Communications in Pure and Applied Mathematics.* **13 (2)**: 217–237.

McCormack R.W., 1969. *The effect of viscosity in hypervelocity impact cratering*. American Institute of Aeronautics and Astronautics Electronic Library, pp 69-354.

McKenney R., Jacobson R., Wertheimer R., 1995. Woody vegetation and channel morphogenesis in low-gradient, gravel-bed streams in the Ozark Plateaus, Missouri and Arkansas, Geomorphology, **13**, 175-198.

Molle, F., Hoanh, Chu Thai. 2011. Implementing integrated river basin management in the Red River Basin, Vietnam: a solution looking for a problem? *Water Policy*, **13(4)**:518-534

Newson, M. D., & Large, A. R., 2006. "Natural" rivers, "hydromorphological quality" and river restoration: a challenging new agenda for applied fluvial geomorphology. *Earth Surface Processes and Landforms*, **31**, 1606–1624.

Nicklow, J. & Mays, L. 2000. Optimization of multiple reservoir networks for sedimentation control. *Journal of Hydraulic Engineering*, **126(4)**: 232-242.

Nones M., Ronco P., Di Silvio G., 2013. Modelling the impact of large impoundments on the Lower Zambezi River, *International Journal of River Basin Management,* **11(2),** 221-236.

Petts, G. E., & Gurnell, A. M., 2005. Dams and geomorphology: Research progress and future directions. *Geomorphology*, **71(1–2)**, 27–47.

Poff, N. L., and Hart, D. D. , 2002. How dams vary and why it matters for the emerging science of dam removal, *Bioscience,* **52 (8)**.

Preissmann A., Cunge J.A., 1961. Calcul des intumescences sur machines électroniques, *Proceedings of the 9th' IAHRE Conference*, Dubrovnik.

Rahmeyer W., Werth D., Cleere R. 1995. The study of Resistance and Stability of Vegetation in Flood Channels. Utah State University Lab report USU-376

Roe, P.L., 1986. Upwind differencing schemes for hyperbolic conservation laws with source terms, in Carasso, Raviart and Serre (ed.), *Proc. First International Conference on Hyperbolic Problems,* Springer, pp. 41 – 51.

Rosatti G., Armanini, A., Galletta, V., Vergnani, M., & Cerchia, F., 2008. L'uso dei pennelli per la riduzione della barra forzata in prossimità del punto di inflessione tra due curve susseguenti: uno studio numerico relativo al Po. *Atti del 31° Convegno di Idraulica e Costruzioni Idrauliche*, Morlacchi, Perugia (in Italian).

Rosatti, G. & Fraccarollo, L. 2003. A well-balanced approach for flows over mobile bed with high sediment transport. *Journal of Computational Physics,* **220**: 312-338.

Schippa, L. & Bernardi D. 2014. *Hydromorphological physically based model of the Red River*, IMRR project intermediate reports, Part 4.2, www.imrr.info

Schippa, L. & Pavan, S. 2008. Analytical treatment of source terms for complex channel geometry, *Journal of Hydraulic Research,* **46(6)**: 753-763.

Schippa, L. & Pavan, S. 2009. Bed evolution numerical model for rapidly varying flow in natural streams, *Computers & Geosciences,* **35**: 390-402.

Schmitt, R. 2014. *Hydromorphological dynamics in the Red River Delta*, IMRR project intermediate reports, Part 4.1, www.imrr.info

Schumm S. A., 1977. *The fluvial system*, Wiley, New York.

Simon A., Rinaldi M., 2006. Disturbance, stream incision, and channel evolution: The roles of excess transport capacity and boundary materials in controlling channel response. *Geomorphology*, **79**, 361–383,

Soncini-Sessa R., Weber E., Castelletti A., 2007. *Integrated and participatory water resources management-theory*, vol. 1, Elsevier Science.

Surian N., Rinaldi M., 2003. Morphological response to river engineering and management in alluvial channels in Italy. *Geomorphology*, **50(4)**, 307-326.

Sweby, P.K. 1984. High resolution schemes using flux-limiters for hyperbolic conservation laws, *SIAM Journal on. Numerical Analysis* **21 (5)**: 995–1011.

Tabacchi E., Lambs L., Guilloy L., Planty-Tabacchi A. M., Muller E., Décamps H, 2000. Impacts of riparian vegetation on hydrological processes, *Hydrological Processes*, **14**, 2959-2976.

Toro, E. F., Spruce, M., Speares, W. 1994. Restoration of Contact Surface in the HLL-Riemann Solver. *Shock Waves*, **4**: 25-34.

Toro E. F., Millington R. C., Nejad L. A. M., 2001. Towards very high-order Godunov schemes. *Godunov Methods: Theory and Applications* (E. F. Toro, ed.), Kluwer Academic/Plenum New York 905-937.

Toro E. F., Siviglia A., 2003. PRICE: Primitive centred schemes for hyperbolic system of equations. *International Journal for Numerical Methods in Fluids* **42**, 1263-1291

Toro, E.F., 2009. *Riemann Solvers and Numerical Methods for Fluid Dynamics, 3rd ed.* Berlin: Springer-Verlag.

Uyen, V.T., 2011. *Warning about sand mining consequence in Red river*, Vietnamese Ministry of Agriculture and Rural Development - MARD, internal report (in Vietnamese).

Valiani, A. & Begnudelli, L. 2006. Divergence form for bed slope source terms in shallow water equations. *Journal of Hydraulic Engineering,* **132(7)**: 652-665.

Warmink J., 2007. *Vegetation Density Measurements using Parallel Photography and Terrestrial Laser Scanning*. MSc Thesis, Utrecht University, January 2007.

Wu W., Wang S. S. Y 2008. One-dimensional explicit finite-volume model for sediment transport. *Journal of Hydraulic Research,* **46(1)**: 87-98.

Wunder S., Lehmann B., Nestmann F., 2011. Determination of the drag coefficients of emergent and just submerged willows, *International Journal of River Basin Management*, **9:3-4**, 231-236.

Acknowledgements

This thesis concludes a three-year long trip. I had the chance to work with valuable persons and good friends. My choice was to mention only people I worked with.

First of all I thank my supervisor Leonardo Schippa for the chance I had to attend a PhD program in hydraulics and for the internship at Bioengineering Group, Inc. in the US. I appreciated the trust he put in me and the possibility I often had to manage the work on my own and being responsible for what I did.

I shall acknowledge IUSS-Unife for the grant funding the trip to United States.

I shall acknowledge Federica Filippi and Sara Pavan at AIPo (*Agenzia Interregionale Fiume Po* in Parma, Italy) for sharing the data I needed to perform the work reported in Chapter 5 and the River Po cross sections surveys for Chapter 3. A thank you goes also to all Vietnamese agencies, especially *IWRP* (Institute of Water Resources Planning, Hanoi) that provided data for the Red River numerical model (Chapter 4).

I want to thank again Sara Pavan, who has been a colleague of mine at the University just for a few months but introduced and connected our group with the group of Prof. Soncini-Sessa at Politecnico di Milano. The collaboration with them has produced the most satisfactory results shown in this thesis.

I want to thank Professor Rodolfo Soncini-Sessa for giving us the opportunity to share with his group part of the research challenges of the IMRR project, for funding part of our work and an unforgettable trip to VietNam in 2013. I'm proud to have worked together with a remarkable professor and person as he is. I thank also Simona Denaro, Marco Micotti, Enrico Weber for their assistance in the work we carried on together.

I want to thank Quang Dinh for being always helpful, patient, for showing me what it means to be determined and dedicated to work and to the accomplishments of results. His commitment and his way to work (not only for himself) will be forever an example for me.

Finally I want to dedicate a few words to Simone Bizzi and Rafael Schmitt: my friends, we shared (with Quang too!) many good moments in Milan and this has given higher value to our collaboration. I liked so much our chats at the bar about Milan, Italy, Germany, politics, everything. I thank you for hosting me often and I hope we will have the chance to work together again. But above all, I wish you all the best for your research career and hope our friendship will continue from now on! I'm looking forward to hosting you very soon in Ferrara.